UNIVERSITY OF TRENTO - Italy
Department of Civil, Environmental and Mechanical Engineering

Doctoral School in Civil, Environmental and Mechanical Engineering
Doctoral Thesis - October 26, 2020

MICHELE BOTTAZZI

Transpiration theory and the Prospero component of GEOframe

Supervisors:

Riccardo RIGON (University of Trento, Italy)

Giacomo BERTOLDI (Eurac research, Italy)

"Tra frammenti di tecniche
sotto prodigi incerti
un affanno continuo"
CCCP - Fedeli alla linea - And the radio plays

Abstract

Evapotranspiration plays a key role in the land-atmosphere interaction and has for long been recognized as the most important process in the determination of the exchanges of energy and mass among them, representing approximately the 40% of total precipitation and of the net radiation absorbed. Our ability to quantify evapotranspiration is limited by several factors such as the scarce availability of its measurements and the high uncertainty they present; and the lack of appropriate modeling methods, as highlighted by some recent papers and its response to climate change ('drought paradox').
In the first part of this thesis we present an extensive literature review of the transpiration theory starting from the milestones until the newest works. In particular we focused on the physics of the process and faced some omissions rising from recent studies. We also addressed some physiological feature of transpiration process and the rising issues from the upscaling techniques.
Later on we introduced a newly developed model called "Prospero", used to estimate the evapotranspiration, that can be used as a component in the GEOframe hydrological modelling system. The physical description of the process provided by Prospero is in agreement with what emerged from the previous literature review and in particular corrects the omissions given by the feedback of the leaf temperature and the wrong representation of the transpiring area, further improved with the inclusion of a model of canopy layers. In addition, it also includes several environmental stress functions based on the physiology of the leaves. These improvements allow the closure of the energy balance and the conservation of the water mass.
Finally the Prospero model is applied on two case studies: the first one is pointwise case study represented by two Alpine grass-

lands (Viote del Monte Bondone, Trentino and Torgnon, Valle d'Aosta) where the estimation of Prospero evapotranspiration is compared with eddy covariance station measurements, and the second one is represented by a small experimental basin in Ressi (Posina, Veneto). Even if not calibrated, Prospero provides good results in the prediction of evapotranspiration, capturing the daily trend and obtaining an error that can be compared with what was found in literature for similar cases. The estimation provided, even if it presents a greater dispersion, gives better results when compared to the other components of GEOframe.
In both case studies the performance of Prospero is compared with the other GEOframe components for evapotranspiration. To this result, Prospero represents an improvement since it gives better performances if compared with the other GEOframe components and allow us to compute other environmental variable like sensible heat and canopy temperature. Thanks to its components-based structure Prospero can be easily improved and represents the core for a future ecohydrological or a lysimiter model.

.

A Carla,
per il suo adamantino e imperituro supporto

TABLE OF CONTENTS

LIST OF TABLES

List of Figures

CHAPTER 1

INTRODUCTION

Evapotranspiration (ET) plays a key role in the hydrological cycle and land-atmosphere interaction, thus, a correct evaluation of this variable is fundamental in several fields of application, such as sustainable water management at the basin scale and irrigation planning, at the field scale.

In fact, the estimation of atmospheric turbulent fluxes (sensible and latent heat) at the land surface has long been recognized as the most important process in the determination of the exchanges of energy and mass among hydrosphere, atmosphere and biosphere (e.g. Bowen, 1926; Penman, 1948; Monteith, 1965; Priestley and Taylor, 1972; Brutsaert, 2013; Morton, 1983; Famiglietti and Wood, 1994; Su et al., 1999; Su and Jacobs, 2001).

At global scale the overland latent heat represents the 38% of the net radiation absorbed and the corresponding evaporated water amounts to the 40% of total precipitation. Transpiration impacts on the evapotranspiration up to 60%. However there is a large uncertainty associated with the vegetation response to water stress (Mastrotheodoros et al., 2020).

There is an urgent need to move towards a more sustainable approach to manage water resources and mitigate and prevent natural hazards. Water-related aspects of climate change (CC) and extremes, such as droughts, put pressure on alpine ecosystems, but their response to hydrological variability is not yet fully understood (Beniston, 2012; Pepin et al., 2015) as the "drought paradox" (Mastrotheodoros et al., 2020, see appendix D).

In recent years, the development of world-wide networks such as the Long-Term Socio-Ecological Research (LTSER) or FLUXNET has led to a deeper experimental knowledge on plant-water interactions.
At the same time, new and improved techniques for area-wide observation (proximal sensing through Unmanned Aerial Vehicle (UAV) devices, RS platforms as European Space Agency (ESA) satellite Sentinel mission, Berger et al., 2012) have provided new options for upscaling to landscape-scale.

Analogously to experimental researches, also theoretical work was very active, in investigating the interactions between the various compartments of the soil-vegetation atmosphere interactions. The paper by Rodrigues-Iturbe (2000) opened twenty years of intense research in hydrology and its interaction with the carbon cycle, although investigations on the effects of the surface and boundary layer parameterization on evapotranspiration go back at least to the seventies, with the work of Sinclair et al. (1976), Jarvis (1976), Norman (1979), Deardorff (1978) to cite a few. As a product of those researches,various models were developed, an effective review of which can be found in the Introduction of Bonan et al. (2018). In addition, various studies accounted explicitly for topographic attributes and lateral water and mass exchanges (Ivanov et al., 2008; Shen et al., 2013; Tague

et al., 2013), but their treatment of plant processes was often oversimplified (Zhou et al., 2013).

Approaching the issues of this thesis from another side, plant water-use strategies are driven by plant functional traits (PFT) (examples are leaf size, toughness and longevity, seed size and dispersal mode, canopy height and structure, capacity for nitrogen fixation, Mitchell et al., 2008) and in recent years, plant-physiology studies provided an increasingly detailed knowledge of plants behaviour (Brodribb et al., 2005), but only some of them started to be implemented in ecohydrological models (Fatichi et al., 2016).
Models simulating plant-hydraulic processes are still rare and confined to specific studies (Hölttä et al., 2009; Mackay et al., 2015; Nikinmaa et al., 2014). In fact, vegetation hydraulic was recently reviewed by Stroock et al. (2014), providing the idea that a new synthesis is necessary between the modelling of water and carbon fluxes, and providing further evidence that an upscaling from cells through plants to landscape is required.
Having collected the information mentioned above made it extremely important to get the right answers, although it was very complicated since it transcend up to 14 orders of magnitude in time and space (Baldocchi, 2019). In mountain terrain, even the effect of plot-scale ($0.01-0.1 km^2$) spatial variability of the energy fluxes is still largely not understood (Rollinson and Kaye, 2015) notwithstanding pioneering studies which account for various feedbacks are available, which show that vegetation productivity and water use do not change linearly through spatial gradients (Niedrist et al., 2016).

Most advanced plot-to-catchment scale models include a three-dimensional treatment of the water fluxes in soil (e.g. Pützc et al., 2013), explicit spatial variability of atmospheric forcing and

turbulence (e.g. Katul et al., 2013) and a well-balanced complexity in the formulation of the water and energy budgets.

In summary, despite the increasing experimental knowledge of plant's hydrology and the availability of high-resolution observations, there is still a lack of appropriate modelling methods able to incorporate this information in a physically consistent way (Demirel et al., 2018) while gathering and blending information from atmospheric boundary layer meteorology, hydrology, plant physiology, thermodynamics and fluid dynamics.
In order to build Reliable, Robust and Realistic (R3) predicting modelling tools (Prentice et al., 2015), there is the need to translate this observational knowledge in mathematical and numerical form, which balances functional complexity to practical needs (Prentice et al., 2015). Two main categories of models can be roughly identify: those who approach the problem mechanistically (Fatichi et al., 2012), by adding detailed processes parameterizations, and those who make reference to optimality principles, claiming that feedback mechanisms were discovered during plants evolution to maintain good performances under sub-optimal conditions (Prentice et al., 2015).
Modellers had to face different challenges, such as joining the plant physiology with the biosphere and considering the interactions with pedo and atmosphere (including spatial and temporal patterns). This task involves an appropriate modelling of the environmental conditions (Bertoldi et al., 2007; Siqueira et al., 2009); the mathematical description of the water flow in the soil interaction with roots and the reciprocal influence of plants for accessing nutrient resources (Manoli et al., 2014); a more accurate separation of soil evaporation from transpiration (Jung et al., 2010); the need to upscale the mathematics of plants behaviour at the landscape scale, with the appropriate degree of complexity (Pappas et al., 2016).

In a recent study I co-authored on Nature Climate Change (Mastrotheodoros et al., 2020), we find that with climate change, the partition between evaporative fluxes and runoff is changing, enhancing the ET during the drought period ('drought paradox', see appendix D). This further highlights the need to have precise models for ET, which calculate separately evaporation and transpiration, in order to better understand the response to climate change of the individual processes (soil and vegetation) but also of model that can be easily implemented in distributed models. To further develop these models, a new synthesis of the theoretical achievements and a software infrastructure are necessary in order to enable comparisons of the alternatives that are emerging from last years of research. In fact, the monolithic informatics of traditional design (Rizzoli et al., 2004) hinder any enhancement of the code and slow-down progresses of research, especially in fields which greatly change. Fortunately, recently "component-oriented" modelling approaches (David et al., 2013; Formetta et al., 2014a; Bancheri, 2017) were deployed. Such approaches make it easier to change modules simulating specific processes, while maintaining unchanged the others.

Therefore the main goals of this thesis are to try a synthesis of many theoretical approaches, and build the basis of the open informatic necessary to implement the various competing approaches. Not all of what discussed discussed in the chapters dedicated to the theory have been implemented though, the effort would have required more than the three years span of a Ph.D. thesis in Italy, but it is hoped that solid foundations have been not only deployed but also tested in a few case studies. The work on informatics has been part of a collective task that involved, just to mention the most recently contributions, works with Francesco Serafin, Marialaura Bancheri and Niccolo' Tubini.

It was aimed to produce a component-based, open source, system called GEOframe able to be a solid base of development for the tools required by Earth Sciences while allowing collective contributions to be introduced seamlessly. The part covered by this thesis was especially to refine and to streamline the process of documenting the material, using Python and Jupyter, designing rules and practices for collaborative work, and copying with the processed of continuous integration of the new software software on the GitHub repository. Notwithstanding being intense and challenging this work is usually not evaluated properly by scientists, in its importance and consequences. Being a collective effort, however, this is reported mainly in the Appendix A but it constitutes the foundation of what presented in the main chapters. The designing principles of the modelling has been to balances functional complexity to practical needs and models robustness, while the scientific aims has been to provide R3 predicting tools (Prentice et al., 2015) to be able to analyze the effects of short-term climatic and small-scale hydrological spatial variability on mountain biophysical cycles.

In chapter 2, I present an extensive literature review of the transpiration theory starting from the milestones until the newest works. In particular, the physics of transpiration is analyzed, defining the energy balance and its components. In particular, some omissions rising from recent studies are highlighted.
In chapter 3, I face the physiological component of transpiration and how it manages the exchange of fluxes between the vegetation and the atmosphere. I also analyze some strategies commonly used to adapt the transpiration's equations at the canopy scale of this work.
In chapter 4, I discuss about the deployment of the Prospero code, where it can be found, where the executable and the documentation are, and I also list a series of rules for improving

the code and the framework that this Thesis helped to delineate, in the perspective of open science and science replicability. Finally, in chapter 5 and 6, Prospero is applied to two different types of case studies, both at point-wise scale and catchment scale. Performances are compared with other GEOframe's tools for evapotranspiration and with observed measurements.
Furthermore, in the Appendixes, two papers I worked on are presented. They are not closely related to the development of Prospero, but certainly to GEOframe, the one about Kriging, and to the general topic I considered about the blue and green waters on the Alps.

CHAPTER 2

TRANSPIRATION AND SOIL EVAPORATION THEORY

The effort in this Chapter is to give an updated overview of the evaporation and transpiration theory. Bonan (2019) and Baldocchi (2019) give an outstanding analysis of the same topic. However, here, the aim is also to present all formulas in a unified notation, to give a balanced view of some hydrological aspects and to add some details which were neglected by the previous contributions . For instance Bonan (2019) analysis, even if complete, is standard in giving account of soil behavior; Baldocchi (2019) is mainly concentrated on the atmospheric/atmospheric boundary layer issues than hydrology. In this literature review, I has been inspired a lot from papers and conferences by G.K Katul (even if we are not able to indicate specific papers) and D. Or in his work with Lehman (on soil) and with Schymanski on vegetation. I tried also to maintain a central view on the water budget. Neglecting its role is a classic in literature which brings to difficulties in interpretation when water limited environment

or situations are the case study. The Penman-Monteith approach (Penman, 1948; Monteith, 1965) is excluding water from being limited when assuming that the vapor pressure in leaves (and soil) is at the free water vapor tension. Limitations are recovered a-posteriori through stomatal resistance and empirical stress functions, which could be not imposed the right way. Unfortunately I was not able to do much progress in this direction but, I could at least, on the basis of Vesala et al. (2017) put some place holder in an aspect of the theory which is usually overlooked. As Baldocchi (2019) shows complexity of various order can be introduced for treating the turbulent transport. In this chapter we stick, however, with the first order closure known as K-theory, and let the other treatments to future works. I have clear also that hydrology needs to be coupled with vegetation grow. Modeling vegetation, however, is not between the feasible scopes of this thesis. Therefore any information about vegetation status is thought here as a given (measured) quantity. I give a framework for treating the resistances which is nothing else than the classical one but, possibly in a consistent way. the same approach I use for informatic, the one of encapsulation of concerns, is applied to the theoretical aspects, that can be substituted by others. In this section, the Daltonian equation and the related heat transport equation (k-Theory) are derived heuristically. A brief theoretical analysis of their sensitivity is also performed, mostly derived from Baldocchi (2019). These equations are coupled to the energy budget, written under the hypothesis that leaves have negligible thermal capacity, and to a linearized form of the Clausius-Clapeyron equation, to a solution of the resulting coupled problem, first solved by Penman (1948) and recently reworked by Schymanski and Or (2017). I highlight that the solution regards also temperature, vapor pressure and sensible heat transport, not only the estimate of evapotranspiration as

popularised in textbook where, sometimes, it seems it is not a solution of a well posed algebraic problem but just one among many formula. Because the radiative coupling between the surfaces and atmosphere is important, this extension is treated in the subsequent section, where the solutions are specialized to the case of leaves. The theory is straightforwardly extended using the Monin-Obukhov stability theory. Subsequently soil evaporation is treated with its specific characterization, at the light of Haghighi, Lehman, and Or experiments and theory (Haghighi and Or, 2013; Lehmann et al., 2018; Lehmann and Or, 2015). It support the idea that soil evaporation after a critical distance of the evaporating front from the surface, is limited by the water vapor transport.

2.1 According to Budyko

Below it is presented the the analysis evaporation by Budyko with the purpose of showing that evaporation can be limited by both energy and water supply. Mass conservation in hydrological cycle can be written as:

$$\Delta S = (ET - P - Q)\Delta t \tag{2.1}$$

where ΔS is the soil moisture storage, ET is the evapotranspiration, P the precipitation, Q the runoff and Δt is the temporal time step.
Considering the runoff as the sum:

$$Q = Q_{sup} + Q_s + Q_G \tag{2.2}$$

Where Q_{sup} is the surface runoff, Q_s is the subsurface runoff and Q_G is the recharge term. Budyko considers that an area is large enough ($\approx$ 1000 km^2), the effect of groundwater is minimized. Furthermore if the time step is quite long (Δ t > 1 year), we can

assume the storage variation is more or less zero.
Inverting the water balance we can express the evapotranspiration as:

$$ET = (P - Q) - A\frac{\Delta S}{\Delta t} \tag{2.3}$$

According to Budyko, it can be deduced that the maximum of evapotranspiration is obtained, besides neglecting the water storage variation, when $Q = 0$. If this happens, the maximum evapotranspiration is equal to the rainfall.

$$ET_{max} = P \tag{2.4}$$

Assuming the soil heat flux G equal to zero and the sensible heat H is positive, the energy balance ΔE can be expressed as:

$$\Delta E = R_n - \lambda ET - H \tag{2.5}$$

where R_n is the net radiation, H is the sensible heat and λ the latent heat of evaporation.
When energy is a limiting factor, the maximum possible ET is when $H = 0$ (only if we are considering long terms average, otherwise H could also be negative) and the first member of the equation (ΔE) is negligible. Then, when energy is the limiting factor, it is:

$$R_n > \lambda ET_{max} = \lambda P \tag{2.6}$$

where ET_{max} indicates the maximum possible evaporation, which therefore is equal to P (from mass conservation equation).
Finally we can say that:

$$ET_{max} = min\left(P, \frac{R_n}{\lambda}\right) \tag{2.7}$$

This equation makes evident that both the water and the energy budgets rule evapotranspiration and limit it. When there is not enough water, ET is said water-limited; when there is not enough energy, ET is said energy limited. We use these concepts later on in the thesis.

2.2 Momentum and water vapor transport in turbulent atmosphere

Below I consider an alternative presentation of the topic in (Bonan 2019, section 6.2). The control volume we are considering is the Earth surface and a portion of atmosphere above it (i.e. the critical zone). In its minimalist conceptualization, a semi-

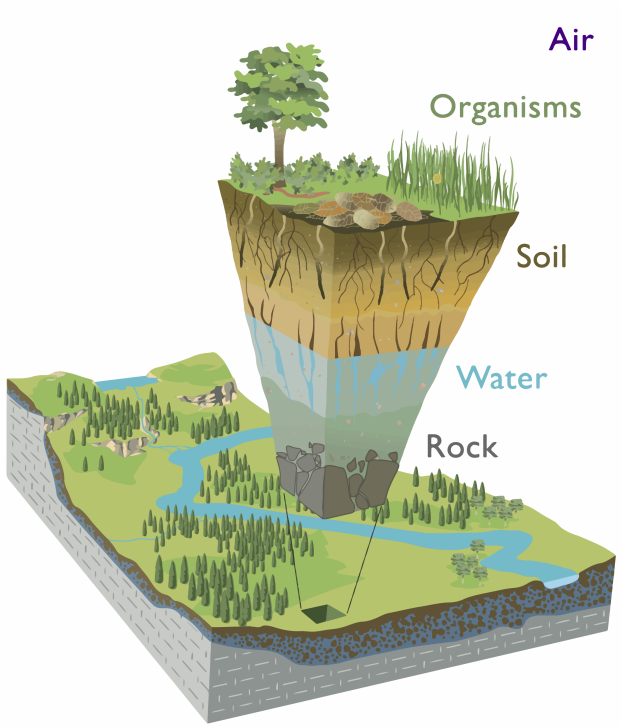

Figure 2.1: Critical Zone surfaces and components (Chorover et al., 2007). Image from Critical Zone Observatories

indefinite volume below, the ground, and a semi-indefinite volume above it, the atmosphere, Dalton's studies were mostly experimental (Brutsaert, 1986), and the current transport theory used to in the area, is the semi-empiric mixing length theory(Prandtl, 1925,1926). It finds that any quantity of concentration x is transported in atmosphere by the vertical fluctuation of velocity, w',

positive upward. So, for instance, it is:

$$\text{Transport of x} = \overline{(\rho_x x)\, w'} \tag{2.8}$$

where:

- x is a generic quantity
- ρ_x is its mass density [kg m^{-3}]
- w' is the fluctuation of air velocity [m s^{-1}]

The rational of the above formula is simply understood, since $\rho_x x$ is the mass of the quantity x present in the control volume, and w' is the upward net velocity excess, so that equation 2.8 is the momentum per unit volume.
The relevant quantities transported in our cases are:

- $-\rho_a u'$ is the momentum [Kg m^{-2} s^{-1}], u' is the fluctuation of horizontal velocity of air [m s^{-1}] and ρ_a is the air density [kg m^{-3}].
- specific thermal energy or sensible heat: $\rho_a c_p T'$ [W m^{-2}], where c_p [J kg^{-1} °K^{-1}] is the thermal capacity of air and T its temperature [°K].
- vapor, $-\rho_a q'$ [Kg m^{-3}], where q is the specific humidity of air (mass concentration of water vapor in air)

Momentum has a negative sign because it is transported downward. Thus we have, accordingly to the above consideration, the momentum flux, τ [N m^{-2}]:

$$\tau = -\overline{\rho_a w' u'} \tag{2.9}$$

Thermal energy flux, H, [W m^{-2}]:

$$H = \overline{\rho_a c_p w' T'} \tag{2.10}$$

Vapor flux, a.k.a as evapotranspiration, ET [m s^{-1}]:

$$ET = \overline{\rho_a w' q'} \tag{2.11}$$

The momentum transfer is regulated by Navier-Stokes equations (NSe):

$$\rho_a \left(\frac{\partial \vec{v}}{\partial t} + \vec{v} \nabla \cdot \vec{v} \right) = -\vec{\nabla} p + \nabla \cdot \mathbf{T} + \vec{f} \tag{2.12}$$

i.e. (Batchelor, 1967), where:

- $\vec{v}$ is the velocity of the air (fluid)
- $\nabla\cdot$ is the divergence operator
- $\vec{\nabla}$ is the gradient operator
- p is the normal stresses (pressure)
- $\mathbf{T}$ is the stresses tensor
- $\vec{f}$ are the external forces acting

NSe can be, in fact, the starting point for a simplifications journey which arrives to results similar to the mixing layer theory based on the assumptions that:

- we can separate the average flow velocity from fluctuations: $\vec{v} = (\bar{u} + u', \bar{v} + v', \bar{w} + w')$
- the flow is over a plane (it throws away the vertical axes dependencies on the left hand side of the equation)
- it is stationary (it eliminates the time derivative)
- homogeneous
- without subsidence
- the molecular viscosity can be neglected

The simplification path takes away almost everything for NSe and leaves only:

$$\frac{\partial}{\partial z}\overline{u'w'} = 0 \rightarrow \overline{u'w'} = constant \tag{2.13}$$

or $\overline{u'w'} = constant$ which gives an important information about the momentum transport in equation (2.9). It can be considered also an empirical results, coming from one hundred year and more of experiments on turbulent flows.
A further leap in Prandtl theory is that:

- fluctuations in equation 2.9, 2.10, 2.11 can be substituted by spatial finite gradients of the same quantities
- the vertical fluctuation of velocity is proportional to the mean horizontal velocity such that:

$$\overline{w'T'} = C_H \Delta\bar{u} \cdot \Delta\bar{T} \tag{2.14}$$

where C_H is called Stanton Number (Gill, 2016).

$$\overline{w'u'} = C(\Delta\bar{u})^2 \tag{2.15}$$

where C is called drag number;

$$\overline{w'q'} = C_E \Delta u \Delta q \tag{2.16}$$

where C_E is called Dalton Number (Gill, 2016).
These assumptions make the Prandtl expressions in 2.9, 2.10, 2.11 evaluable once the coefficients C, C_H, CE are determined.
Concentrating our attention to the momentum transfer, the horizontal flow velocity at the surface is zero and, therefore, $\Delta\bar{u} = u$.
Besides, because $\overline{u'w'} = constant$, we can define:

$$\overline{u'w'} := u_*^2 \tag{2.17}$$

where u_*^2 is called friction velocity. By comparison of (2.17) with (2.15), it results then:

$$C \equiv \frac{u_x^2}{\bar{u}^2} \tag{2.18}$$

which does not help yet, but will be useful soon. Finally, experiments (McDonough, 2007) and recent mathematical treatments of the NSe (She et al., 2017), confirm that, closely to the boundary, in the conditions above specified, the velocity in a turbulent field grows with a logarithmic profile. This translates, in our notation into:

$$\bar{u} = \frac{u_*}{k} \ln\left(\frac{z - z_d}{z_0}\right) \tag{2.19}$$

where

- $k \sim 0.41$ is the von Karman constant
- z is the height above the plane,
- z_d is the zero displacement level and
- z_0 is the surface roughness.

Consequently, it is:

$$C = \frac{u_*^2}{\bar{u}^2} = \frac{k^2}{\ln^2 \frac{z - z_d}{z_0}} \tag{2.20}$$

which is the well known formula for *aerodynamic conductance*. We do not enter for now in the estimation of C_E and C_H which, however, should be related to C and, in some peculiar cases, should be set equal to it.

2.2.1 Dalton's law of evaporation

Therefore our starting point is the acceptance of the Dalton equation:

$$ET = C_E \bar{u}(q_{z_0} - q_z) \tag{2.21}$$

which derives directly from (2.16) where:

- ET is evapotranspiration, [m s^{-1}]
- C_E is a dimensionless evaporation "conductance"
- $\bar{u}$ is the mean horizontal velocity (of a turbulent air field), [m s^{-1}]
- q_{z_0} is specific humidity at the evaporation source position (z_0, [m]) [non-dimensional]
- q_z is the specific humidity of air at quote z [non-dimensional]

Dalton's law expresses that a certain quantity of water vapor is taken from a region where its concentration is q_{z_0} to a region where it is q_z, if $q_{z_0} > q_z$. Also viceversa can happen if $q_{z_0} < q_z$. Nothing moves in case of equality of q_{z_0} and q_z. It does not express anything on the physical reasons that cause concentration having those values at the bottom and top boundaries of the control volume.
All the expression and, in particular, C_E is a suitable simplification of the turbulence that moves it all. In principle, it can be substituted by the direct resolution (by numerical integration) of the NSe or one of its simplification, like large eddy simulations (LES), (e.g. McDonough (2002)) and the appropriate transport equation. As reported in Bonan (2019) Figure 1.1 such law assume different notations according the disciplines. We have adopted here the convention to use dimensionless coefficients, which forces to explicit whole the known dependencies from dynamical variables. If the water mass flux of water is desired, the Dalton equation must be multiplied by the density of air ρ_a so that the formula, in that case is:

$$ET^{[m]} = \rho_a C_E \bar{u}(q_{z_0} - q_z) \tag{2.22}$$

[Kg m^{-2}] If the equivalent (latent) energy transported is desired, the mass formula must be further multiplied by the latent heat

of (water) vaporization, usually denoted as λ. Its value is $\lambda = 2264.705$ [KJ Kg^{-1}]. We will denote the latent heat flux as λET (λ multiplied by ET). Specific humidity is the mass of water divided by the mass of air (air gas plus water vapor). Therefore:

$$q := \frac{M_w}{M_a} = \frac{\rho_a}{\rho_a} \tag{2.23}$$

where:

- M_w and M_a are the water vapor mass and the air mass,
- ρ_w and ρ_a are the water vapor and air density.

the expression containing the densities allows for using the ideal gas law and relating the previous expression with those containing the partial pressures of water vapor.
Traditionally for water vapor, pressure is denoted as e and therefore the ideal gas law reads:

$$e = \rho_a R_v T \tag{2.24}$$

where:

- ρ_w is the density of water vapor,
- $R_v = 461$ [J $^\circ$ K^{-1} kg^{-1}] and

For dry air we can write:

$$p_d = \rho_d R_v T \tag{2.25}$$

where:

- ρ_d is the density of dry air, $R_v = 287$ [J $^\circ$K^{-1} kg^{-1}].

Therefore, it is

$$q \sim \epsilon \frac{e}{p_d} \tag{2.26}$$

where:

- $\epsilon := R_d / R_v \sim 0.622$.

This allows for writing the Dalton evaporation law in term of mass flow as:

$$ET^{[m]} = \underbrace{\rho_a C_E \bar{u} \frac{\epsilon}{p_d}}_{g_{tw}} (e^{\#}(z_0) - e(z)) \tag{2.27}$$

where $e^{\#}(z_0)$ is the vapor pressure at the evaporating surface, assumed at quote z_0. Evapotranspiration, is also expressed in terms of moles:

$$ET^{[m]} = E_{l,mol} M_{w,mol} \lambda_E \tag{2.28}$$

Where:

- $M_{w,mol}$ is the molar mass of water [kg mol^{-1}];
- λ_E is the latent heat of vaporisation [J kg^{-1}];
- $E_{l,mol}$ was computed in molar units [(mol m^{-2} s^{-1})] as a function of the concentration of water vapour at the emitting surface (C_{wl}, [mol m^{-3}]) and in the free air (C_{wa}, [mol m^{-3}]) (Frank P. Incropera, David P. DeWitt, Theodore L. Bergman, 2002).

In this case the Dalton laws takes the form:

$$E_{l,mol} = g_{tw}(C_{wl} - C_{wa}) \tag{2.29}$$

g_{tw} is the total conductance for water vapor [ms^{-1}].

2.2.2 Convective transport of thermal energy (sensible heat)

As we can derive from section 2, transport of thermal energy (or sensible heat, as it is known), follows a law similar to Dalton law:

$$H = \underbrace{\rho_a C c_p \bar{u}}_{S_T} (T_{z_0} - T_z) \tag{2.30}$$

where:

- H is the latent heat flux per unit area [W m^{-2}]:
- ρ_a is the air density [kg m^{-3}];
- C is the dimensionless Stanton number [-];
- c_p is the specific thermal capacity or air, [J Kg^{-1} °K^{-1}];
- $\bar{u}$ is the mean horizontal velocity [m s^{-1}];
- T is temperature [K];
- S_T is the Stanton (Frank P. Incropera, David P. DeWitt, Theodore L. Bergman, 2002).

Inspection of the formula makes clear that it is homogeneous dimensions with λET.

2.3 Derivation of the energy balance

2.3.1 The energy budget

A third equation that contains evapotranspiration is the energy budget. It can be written, for a unit area, as:

$$\frac{dU}{dt} = \overbrace{\underbrace{P+E_A}_{advection} + \underbrace{R_s+R_l}_{radiation}}^{S_{rc}} - \overbrace{\underbrace{aH-b\lambda ET^{(m)}}_{convection} - \underbrace{G}_{conduction} - \underbrace{E_V}_{chemical\,energy}}^{S_{nk}} \tag{2.31}$$

where:

- U is the internal energy of the element considered [J m^{-2}]
- R_s is the net shortwave radiation [W m^{-2}]
- R_l is the net longwave radiation [W m^{-2}]

- a is the ratio between the heating/cooling surface and its projection (usually equal to 1 or 2)
- H is the thermal energy transport
- b is the ratio between the evaporating surface and its projection on a horizontal plane (equal to 1 or 2, depending on the surface)
- ET is evapotranspiration
- G is the ground heat flux [W m^{-2}]
- P is the incoming energy due to precipitation [W m^{-2}]
- E_A is the advected energy into the control volume [W m^{-2}]
- E_V is the energy stored in chemical bounds (due, for instance, to photosynthesis that produces carbohydrates) inside the control volume [W m^{-2}]
- S_{rc} are positive if source of energy
- S_{nk} are positive if sink of energy

We neglect in the budget the action of external force fields, like gravity, which can be added when required. As written, the equation is of general validity, but usually P, E_A and E_V are neglected. In the simplest approaches also dU/dt is neglected, assuming either that the system is stationary or that its dynamics can be considered as a sequence of stationary states, in equilibrium with the energy forcings. For leaves this assumption is supported by various experiment. In particular Gates (1968) reports that leaves temperature adapts to the forcing in, at most, some minutes. Therefore, at least for vegetation canopies, the assumption can be considered valid. For sure if these equations are going to be used in modelling at hourly time scale, the adaptation can be

considered instantaneous and system considered to move from one stationary states to another abruptly. The same assumption could not be valid for soil, whose thermal capacity is not negligible. Therefore, the form of the equation we deal with here is:

$$R_s + R_{ll} = aH + b\lambda ET + S_{nk} \tag{2.32}$$

where we have taken away the sources of energy and left all the sinks in aggregate form.

2.3.2 The Clausius-Clapeyron equation and its modifications

As product of the previous analysis, we have then three equations that need to be solved simultaneously:

$$ET^{(m)} = \rho_a C_E \bar{u}(q^{\#}(z_0) - q_z) = \frac{\epsilon}{p_d}\rho_a C_E \bar{u}(e^{\#}(z_0) - e(z)) \tag{2.27}$$

$$H = \rho_a C c_p \bar{u}(T_{z_0} - T_z) \tag{2.30}$$

$$R_s + R_{ll} = aH + b\lambda ET^{(m)} + S_{nk} \tag{2.32}$$

The unknown of these equations are, however, four: (1) ET, (2) $q_\Delta := (q^{\#}(z_0) - q_z)$, (3) H and (4) $T_\Delta := (T_{z_0} - T_z)$, if R_{ll} is assumed measured (in this case we are dealing with the so called radiatively uncoupled-energy budget). With three equations and four unknowns, we cannot get the solutions, and, therefore, we need to find out another equation. Under the hypothesis that the specific humidity at the evaporating surface is the saturation one, this equation, can be provided by the Clausius-Clapeyron equation (CCe). This is, often forgotten, a strong assumption, that requires, in particular that the system is not water limited.

It relates saturation vapor pressure to temperature and reads, for the case of ideal gases:

$$e^*(T) = e^*(T_{ref}) \exp^{-\frac{\lambda}{R}\left(\frac{1}{T}-\frac{1}{T_{ref}}\right)} \tag{2.33}$$

where $e^*(T_{ref})$ and T_{ref} are respectively the saturation water vapor pressure at T_{ref} and T_{ref} is a reference temperature (in Kelvin). The derivation of (2.33) is of public domain and can be found, for instance on Wikipedia (search for Clausius-Clapeyron relation). As we said, the form of Dalton equation that derives from the use of saturated specific humidity in it is an educated guess which could not work in all occasions. Certainly it works for a water surface (with corrections for salinity, if the case applies) but could not work for vegetation or soil under scarce water supply. For water not in free conditions, e.g. capillary water and water with solutes, the vapor tension can be less than e^*. A complete treatment of the phenomena (for leaves) is made in Vesala et al. (2017). But, in the following sections, we ignore this fact. The actual $e^{\#}$, in substitution of e^* can be estimated (as in the paper by Vesala et al. (2017):

$$e\# = e^* \exp\left(\frac{\psi V_{H_2O}}{RT}\right) \tag{2.34}$$

where:

- ψ is the water potential in leaves (negative) [Pa];
- V_{H_2O} is the molar volume of water (18×10^{-6} m^3 mol^{-1});
- R is the universal gas constant, equal to 8.31446261815324 [J K^{-1} mol^{-1}];
- T is the temperature in Kelvin degrees.

As Vesala et al. (2017) reports, this factor can cause up to 15% reduction of evaporation from leaves, due to the high tension under which water can be present in plants. In soil its contribution

is instead usually negligible. This expression can be combined with the expression of the Clausius-Clapeyron formula to obtain the value also in dependence from temperature.
The set of equations (2.27),(2.30),(2.32) and(2.33) is now well formed. However, it is a non linear system (because CCe is a non-linear relation) and a closed solution cannot be found for it.

2.3.3 The Penman linearization

To get a linear system instead of the previous non linear one, Penman (1948) had the idea to eliminate the specific saturation humidity as a function of surface temperature by using its Taylor's expansion, around air temperature (which is actually the same that linearizing the CCe):

$$q^*(z_0) \approx q^*(T_{z_0}) \tag{2.35}$$

$$q^*(T_{z_0}) = q(T_z) + \frac{dq^*}{dT}|_{T=T_z}(T_{z_0} - T_z) + O((T_{z_0} - T_z)^2) \tag{2.36}$$

where:

$$\frac{dq^*}{dT} = \frac{\epsilon}{p_d}\Delta_{e_T} \tag{2.37}$$

and Δ_{e_T} is the derivative of the Clausius-Clapeyron equation with respect to temperature.

$$\Delta_{e_T} = \frac{de^*}{dT} = \frac{25083}{(T+273.3)^2} e^{\frac{17.3T}{T+273.3}} \tag{2.38}$$

where:

- T is the temperature [°C],
- e is the pressure [mb].

Accordingly to previous equations we also define:

$$e^*(z_0) := e^*(z) + \Delta_{e_T}(T_{z_0} - T_z) \tag{2.39}$$

and

$$e^*(z_0) - e(z) = \underbrace{e^*(z) - e(z)}_{\delta e(z)} + \Delta_{e_T}(T_{z_0} - T_z) \tag{2.40}$$

where:

- $\delta e(z)$ is called evaporation deficit.

Finally (2.39) can be rewritten as:

$$e_\Delta = \delta e(z) + \Delta_{e_T} T_\Delta \tag{2.41}$$

where $e_\Delta := e^*(z_0) - e(z)$. Other authors, used quadratic or ore complex approximation of the CCe (still obtaining a closed form solution (McColl, 2020).

2.3.4 Solving the Penman-Monteith System step by step

We call Penman-Monteith system (PMs), the system of equations (2.27), (2.30), (2.32) and (2.41). Monteith (1985) in fact, is the one who assumed first that drag and Dalton coefficients could be different. PMS is linear and can be solved by substitution.
First insert (2.27) into (2.32), obtaining:

$$R_s = a_{sH} H + a_{sE} \lambda \rho_a C_{Da} \frac{\epsilon}{p} \bar{u} e_\Delta + R_{ll} + S_{nk} \tag{2.42}$$

Equation (2.30) can be then inserted into (2.42), obtaining:

$$R_s = a_{sH} \rho_a C_{Dr} c_p \bar{u} T_\Delta + a_{sE} \lambda \rho_a C_{Da} \frac{\epsilon}{p} \bar{u} e_\Delta + R_{ll} + S_{nk} \tag{2.43}$$

Substituting (2.41) into the previous equation, we then obtain an expression where the only variable is T_Δ:

$$R_s = a_{sH} \rho_a C_{Dr} c_p \bar{u} T_\Delta + a_{sE} \lambda \rho_a C_{Da} \frac{\epsilon}{p} \bar{u} (\delta e(z) + \Delta_{e_T} T_\Delta) + R_{ll} + S_{nk} \tag{2.44}$$

Collecting T_Δ, we obtain:

$$R_s - R_{ll} - S_{nk} - a_{sH}\lambda\rho_a C_{Da}\frac{\epsilon}{p}\bar{u}\delta e(z) = T_\Delta(a_{sH}\rho_A C_{Dr} c_p \bar{u} + a_{sH}\lambda\rho_a C_{Da}\frac{\epsilon}{p}\bar{u}\Delta_{e_T}) \quad (2.45)$$

or:

$$T_\Delta = \frac{R_s - R_{ll} - S_{nk} - a_{sE}\lambda\rho_a C_{Da}\frac{\epsilon}{p}\bar{u}\delta e(z)}{a_{sH}\rho_a C_{Dr} c_p \bar{u} + a_{sE}\lambda\rho_a C_{Da}\frac{\epsilon}{p}\bar{u}\Delta_{e_T}} \quad (2.46)$$

Collecting $\rho_a\bar{u}$ at the denominator results:

$$T_\Delta = \frac{R_s - R_{ll} - S_{nk}}{\rho_a\bar{u}\left(a_{sH}C_{Dr}c_p + a_{sE}\lambda C_{Da}\frac{\epsilon}{p}\Delta_{e_T}\right)} - \frac{a_{sH}\lambda C_{Da}\frac{\epsilon}{p}\delta e(z)}{aCc_p + b\lambda C_{Da}\frac{\epsilon}{p}\Delta_{e_T}} \quad (2.47)$$

Once defined the psychrometric "constant" as:

$$\gamma := \frac{c_p p}{\epsilon\lambda} \quad (2.48)$$

equation (2.47) becomes:

$$T_\Delta = \frac{\gamma}{a_{sH}C_{Dr}\gamma + a_{sE}C_{Da}\Delta}\frac{R_s - R_{ll} - S_{nk}}{\rho_a\bar{u}c_p} - \frac{C_{Da}}{a_{sH}C_{Dr}\gamma + a_{sE}C_{Da}\Delta_{e_T}}\delta e(z) \quad (2.49)$$

A this point the value of T_Δ can be substituted back into the other equations. Using (2.41) first, we obtain:

$$e_\Delta = \delta e(z) + \Delta_{e_T}\left[\frac{\gamma}{a_{sH}C_{Dr}\gamma + a_{sE}C_{Da}\Delta_{e_T}}\frac{R_s - R_{ll} - S_{nk}}{\rho_a\bar{u}c_p} - \frac{C_{Da}}{a_{sH}C_{Dr}\gamma + a_{sE}C_{Da}\Delta_{e_T}}\delta e(z)\right] \quad (2.50)$$

which results in:

$$e_\Delta = \frac{\gamma\Delta_{e_T}}{a_{sH}C_{Dr}\gamma + a_{sH}C_{Da}\Delta_{e_T}}\frac{R_s - R_{ll} - S_{nk}}{\rho_a\bar{u}c_p} + \frac{a_{sH}C_{Dr}\gamma + (a_{sE}-1)C_{Da}\Delta_{e_T}}{a_{sH}C_{Dr}\gamma + a_{sH}C_{Da}\Delta_{e_T}}\delta e(z) \quad (2.51)$$

For what regards the enthalpy transport in (2.30):

$$H = \frac{C_{Dr}\gamma}{a_{sH}C_{Dr}\gamma + a_{sE}C_{Da}\Delta_{e_T}}(R_s - R_{ll} - S_{nk}) - \frac{\rho_a c_p \bar{u} C_{Dr} C_{Da}}{a_{sH}C_{Dr}\gamma + a_{sE}C_{Da}\Delta_{e_T}}\delta e(z) \quad (2.52)$$

Finally for ET substitution results in:

$$ET = \rho_a C_{Da}\frac{\epsilon}{p}\bar{u}\left[\frac{\gamma\Delta_{e_T}}{a_{sE}C_{Dr}\gamma + a_{sE}C_{Da}\Delta_{e_T}}\frac{R_s - R_{ll} - S_{nk}}{\rho_a \bar{u} c_p} + \frac{a_{sH}C_{Dr}\gamma + (a_{sE}-1)C_{Da}\Delta_{e_T}}{a_{sH}C_{Dr}\gamma + a_{sE}C_{Da}\Delta_{e_T})}\delta e(z)\right] \quad (2.53)$$

from which, by multiplying for λ and using the definition of the psychometric constant, it is obtained:

$$\lambda ET = \frac{C_{Da}\Delta_{e_T}}{C_{Dr}\gamma + a_{sE}C_{Da}\Delta_{e_T}}(R_s - R_{ll} - S_{nk}) + \frac{\rho_a \bar{u} c_p a_{sE} C_{Dr} C_{Da} + (a_{sE}-1)C_{Da}^2\Delta_{e_T}/\gamma}{a_{sH}C_{Dr}\gamma + a_{sE}C_{Da}\Delta_{e_T}}\delta e(z) \quad (2.54)$$

Equations (2.49), (2.51), 2.52 and (2.54) are an explicit solutions of the Penman-Monteith system, as obtained by Schymanski and Or (2017), and we call them PMSO solutions.
There are a few remarks to be done on PMSO (excluding those implied by the approximations they contain).

- The first is that those equation are valid for any time interval (not specifically for hourly, daily or monthly intervals), as soon as the forcings are given with the appropriate time step.
- The second is that, and the merit of this has to be given to Schymanski and Or (2017), that is a system resolution, which gives, not only ET, but also H, e_Δ, and T_Δ.

If, for a given problem, we have $e(z)$ and T_z as Dirichlet type of boundary conditions, then we immediately have $e^*(z)$ (which

is not a surprise when understood that CCe was used) and T_{z_0} as a consequence. The solutions obtained are the so called radiatively uncoupled solutions. In fact it was assumed R_{ll} to be independent from the evaporating surface temperature, which is not actually the case. The coupled system implies further linearizations to obtain closed form solutions of the PMs, which we will describe in next sections.

2.3.5 Different transpiring surfaces: the case of leaves and soils

We now specialise the budget for a single leaf. The problem with leaves, as brought to evidence by Schymanski and Or (2017), is that leaves have 2 faces and, therefore they exchange heat from the two sides, i.e., in the previous formulas, $a_{sH} = 2$. Stomata are instead can be either on the bottom side of the leaves ($a_{sE} = 1$), which is the most diffuse case and it is called hypostomatous case, and on both the sides of a leave (amphistomatous, $a_{sE} = 2$). Besides, for leaves, conduction of heat can be neglected and $S_{nk} = 0$. So, for the hypostomatous case, the PM solutions read:

$$T_\Delta = \frac{\gamma}{2C_{Dr}\gamma + C_{Da}\Delta_{e_T}} \frac{R_s - R_{ll}}{\rho_a \bar{u} c_p} - \frac{C_{Da}}{2C_{Dr}\gamma + C_{Da}\Delta_{e_T}} \delta e(z) \quad (2.55)$$

$$e_\Delta = \frac{\gamma \Delta_{e_T}}{2C_{Dr}\gamma + C_{Da}\Delta_{e_T}} \frac{R_s - R_{ll}}{\rho_a \bar{u} c_p} + \frac{2C_{Dr}\gamma}{2C_{Dr}\gamma + C_{Da}\Delta_{e_T}} \delta e(z) \quad (2.56)$$

$$H = \frac{C_{Dr}\gamma}{2\Delta_{e_T}\gamma + C_{Da}\Delta_{e_T}} (R_s - R_{ll}) - \frac{\rho_a c_p \bar{u} C_{Dr} C_{Da}}{2C_{Dr}\gamma + C_{Da}\Delta_{e_T}} \delta e(z) \quad (2.57)$$

$$\lambda ET = \frac{C_{Da}\Delta_{e_T}}{2C_{Dr}\gamma + C_{Da}\Delta_{e_T}} (R_s - R_{ll}) + \frac{2\rho_a \bar{u} c_p C_{Dr} C_{Da}}{2C\gamma + C_{Da}\Delta_{e_T}} \delta e(z) \quad (2.58)$$

The case of amphystomatous leaves has instead both $a_{sH} = 2$ and $a_{sE} = 2$ and the related formulas are easily obtainable. In the case of soil, a trivial application of the Schymanski and Or equations is obtained with both $a_{sH} = 1$ and $a_{sE} = 1$. This is actually used in

literature but it is known not to work well, unless corrections, in form of limitation of fluxes in dependence on water soil content, is used. We do not start this debate here but we will try to dig into the topic later on.

2.3.6 The radiatively coupled system

Unfortunately, even if the previous equations (in some wrong form) were applied for more that fifty years, the longwave radiation, R_{ll} is coupled to the evaporating surface temperature. In fact, it can be usually decomposed into two main contribution:

$$R_{ll} = R_{ll}\uparrow - R_{ll}\downarrow \tag{2.59}$$

where:

- $R_{ll}\uparrow$ is the upwelling longwave radiation outgoing from the surface and
- $R_{ll}\downarrow$ is the downwelling longwave radiation, coming mainly from the sky and clouds

For the parameterization of the latter, please see for instance Formetta et al. (2016). The first simply depends on the evaporating surface temperature according to the Stefan-Boltzmann law:

$$R_{ll}\uparrow = \epsilon\sigma T_{z_0}^4 \tag{2.60}$$

where:

- $\epsilon \approx 1$ is the surface emissivity (for the most of surfaces),
- σ is the Stefan-Boltzman constant [$\sigma = 5.670374419 \times 10^{-8}$ W m^{-2}K^{-4}]

We can then assume that $R_l \downarrow$ is given, while $R_l \uparrow$ must be obtained by the resolution of the system. Unfortunately, the energy budget becomes a non linear equation in T_{z_0}. In fact, it is:

$$R_s = a_{sH}\rho_a C_{Dr} c_p \bar{u}(T_{z_0} - T_z) + a_{sE}\lambda\rho_a C_{Da}\frac{\epsilon}{p}\bar{u}(\delta e(z) + \Delta(T_{z_0} - T_z)) + \epsilon\sigma T_{z_0}^4 + S_{nk} \quad (2.61)$$

This is a polynomial system of the type:

$$aT_{z_0}^4 + bT + c = 0 \quad (2.62)$$

and the four exact solutions can be found (with only one of physical significance).
Alternatively it can be implemented an iterative solution of the system, assuming for instance $T^4(z_0) = T_0^3 T_{z_0}$ where:

- T_0 is some approximate value of T (for instance the one given by the solution at the last past time interval).

Notably, because here, we have to possibly resort to iterative numerics, the CCe can be used directly in the system, instead of using one of its approximations.

2.3.7 Including the Monin-Obukhov Similarity Theory (MOST)

All the previous derivation is affected by the treatment of turbulence according to the mixing length theory especially for the Dalton's law and the thermal energy flux. The obvious extension of Prandtl's theory is the application of the MOST (Foken, 2006), which brings the following corrections to the drag coefficient (e.g. Yang et al. 2001, Banerjee et al. 2017; Bonan, 2019, Section 6.6):

$$C = k^2\bar{u}(z)\left[\ln\left(\frac{z-z_d}{z_{0m}}\right) - \psi_m(\zeta_d,\zeta_{0m})\right]^{-1}\left[\left(\frac{z-z_d}{z_{0*}}\right) - \psi_*(\zeta_d,\zeta_{0*})\right]^{-1} \quad (2.63)$$

where:

- z_{0m} is the roughness length for momentum transfer;
- z_{0*} is the roughness length for the specific transport (i.e. thermal energy or enthalpy);
- ψ_m is an integral stability correction function for momentum;
- ψ_* is an integral stability correction function for the specific transport $*$;
- $\zeta_d := (z - z_d)/L$;
- $\zeta_{0m} := z_{0m}/L$ is the roughness length for momentum;
- $\zeta_{0*} := z_{0h}/L$ is the roughness length for the specific transport;
- $L = -u_*^3 * /(kg\overline{w'*'})$ is the Obukhov length for the specific transport;
- $g = 9.81$ [m s^{-2}] is the gravitational acceleration;
- $*$ Is the transported quantity.

Banerjee et al. (2017) suggests also that a correction must be given for obtaining the conductance for thermal energy transfer and latent heat transfer such that:

$$C_E = \frac{C_{Dr}}{P_E} \tag{2.64}$$

and

$$C_H = \frac{C_{Dr}}{P_H} \tag{2.65}$$

where P_E is the turbulent Prandtl number for latent heat transport and P_H is the Prandtl number for sensible heat:

- $P_E := \frac{K_m}{K_E}$;

- $P_H := \frac{K_m}{K_H}$;
- K_m is the momentum eddy diffusivity;
- K_E is the latent heat eddy diffusivity;
- K_H is the sensible heat eddy diffusivity.

The so called stability parameters ζ_{0*} can be obtained as follows:

- $\zeta_{0m} = \frac{z_{0m}}{L}$
- $\zeta_{0H} = \frac{z_{0H}}{L}$
- $\zeta_{0E} = \frac{z_{0E}}{L}$

Negative ζ indicates unstable stratification; positive values indicate stable stratification.

Finally, the integral stability correction functions ψ can be obtained as in Liu et al. (2007) such that:

$$\psi_m(\zeta,\zeta_{0m}) = 2\ln\left(\frac{1+x}{1+x_0}\right) + \ln\left(\frac{1+x^2}{1+x_0^2}\right) - 2\tan^{-1} z + 2\tan^{-1} x_0 \tag{2.66}$$

where:

- $x := (1-\gamma_m\zeta)^{1/4}$
- $x_0 := (1-\gamma_m\zeta_{0m})^{1/4}$

$$\psi_H(\zeta,\zeta_{0h}) = 2\ln\left(\frac{1+y}{1+y_0}\right) \tag{2.67}$$

where:

- $y = (1-\gamma_H\zeta)^{1/2}$
- $y_0 = (1-\gamma_H\zeta_{0H})^{1/2}$

The γs are parameters whose values differ in literature. Paulson (1970) suggests $\gamma_H = \gamma_m = 16$. For more details, please refer to Banerjee et al. (2017).

2.4 Introducing the water budget

The water budget is missing in the previous sections after the introduction of the Clausius-Clapeyron equation as key for getting solutions. It reads, for a generic control volume:

$$\frac{dS}{dt} = P - ET - R \tag{2.68}$$

where:

- S [kg] or [m] is the water content
- P [kg] or [m] is (any type of) precipitation
- ET is evapotranspiration [kg] or [m]
- R represents all the runoffs [kg] or [m]

Either the mass or the length or the mass units must be used consistently. Given for granted that this equation has to be satisfied simultaneously with the other four that we dealt with in the previous sections, it remains unclear how it interacts with the others. The hypothesis to use the saturated water vapor and the Clausius-Clapeyron formula, in fact, decouples the mass budget from the other equations.

It is evident that mass budget poses a limiting behavior, i.e. ET cannot be greater than $P - \frac{dS}{dt}$ and in literature, this limitation is accomplished by introducing a stress factor, f such that:

$$AET = f\,ET \tag{2.69}$$

where:

- f is a dimensionless stress factor
- AET is the actual evapotranspiration

The stress factor is usually function of the relative water content, the fraction of the existing water content over the maximum water content possible in the control volume. Another approach, popularized by Monteith (1985) is that missing water acts like an additional resistance, to add to the aerodynamic ones, given by $1/C_{Dr}$, $1/C_E$ and $1/C_H$. In this case the derivation made in the previous section remains valid after the appropriate substitution of C_E with the appropriate conductances.
For example, assuming soil produces a resistance, it will be:

$$\hat{C} = \frac{1}{1/C_E + 1/C_s} \tag{2.70}$$

where

- $\hat{C}$ is the new total conductance
- C_s is the soil conductance

The analogy with the electric circuitry is evident. In the case of vegetation, the stomatal (g_{sw}) and the boundary layer conductance (g_{bw}) are those that enters in a similar formula:

$$g_{tw} = \frac{1}{\frac{1}{g_{sw}} + \frac{1}{g_b w}} \tag{2.71}$$

As the analysis performed in this manuscript supports, we suggest that a more proper way to cope with the phenomenon of water stress is to give a proper expression of $e^{\#}(z_0)$ in Eq. 2.27, substituting an appropriate value for it which differ from the CCe derived $e^{*}(z_0)$.
Another, more subtle maybe, aspect is that, when we deal with evaporating surfaces like the leaf or soil, because evaporation ultimately is emitted from stomata or pores, the effective evaporating surface can be less than the total surface, a fact enlightened by Shahraeeni et al. (2012). We propose therefore below a more detailed analysis of these aspects, starting from soils in the next section and for vegetation in the next chapter.

2.4.1 The case of soils

Lehmann et al. (2008) provides a comprehensive analysis of the dynamics of evaporation from soil. At the small scales, soil is a fractal random medium: a set of voids of different diameter, that, as a first approximation, can be considered, as a 3D bundle of tubes of varying radius with a certain distribution which varies with soils texture and structure. When we have stratified soil where the mean properties and the statistics can vary abruptly from one horizon to the other, still each horizon is described as a random porous medium.
As all know, water is retained with different energies inside these pores, according to the radius and the Young-Laplace law (e.g., Lu and Godt, chapter 3)

$$\psi = -\frac{2\gamma}{\rho_w g r} \tag{2.72}$$

where ψ [m] is the pressure head in the vadose soil, $\gamma = 0.0728$ [J m^2 at 20 °C] is the surface tension and r [m] the pore radius.
Thus, when soil is filled with water and water starts to evaporate, large pores are emptied first because their suction is smaller than that of smaller pores. The evaporating demand is uniform and withdraw water from any place, but, at the same time, water is supplied from the largest pores to the smaller ones when they are emptied. Experiments and measures (e.g. Or et al., 2013) show that evaporation is working as $e^{\#} = e^{*}$ even in non saturated conditions (stage I evaporation) up to a threshold condition when it start to decrease fast to zero. The latter is called stage II, evaporation.

2.4.2 Stage I evaporation from soil

According to Lehmann et al. (2008), stage I evaporation continues until water capillary flow can arrive at the soil surface and

falls when the water supply to the surface breaks. During stage I evaporation, the liquid phase is connected, in phase II is disconnected, at least at the surface, and evaporation is supported by water flow (as opposed by water flow). We are concerned here with the duration of stage I, under which we can think that the vapor phase at the surface is closely at the saturation content.
According to Lehmann et al. (2008), we can recognize a bulk water phase, below a certain level from the surface, i.e a water table, which feeds an upward water flow until this depth arrives to a critical value, L_C. Below this level, continuity of the water phase cannot be sustained anymore. To estimate this L_C capillary forces, gravity and viscous losses must be in equilibrium as Lehmann et al. (2008) accurately derives. L_C depends on soil characteristics and it is:

$$L_C = \frac{L_G}{1 + \frac{ET(z_0)}{k(\theta)}} \tag{2.73}$$

where L_G can be expressed as a function of soil parameters. i.e., choosing for the soil characteristics the van Genuchten-Mualem curves:

$$L_G = \frac{1}{\alpha(n-1)} \left(\frac{2n-1}{n}\right)^{(2n-1)/n} \left(\frac{n-1}{n}\right)^{(1-n)/n} \tag{2.74}$$

The variables present above are:

- α [m^{-1}]is the van Genuchten (vG) α parameter, usually associated with the air entry point
- n [-] is another vG parameter
- $ET(z_0)$ is the evaporation demand at the surface
- $K(\theta)$ [m s−1] is the vG-Mualem hydraulic conductivity
- θ [-] is the dimensionless volumetric water conductivity

To put forward some numbers, in sandy soil, this length results of the order of 5 to 10 cm.
Assuming to have a completely saturated soil at the beginning, thus evaporation works as we have vapor saturation at soil surface until the water table depth arrive to L_C.
To control how this happens, we can use Richards equation or, if we adopt a simpler reservoir model, we can follow the water budget:

$$\frac{d(\theta_s - \theta_r)\xi}{dt} = +ET + R - P \tag{2.75}$$

where:

- θ_s is the porosity [-];
- θ_r is the residual water content;
- ξ [m] is the water deficit $\xi = S_{max-S}$ where S_{max} is the maximum storage available in the control volume;
- ET is evaporation [m s^{-1}];
- R contains all the types of runoff [m s^{-1}];
- P is the liquid precipitation [m s^{-1}].

when $\xi > L_C$ stage I evaporation ends. The resilience of the stage I evaporation reminds that water is a cohesive medium, which can resist to large tensions, as shown in plants hydromechanics (e.g. Choat et al., 2005). Soils do not have the mechanism that vegetation has to prevent embolism.

2.4.3 Stage II evaporation from soil

Stage II Et is controlled by the fractal nature of the evaporating medium. As anticipated above, according to Lehmann et al. (2008), a dynamic capillary fringe whose extension to the soil surface is responsible for the evaporation rates. When the capillary

fringe lowers and detaches from the surface, evaporation stage II starts. This situation is well represented in Figure 1 of Shokri and Or (2011) and seems to be appropriately described by the percolation theory developed by Wilkinson (1986) and Sapoval et al. (1985).
Equation (3) from Shokri and Or (2011) can be used to establish the evaporative flux. It reads:

$$ET_0 = D\frac{dq}{dz} \sim \frac{\theta_a^{2.5}}{\theta_s} D_{atm} \frac{q^* - q(z_0)}{\xi} \tag{2.76}$$

with $\xi > L_C$ defined above and:

- ET_0 [m s^{-1}] evaporation at the soil surface (technically at the end of the viscous layer);
- D is the water vapor diffusion in porous media;
- θ_a is the vapour dimensionless (volumetric) content;
- D_{atm} is the water vapor diffusion coefficient in free air $\sim 2.5 \cdot 10^{-5}$ [m^2 s^{-1}] ;
- q^* is the specific humidity at saturation ($27 \cdot 10^{-3}[kgm^{-3}]$) [-];
- q is the actual specific humidity at the soil surface [-].

In the following, we will use the finite difference form of the above equation, but approximate solution for the diffusion process at constant coefficient are also available and worth to be explored (e.g. Nobel et al., 1999).

2.4.4 A new set of equations for the evaporation processes in soil

The above indications refers to lab experiments in controlled situations and we try now to give indication of how to use them

in daily modelling of soil evaporation.
The first suggestion is that we can continue to use the PMSO solutions until the critical depth is obtained. This critical depth can be computed from (2.74) and its overcoming monitored by solving the deficit budget (2.75).
After the stage II evaporation starts, we can possibly subdivide the evaporation domain into two. One going from the depth ξ to the end of the viscous atmospheric layer. And a second one form the top of the viscous layer to the open atmosphere.
Dalton equation should remain valid (as soon as we consider the Prandtl mixing layer theory valid) but the lower level of specific humidity, $q^{\#}$ should be the one made available by the molecular diffusion at the domain from the dry domain.
In this domain, we can consider, as suggested by the PMSO treatment in the previous section and having made the appropriate changes, the energy budget, the water mass budget, the molecular diffusion of vapor, the Fourier law for heat transfer, and, if reasonably, the sensible heat molecular transport. The energy budget reads:

$$c_p \frac{dT}{dt} = R_n - \lambda E T_0 - G - H + \rho_w \lambda P \tag{2.77}$$

where:

- c_p is the soil bulk specific thermal capacity (depending on water content, i.e. on ξ) [J/K];
- T is temperature [K];
- R_n is the net radiation [W/m^2];
- G the heat transfer by conduction [W/m^2];
- H the heat transfer by molecular diffusion [W/m^2];
- $\rho_w \lambda P$ the energy content of precipitations [W/m^2].

The water budget is instead:

$$\frac{d(\theta_s - \theta_r)\xi}{dt} = +ET_0 + R - P \tag{2.75}$$

whose quantities were defined previously and where:

$$ET_0 = D\frac{dq}{dz} \sim \frac{\theta_a^{2.5}}{\theta_s} D_{atm} \frac{q^* - q(z_0)}{\xi} \tag{2.76}$$

where we can use CCe:

$$q^*(T) = \frac{\epsilon}{p} e^*(T) = \frac{\epsilon}{p} e^*(T_{ref}) \exp^{-\frac{\lambda}{R}\left(\frac{1}{T} - \frac{1}{T_{ref}}\right)} \tag{2.33}$$

for determining the value of $q*$. In case, equation (2.33) can be corrected by Kelvin's effect as in proposed by Vesala et al. (2017). We can decide, at present to neglect H and, finally,

$$G = -\lambda_T (T(z_0) - T(\xi)) \tag{2.78}$$

The unknowns of this systems are ξ, $q(z_0)$, $T(z_0) - T(\xi)$, ET_0, G and their number is matched by the number of equations available which now however, contain the water budget.

2.4.5 Some simplification to show that the system above is actually solvable

In this section, we simplify the non linear problem posed by the above equation to actually show that we can arrive to a solution, a fact that could not be so evident to the reader. To sketch this, we do some simplifications and assume that:

- c_p and λ_T are independent from ξ
- $\rho_w \lambda P$ can be neglected
- the Penman approximation of q^* can be used

- the system is radiatively decoupled

The Penman ansatz (2.36) can then be used inside the energy budget, discretized at this point, as a finite difference:

$$c_p \frac{T_{z_0}^n - T_{z_0}^{n-1}}{(\delta t)} = R_n - \frac{\lambda D}{\xi^n} \Delta (T_{z_0} - T(\xi)) - \lambda_T (T_{z_0} - T(\xi)) \quad (2.79)$$

where:

- D is the water vapor diffusion in porous media
- ξ^n is the deficit at time interval $t = n$
- δt is the discretized time interval

The above equation (2.79) would be an equation containing the only independent variable $(T_{z_0} - T(\xi))$ if ξ was not there. ξ, in turn, is a product of the water budget (2.75), which ca be rewritten also as a finite difference:

$$(\theta_s - \theta_r) \frac{\xi^n - \xi^{n-1}}{\delta t} = ET_0 + R_n - P \quad (2.80)$$

or:

$$(\theta_s - \theta_r)\xi^n = (\theta_s - \theta_r)\xi^{n-1} + (\delta t)\left(\frac{\lambda D \Delta}{\xi^n} (T_{z_0} - T(\xi)) + R_n - P \right) \quad (2.81)$$

where the expression for ET_0 has been already substituted in producing a quadratic equation in ξ. We can now observe that (2.79) and (2.81) are a non linear system in ξ and $(T_{z_0} - T(\xi))$ which can be solved iteratively. Once (2.81) is solved for ξ as a function of $(T_{z_0} - T(\xi))$, the result can be introduced in (2.79) to obtain T_{z_0}, substitutions then give the solution for ξ, ET_0, G and $q^{\#}$.

These solutions provide what happens in the viscous transport zone, inside the soil and up to the viscous layer). What happens instead in the overlying turbulent layer ?

2.4.6 Vapor, momentum and energy budget in the turbulent layer

Obviously in the turbulent layer are still valid Dalton law and the turbulent exchange equation:

$$ET^{(m)} = \underbrace{\rho_a C_E \bar{u}}_{\bar{g}_{tw}}(q^{\#}(z_0) - q_z) \tag{2.27}$$

$$H = \rho_a C c_p \bar{u}(T_{z_0} - T_z) \tag{2.30}$$

Now, however, temperature at soil level, T_{z_0} can be given by the results of the previous section and, upon measuring T_z, H is determined. The same argument apply to the Dalton law: $q^{\#}$ is given as well as q_z could be measured. Otherwise, we can assume that one of q_z and T_z are unknown, and therefore use the energy budget to determine it. Following the classic use of the stationary energy budget, it reads, for the turbulent control volume:

$$0 = R_l \uparrow - ET - H = \epsilon\sigma T_{z_0}^4 - \lambda C_E(q^{\#}(z_0) - q_z) - C_H(T_{z_0} - T_z) \tag{2.82}$$

assuming that:

- shortwave radiation does not interacts with air;
- the air thermal capacity is negligible.

Using (2.82), as promised, either q_z or T_z can be estimated instead than measured. However, if we measure both, we can consider to solve (2.82) simultaneously together with the soil vapor budget equations to obtain $T(\xi)$, the temperature at a certain depth. Realistically, we can also think to introduce a calibration parameter where appropriate in the soil budget to cope with simplifications made and use both measurements for calibration of such a parameter, when both q_z and T_z are available. In any case, the previous estimations show that there is a flux out of the viscous layer ET_0 and a different flux out of the turbulent

layer, ET whose difference gives the water vapor budget in the turbulent layer as:

$$\frac{dV}{dt} = ET_0 - ET + v_{adv} \tag{2.83}$$

where:

- $v_a dv$ is the net advected vapor [m s^{-1}].

2.5 A disclaimer

Of the theory presented in this section, MOST was not implemented yet in the Prospero code discussed in the next sections. Prospero does not deploys the solutions of the radiatively uncoupled problem too, but solves directly the radiatively coupled one. Also the soil evaporation theory was formulated, but not implemented because of time constraints and the Vesala et al. (2017) corrections to the evaporation formulas are not coded yet, waiting for a significant introduction of plants hydraulics in the system. As told in the previous text no much investigation was performed for returning a more realistic account of the turbulent transport in canopies. A nice and feasible extension is the one proposed by Poggi et al. (2004) which, however, will be certainly considered in the next future.

CHAPTER 3

UPSCALE THE TRANSPIRATION THEORY

The case of the evaporation from the vegetation, i.e. transpiration, is different from the ground/soil evaporation. The soil is a porous medium from which evaporation is essentially governed by the energy balance and water balance. The case of vegetation involves also plants physiology with the energy budget and the water budget more tightly entangled in the process of photosynthesis.

Transpiration is not simply a loss of water but a necessary functional activity of plants. With stomata closed (no transpiration), the plants carbohydrate building engine does not work and photosynthesis does not happen since it is the water flow that makes it possible. Water transpiration is not just a byproduct of photosynthesis, but full part of it.

The core of the theory developed in previous chapters remains valid and the task to perform is to go and determine $e^{\#}$ above the leaves surface. However, it depends on leaves and stomata control on the vapor (and CO_2) fluxes.

There is another apparent difference between vegetation and

soils. Soils are a random medium and water related equations deal with by averaging the local properties at the Darcy scale. Therefore in Richards equations, the soil water retention curves and hydraulic conductivities are statistical outcomes (Mualem, 1976). In plants, water movements are laminar, as in soils, but they move in a medium which is the product of the organisation of the flow in the xylem whose structure evolved through the ages (Stroock et al., 2014). Caused by this, while in soil the liquid phase becomes discontinuous at low suction (limited negative pressures), plants can sustain a large negative suction, which is due to the water vapor demand by the atmosphere, without producing any embolism, according to the so-called cohesion-tension theory (Holbrook et al., 1995). In this thesis we do not discuss the complex issues of plants hydraulics.

I concentrate my attention then on three aspects: what happens at leaf level (Sec. 3.2), what at canopy level (Sec. 3.4) and what at catchment level (Sec. 3.7).

Vapor diffusion, according to Fick's law, can be casted in a form similar to Dalton law. Therefore, changed what has to be changed, the solutions for $E_T.H$, T, and e obtained in the previous chapter can be used also for this phenomena. Eventually the two type of solution can be arranged together. Stomatal stresses are analyzed accordingly to the main approaches in literature. Among the various possibilities a simple multi-layer model is illustrate which comprises a separation between leaves on full light, shadows and soil evaporation. This simplification is used because my main interest is to avoid excessive complication to extend the model at catchment scale where heterogeneity of parameters, hydro-meteorological quantities, plant species, play a dominat role. The latter case is discusses in section 3.7

3.1 Where does water go in plants?

The answer to the question is simple: the water from soil goes into the roots, then to the stems and then evaporates or goes back with solute through the phloem. In fact, the right questions is: how the water goes where it goes ?
The current understanding is that the water is pulled along the plants by differences in pressures between the atmosphere and the soil. These differences are very high and often around 30 MPa, as shown in Figure 3.1. In doing this, plants resolve various problems like the one of avoiding cavitation, and providing water flux at leaves at all tree heights heights with almost equal efforts (Olson et al., 2018, Rosell et al., 2017). This is obtained in vascular plants by appropriately dimensioning of the xylem vessel (Anfodillo et al., 2006). Due to the fact that most of the resistances to water flow are in leaves, justifies neglecting, as first approximation, the hydraulic of stems, as it is done in this thesis.

A couple of papers, in particular, Manzoni et al. (2013) and Bonan et al. (2014a) offer two remarkable points of view on the dynamics of water in plants and we left to those papers the duty to summarize the issues and their current solutions of the matter. Manzoni et al. is more interested to processes, equations and general issues with plants hydraulics. Bonan et al. goal is the implementation of a model of the soil-plant-atmosphere continuum and therefore its appendixes can be useful to understand some of the details that can be perceived as ambiguous by the beginners in the field in other treatmes of the subject. Bonan et al.'s treatment is "traditional" being based on a set of assumptions commonly used and which give you back an already well packaged simplification of the physics involved. Manzoni et al. put more emphasis on the biophysical aspects and their connections with plants physiology and use partial differential equations to

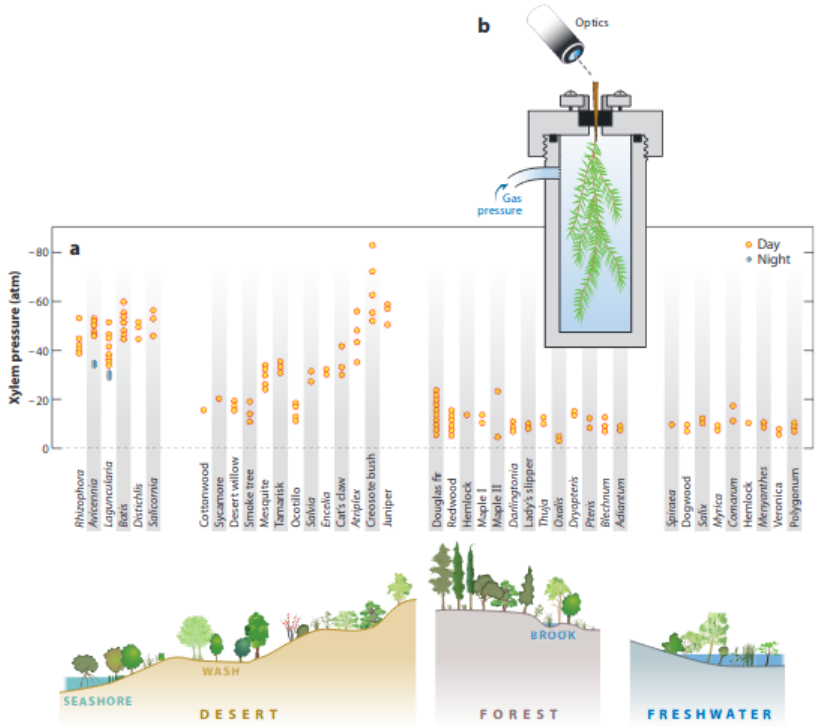

Figure 3.1: Pressure in the xylem. (a) The pressure relative to atmospheric pressure in leaves and needles ($P_{X,l} - P_0$) is reported in atmospheres (≈ 0.1 MPa) for a variety of species in a variety of climates. The values are negative. (b) Schematic depiction of the Scholander leaf pressure chamber. A cut leaf or terminal shoot is placed in the chamber with its stem exposed through a seal. The air pressure is raised within the chamber until a droplet of liquid is observed optically at the cut surface of the stem. This positive balance pressure is taken as an estimate of the negative pressure in the xylem before excision. This method has been shown to agree with more direct, mechanical measurements (Holbrook et al., 1995; Melcher et al., 1998). Figure taken from Stroock et al. (2014) and readapted from Scholander et al. (1965).

illustrate the concepts. Both of them have a large list of references and, together with the recent works of Verhoef and Egea (2014) and of Dewar (2002b), can be a solid start for any study of the subject. The latter papers, in particular, compare various approaches to modelling the water stress and discuss their ability to reproduce experimental data which is a task close to our goals. General references worth to be consulted are also Baldocchi (2019) and Bonan (2019).

3.2 Leaves

If all the machine starts from atmosphere demanding an given for granted that resistances are minor in stems and roots (Anfodillo et al., 2006), the very next thing to consider in plants is the leaves functioning.
In order to obtain this result it is useful to understand the structure of a typical angiosperm leaf, as presented in many textbooks, for instance in Molles (2015). Looking at the cross section of a leaf (as shown in Fig. 3.2), an epidermis cover both the upper and lower surface and the thick of a leaf is generally few hundred micrometers.
Epidermis (epidermal cells) is a relatively thick waterproof cuticle placed on the upper and lower side. Between the two epidermal layers there is the mesophyll tissue, which is usually differentiated into chloroplast, "palisade" and "spongy" cells, Fig. 3.2.
The palisade cells are often elongated perpendicular to the upper epidermis and are found immediately beneath it. The spongy mesophyll cells are located between the palisade mesophyll cells and the lower epidermis, are loosely packed, and intercellular air spaces are conspicuous. In fact, most of the surface area of both spongy and palisade mesophyll cells is exposed to air in the intercellular spaces, facilitating diffusion of gases into or out of

the cells.
The pathway of least resistance for gases to cross the epidermis and enter or to exit into the leaf is through the adjustable space between a pair of guard cells.
The pore and the surrounding guard cells are called stoma or

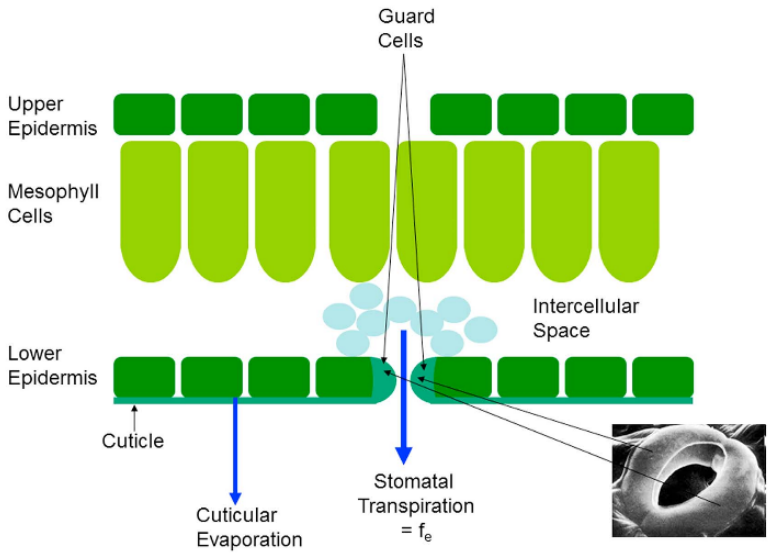

Figure 3.2: Cross section of typical angiosperm leaf. Image taken from Katul et al. (2012)

stomata if more than one.

When guard cells are open, the stomatal pores allow exchange of incoming CO_2 into the leaf and the emission dioxygen, produced by photosynthesis. However this implies the loss of water vapor (i.e. transpiration) also occurs mainly through the stomatal pores.
The degree of stomata opening depends also by the CO_2 concentration near to the guard cells. When a leaf is illuminated, the CO_2 concentration start to decrease, due to the fixation inside the leaf for photosynthesis activity, this decrease triggers the stoma opening in order to get more water from roots to supply

oxigen and nutrients necessary and assimilate more CO_2 and build carbohydrates (Nobel et al., 1999).
In leaves, and especially for those in shade, the degree of stomata opening increases with the photosynthetic photon flux (PPF) until they reach the saturation point (around 45 W/m^2 and generally expressed as micromoles of photons, μmol $m^{-2}s^{-1}$) beyond this value the opening degree does not change even if the PPF value keeps increasing (Nobel et al., 1999). On the other hand, others leaves show an increment of the opening degree up to a PPF of approximately 2000 μmol $m^{-2}s^{-1}$. This is because the leaves in shadow seem to be more efficient in the absorption of CO_2 than those placed in sunlight.
The lack of water in a leaf can be intuitively dangerous for the survival of the leaf itself. To avoid losing too much water in fact stomata tend to close when there is a decrease in the leaf water potential, that varies between 1MPa for garden vegetables up to 6MPa for some desert shrubs. For the same reason, even a decrease in the humidity of the air leads to a partial or complete closure of the stomata. If there is no closure of the stomata for these reasons, if a leaf is exposed it will tend to open the stomata with the increase in temperature: in fact the optimal photophosphorylation temperature is between 30 to 40°C, depending on the species and the growth temperature. (June et al., 2004), a value that is generally higher in leaves in shadow (Nobel et al., 1999).
Stomata provide a control on this trade off, between the freely assimilation of the CO_2, supply of water oxygen, needed for photosynthesis and at the same time preventing excessive loss of water vapor from the plant, which would cause the stop of the photosynthesis engine caused by cavitation. The loss of water at the same time helps to lower the temperature of the leaf avoiding that it overheats and keeps, as much as possible, the optimal

temperature for photophosphorilation to happen.
Since CO_2 diffuses across the same pathway used by vapour, when the carbon dioxide fixation starts, water vapour movement takes place. The PAR threshold for photosynthesis activation is different for each species and also for sunlit and shaded leaves (Nobel et al., 1999).
A few major factors were identified to control transpiration from stomata: water content, light availability, radiation input and temperature.
To further summarize: water is transported with relatively low resistance from root to leaves (Anfodillo et al., 2006) but under tension. This cause a non-stomatal resistance to evaporation because, according to Kelvin's law, the vapor tension is decreased (Vesala et al., 2017), subsequently vapor has to be moved out the VBL according to Fick's law but limited by stomatal closure, and finally is transported away from plant's canopies by turbulence, i.e., in our approximation, by Dalton's law. In the next sections we discuss how we can deal with molecular diffusion and stomatal closure, while non stomatal resistances where already discussed in section 2.

3.2.1 Water vapor diffusion in leaves boundary layer

Whatever the controls on water and vapor movements, the key passage in modelling is to understand how to get them in equation and understand if the tool set developed for the turbulent transport can be re-arranged for the vapor movements in leaves. On this topic we follow the treatment by Nobel et al. (1999).
Fick's first law is usually used to represent concentration-driven

gas diffusion of a generic gas j:

$$J_j = D_j \frac{\partial c_j}{\partial x} \tag{3.1}$$

Fortunately, it can be recasted in a form that is similar to Dalton's law:

$$J_j = D_j \frac{\partial c_j}{\partial x} = D_j \frac{\Delta c_j}{\Delta x} = D_j \frac{\delta c_j^{bl}}{\delta^{bl}} \qquad = g_j^{bl} \Delta c_j^{bl} = \frac{\Delta c_j^{bl}}{r_j^{bl}} \tag{3.2}$$

$$g_j^{bl} = \frac{J_j}{\Delta c_j^{bl}} = \frac{D_j}{\delta^{bl}} == \frac{1}{r_j^{bl}} \tag{3.3}$$

Where:

- J_j is the net flux density in $[molm^{-2}s^{-1}]$,
- c_j is the concentration coefficient in $[molm^{-3}]$,
- D_j is the diffusion coefficient in $[m^2s^{-1}]$,
- δ^{bl} is the boundary layer thickness in [mm],
- g_j^{bl} is the boundary layer conductance in $[ms^{-1}]$,
- r_j^{bl} is the boundary layer resistance in $[sm^{-1}]$,

Therefore, arguments similar to those already expressed in Chapter 2 to obtain E_T, H, T and e under the vapor removal by turbulence, can be used for transpiration and vapor movements insides leaves but using Fick's law coefficients instead of those derived by turbulent analysis. Thus, once the stomatal conductances are appropriately estimated, PMSO solutions form remain valid, changed what has to be changed, also in this case. In fact, one can also use the above solution for the VBL and then use it to feed any scheme of turbulent transport. Not necessarily, the K-theory we adopted here. To give values to the resistances in leaves, Nobel et al. (1999) essentially identifies 3 different conductance to water vapor diffusion in VBL:

- stomatal conductance: linked to the size of the stoma,
- boundary layer conductance: that is the resistance that meets the water vapor spreading in the turbulent atmosphere
- intercellular air space conductance: due to the irregular shape of the air space inside the leaves.

Typical values of these resistances are reported in table 3.1.
Water availability in leaves is ultimately related to the water available in soil.
However, there is a variety of ways plants actually regulate the stomatal resistance, in accordance to water deficencies but they can be simplified in two type of behavior: the isohydric and anisohydric types (Martínez-Vilalta and Garcia-Forner, 2017).
In the first case, the plant progressively closes the stoma as reaction to water stress to maintain as much as possible a balanced water content. In the other case the plant delays stoma closure in the measure it can resist to manifestation of cavitation and produces in its interior a very uneven water distribution.

3.2.2 Stomatal conductance in the absence of stress

According to the previous analysis, one important information is derived from the determination of stomatal opening. First we determine the maximum one, according to Lehmann and Or (2015). The stomatal resistance is computed as the sum of two terms:

- the throat resistance (r_{sp}), dependent on the area and the thickness of the pores (respectively A_n and d_p),

Components	Conductance		Resistance	
Condition	$\frac{mm}{s}$	$\frac{mmol}{m^2 s}$	$\frac{s}{m}$	$\frac{m^2 s}{mol}$
Boundary layer				
Thin	80	3200	13	0.3
Thick		320	130	3
Stomata				
Large stoma/open	20	800	50	1.3
Small stoma/open	1.8	72	560	14
Closed	0	0	∞	∞
Cuticle				
Crops	0.1-0.4	4-16	2500-10000	60-250
Trees	0.05-0.2	2-8	5000-20000	125-500
Intercellular air space				
Typical	40-100	1600-4000	10-25	0.2-0.6
Leaf				
Crops/open stomata	2-10	80-400	100-500	2.5-13
Trees/open stomata	0.5-3	20-120	300-2000	8-50

Table 3.1: Representative values of conductances and resistances for water vapor diffusing out of leaves (Nobel et al., 1999).

- the vapour shell resistance (r_{vs}), related to the distribution of the water vapor sources over the layer, i.e. to the size and the spacing of the stomata .

The throat resistance is computed as (Lehmann and Or, 2015):

$$r_{sp} = \frac{d_p}{A_p k_{dv} n_p} \tag{3.4}$$

where k_{dv} is the ratio of the vapour diffusion coefficient and the molar volume of air (D_{va}/V_m), and $A_p = \pi r_p^2$.
The vapour shell resistance was proposed by Bange (1953):

$$r_{vs} = \left(\frac{1}{4r_p} - \frac{1}{\pi s_p}\right)\frac{1}{k_{dv} n_p} \tag{3.5}$$

Where s_p is the spacing between stomata expressed in meters, and $n_p = 1/s_p^2$.
The stomatal conductance to water vapour $g_{tw,mol}$, expressed in $mol m^{-2} s^{-1}$, can be computed as:

$$g_{sw,mol} = \frac{1}{(r_{sp} + r_{vs})} \tag{3.6}$$

In order to obtain g_{sw} in m s^{-1}:

$$g_{sw} = \frac{g_{sw,mol} R_{mol} T_a}{P_a} \tag{3.7}$$

Typically we can assume $g_{sw,mol} \approx 40$ mol m$^{-3} \cdot g_{tw}$
Even if this method gives a very good representation of the physical resistance (or conductance) of the pores it does not consider physiological response. In this way there is no closure of the stoma, especially during the night.

3.3 The families of conductance models with stress

Of particular importance for leaf energy fluxes is that leaf temperature, transpiration, and photosynthesis are linked through stomatal conductance. In fact, stomata act to balance the need for photosynthetic CO_2 uptake while limiting water loss during transpiration. An accurate depiction of stomatal conductance is required to determine the transpiration and leaf temperature. Even if Bonan et al. (2014b) recognizes that the biophysics of

stomatal conductance is understood in relation to the biochemistry of photosynthesis, he identifies four main types of models:

- empirical multiplicative models;
- semi empirical models that relate stomatal conductance and photosynthesis;
- water-use efficiency optimization models;
- plant hydraulic models.

Early models of stomatal conductance were empirical and did not link stomatal behavior with photosynthesis. A subsequent model of stomatal conductance recognized the empirical dependence between A_n and g_{sw}, in what is commonly referred to as the Ball-Berry model (Ball et al., 1987). Collatz et al. (1991) coupled photosynthesis and stomatal conductance models for C_3 plants, and Collatz et al. (1992) extended the work to C_4 plants. Alternatively, water-use efficiency optimization theory provides an expression for g_{sw}. It is based on the principle that the physiology of stomata has evolved to maximize carbon uptake while minimizing water loss (Cowan and GD, 1977). A fourth class of models relates stomatal conductance to plant water uptake. Since, at present, we are looking for a simple methodology to model the stomatal conductance, we only analyze the first two models.

3.3.1 Models based on climatic control only

The hypothesis on which these models are based is that the stoma responds independently to the variation of each environmental forcing such as radiation and temperature. When these quantities vary, the stoma will open or close to increase

or decrease the conductance, therefore to favor or limit the assimilation of CO_2. In particular, the stomata tend to close in the presence of those conditions that lead to a high vapor loss as in the case of high pressure deficits or that the external temperature is too high or low compared to the optimal photosynthesis temperature (generally between 15-25°C). Obviously it will also depend on the amount of PAR incident (Nobel et al., 1999; Schymanski and Or, 2017).

$$g_s = f(R_{PAR}) \cdot f(T_l) \cdot f(VPD) \cdot f(C_a) \cdot f(\Psi_l) \tag{3.8}$$

Where:

- R_{PAR} is the PAR,
- T_l is the leaf temperature ($\approx T_a$),
- VPD is vapour pressure deficit,
- C_a is the Co_2 concentration,
- Ψ is the leaf water potential.

Jarvis (1976) was the first to propose this type of approach, currently very widespread. Despite its simplicity, a validation laboratory concluded that this model explains 95% of the observed variation of g_s (Jarvis and Mcnaughton, 1986, Damour et al., 2010). In some variants of this model the function of the leaf water potential $f(\Psi)$ is replaced with a function of the soil water content (Dewar, 2002b).
There are different versions of this model in which only part of the stress is considered. A partial list can be found in Damour et al. (2010).
White et al. (1999) proposes a variant of this model in which

the factors are normalized and multiplied by a value of maximum conductance, i.e. the conductance value obtained in well-watered condition (g_{smax}) and without any stress. A further variation was proposed by Noe and Giersch (2004), in which the factors are not multiplied, but the minimum among the factors is considered. This last approach is used to obviate the reduction in conductance due to the multiplication of individual stress factors. In fact, if two stress factors cause a reduction of the 80%, the total reduction is equal to 64%. This effect is the greater the number of stress factors considered, so it needs an accurate parametrization or a parameters calibration.
The main criticism of this approach is that the interaction between these factors cannot be ignored, such as that between the vapor pressure deficit and the leaf water potential (Tardieu et al., 1996). Furthermore, even if successfully tested in numerous circumstances, multiplicative or limiting factor-based models are essentially empirical and require new parameterization for each new environmental condition. This is their main drawback, likely resulting from the assumption that environmental factors have independent effects.

3.3.2 Models based on the conductance-photosynthesis relationship

Another type of models are those based on the relationship between g_s and the photosynthesis rate A_{net} [mol $CO_2 m^{-2} s^{-1}$]. The ratio g_s / A_{net} remains constant if other environmental and soil variables remain constant as the radiation changes (Wong et al., 1979; Mott, 1988; Aphalo and Jarvis, 1991; Buckley et al., 2003).
These models are designed to maximize water use efficiency (WUE): the basic idea is that the plant regulates the opening of

the stomata in order to maximize the assimilation of CO_2 and minimize the loss of H_2O.
One of the most common models is the Ball-Berry-Leuning model (Ball et al., 1987):

$$g = g_0 + \frac{a_1 A_{net}}{(c_s - \Gamma)(1 + \frac{D_s}{D_0})} \tag{3.9}$$

where:

- A_{net} is the net leaf CO_2 assimilation rate,
- D_s is the vapour pressure deficit (VPD) and
- c_s is the CO_2 concentration at leaf surface,
- Γ is the CO_2 compensation point,
- g_0 is the value of g at the light compensation point. The light compensation point is the intensity of light whereby the frequency of photosynthesis corresponds exactly to the frequency of cellular respiration.
- a_1 and D_0 are empirical coefficient.

Ball et al. (see also Collatz et al. (1992)) has been built out of empirical bases and it was subsequently modified (e.g Verhoef and Egea (2014)) to include physiological reactions and the production of abscisic acid, ABA (Buckley, 2016).
These kind of models (Ball et al., 1987; Leuning, 1995) can be used successfully both at leaf or canopy scale (Misson et al., 2002; Alton et al., 2007). They are easy to use and to parametrize but generally they do not include the soil water stress even if they can be modified in order to model it using an empirical function (Ball et al., 1987; Leuning, 1990; Aphalo and Jarvis, 1993; Leuning, 1995; Damour et al., 2010).

3.4 Canopies

All the considerations made so far are valid at leaf scale. What happens when they are applied to a canopy scale?
For what we saw before we can therefore argue that transpiration is strictly dependent on photosynthetic activity and therefore on radiation.
Radiation, in fact, presents strong heterogeneity since we have part of leaves in shadow and part in sunlight.
Traditionally, many models of ecosystems have used a simple efficiency approach in the use of light (Monteith, 1972,1973) to estimate the assimilation of photosynthetic activity. But starting from the work of Farquhar et al. (1980), the leaf-level model has been adopted more and more often as the basis for canopy scale upscaling, using common parameters throughout the canopy or dividing it into different layers with distinct light response characteristics.

The simplest of these upscaling methodologies is the big leaf approach, which assumes that the canopy have the same responses to the environment as each individual leaf not shaded in the canopy (Sellers et al., 1992, Dai et al., 2004).
Despite its widespread use for the modeling of evapotranspiration at different spatial scales (Raupach and Finnigan, 1988; Moran et al., 1996; Samson and Lemeur, 2001; Weiß and Menzel, 2008), subsequent theoretical and experimental developments (De Pury and Farquhar, 1997; Carswell et al., 2000; Lai et al., 2000; Meir et al., 2002) questioned the assumptions underlying the big-leaf approach in modeling vegetation productivity. Recently it has been discovered that most of the leaves are not saturated with light. These results dispute the assumption that the photosynthetic capacity is exclusively proportional to the absorbed radiation (Friend, 2001; Sprintsin et al., 2012).

According to Baldocchi (2019) the various way to treat the issue can be summarised in:

- big-leaf (Monteith, 1981);
- two-layer systems (plant/soil) (Shuttleworth and Wallace, 1985);
- dual-source system (sun/shade) (De Pury and Farquhar, 1997; Wang and Leuning, 1998);
- two-layer/dual source (plant/soil, sun/shade; Norman, 1980; Sinclair et al. 1976);
- one-dimensional multi-layer system (Baldocchi and Harley, 1995; Goudriaan, 1977; Norman, 1979);
- two-dimensional array (Chen et al., 2008);
- three-dimensional array (Kobayashi et al., 2012; Medlyn, 2004; Wang and Jarvis, 1990);

We summarize in the section below some of their main characteristics.

3.4.1 Big-Leaf Approach

On the leaf scale, Farquhar describes the photosynthetic capacity as the sum of the chloroplastic capacities per surface unit (Farquhar and Von Caemmerer, 1982). It has therefore been hypothesized that the distribution of chloroplasts within the canopy was proportional to the average absorbed radiation, so as to optimize photosynthetic production. This implies that there will be a higher concentration of chloroplasts at the top of the canopy than at the base of the canopy (Nobel et al., 1999). If we assume that the distribution of photosynthetic capacity between the

leaves in a canopy is proportional to the irradiance profile absorbed by the Lambert-Beer law, the canopy can be treated as a single homogeneous entity, ie a large leaf. The equations normally applied to the individual leaves can be extended to the entire canopy (De Pury and Farquhar, 1997; Farquhar, 1989).

3.4.2 Two-Leaf Approach

A simpler approach of separating the leaves from the sun-lit shadow, in which the vegetation is treated as two big leaves in different lighting conditions (Sinclair et al., 1976) and since then it has been continuously investigated (De Pury and Farquhar, 1997; Wang and Leuning, 1998; Chen et al., 1999; Mercado et al., 2006). Two-leaf models have been successfully tested for local and regional scale applications and have been found to sufficiently capture much of the variation present in complex multi-level approaches to separating sun-shaded leaves (Kotchenova et al., 2004) that broad-leaf upscaling cannot reach (De Pury and Farquhar, 1997; Chen et al., 1999; Dai et al., 2004; Mercado et al., 2006; Mercado et al., 2007).
In the two-leaf models, the photosynthetic activity is computed separately for sunlit (LAI_{sun}) and shaded (LAI_{sh}) parts of the canopy Norman (1979). Given the close link that exists between photosynthesis and transpiration, we decide to extend this result to compute the transpiration both from sunlit and shaded canopy. So the total leaf area index (LAI) is separated into sunlit and shaded:

$$LAI = LAI_{sun} + LAI_{sh} \tag{3.10}$$

$$A_c = A_{sun} \cdot LAI_{sun} + A_{sh} \cdot LAI_{sh} \tag{3.11}$$

$$E_c = E_{sun} \cdot LAI_{sun} + E_{sh} \cdot LAI_{sh} \tag{3.12}$$

where A_c and E_c are respectively the total canopy photosynthesis and transpiration.

$$LAI_{sun} = 2 \cdot \cos\theta \left(1 - \exp^{-G(\theta)\,\Omega\,LAI/\cos\theta}\right) \tag{3.13}$$

where

- θ is the solar zenith angle in radiant [rad];
- $G(\theta)$ is the foliage projection coefficient taken as 0.5 assuming a spherical leaf angle distribution [adimensional];
- Ω is the leaf spatial distribution pattern factor [adimensional].

Ω is expressed in terms of the degree of its deviation from the random case (assume equal to 1 for randomly distributed leaves and less than one for clumped canopies) and it influences radiation interception by the canopy at a given θ as described by Beer's law (Beer, 1852).

3.4.3 Clumping foliage

Foliage clumping increases the probability of leaf overlapping and decreases the probability of a leaf exposure to the direct radiation. A decrease in Ω (increasing clumping) results in a decrease of LAI_{sun} and a consequent increase in the fraction of the shaded leaves. Since shaded leaves typically have higher light-use efficiency (photosynthetic performance per unit incident photon flux density), then for extremely clumped canopies such as coniferous forests ($0.5 < \Omega < 0.7$) (Chen and Leblanc, 1997), LAI_{sh} should contribute significantly to total canopy productivity. Furthermore, since Ω influences the ratio between sunlit and shaded leaves (as in the two-leaf case) or changes in PAR-intercepted area (as in the big-leaf case), it should have a considerable effect

on canopy-level GPP (Baldocchi and Harley, 1995; Chen et al., 2003; Chen et al., 2012). Typical values of Ω are 0.5-0.7 for conifer forests, 0.7-0.9 for broadleaf forests, and 0.9-1.0 for grass and crops (Chen and Cihlar, 1996; Chen et al. (1997)).

3.5 Upscaling at the canopy scale

The Schymanski and Or method is validated for a single leaf, with the surface perpendicular to the shortwave radiation and in well-watered condition. In order to extend this approach to be used in the hydrological models, we need to introduce an upscale of this method at the canopy level and to include the water stress factors.

3.5.1 Upscaling strategy

The upscaling problem rises since we are not able to compute the energy balance on each leaf: we need to consider the inclination of sun rays with respect to the leaf surface, if the leaf is exposed to the direct solar radiation or not (or even partially) and various local variables we do not usually know.
Therefore we try a method by doing some simple statistical assumptions:

- the first assumption is to consider air temperature, relative humidity, wind and longwave radiation more or less constant inside the canopy. This implies also to assume the longwave radiation is isotropic inside a canopy level. If the other environmental forcing are constant inside the canopy, the energy balance and the consequently the equilibrium temperature for a leaf depends only by the shortwave radiation, both for sunlit and shaded leaves.

- The second assumption made is to consider the the canopy divided in two parts: the one in sunlight and the one in shadow.

Each of these fractions can be considered as a single big leaf that emits latent heat proportionally to the corresponding area and to the shortwave radiation received.
It is fundamental compute the fraction of canopy area in sunlight and in shadow and the radiation intercepted by these parts of canopy and the one that reach the soil

$$R_s = R_s^{c,Sun} + R_s^{c,Sh} + R_s^{soil} \tag{3.14}$$

Where:

- R_s is the total solar radiation $[W/m^2]$;
- $R_s^{c,Sun}$ and $R_s^{c,Sh}$ are respectively the solar radiation collected be the by the fraction of canopy in sunlight and in shadow $[W/m^2]$;
- R_s^{soil} is the solar radiation reaching the soil $[W/m^2]$.

$$A_c = A_c^{Sun} + A_c^{Sh} \tag{3.15}$$

Where:

- A_c is the total area of the canopy per unit of ground surface $[m^2 m^{-2}]$;
- A_c^{Sun} and A_c^{Sh} are the total area of the sunlit and shaded canopy per unit of ground surface $[m^2 m^{-2}]$.

This allow us also to separate transpiration and evaporation because we can write three different energy balance, being:

$$E_T = E_c^{sun} + E_c^{sh} + E_{soil} \tag{3.16}$$

$$= E_c^{sun}(R_{c,sun}) + E_c^{sh}(R_{c,sh}) + E_{soil}(R_{soil}) \tag{3.17}$$

where:

- E_T is the total evapotranspiration per unit of ground surface $[Wm^{-2}]$;
- E_c^{sun} and E_c^{sh} are the total transpiration from sunlit and shaded canopy per unit of ground surface $[Wm^{-2}]$;
- E_{soil} is the total evaporation from soil per unit of ground surface $[Wm^{-2}]$.

$$E_l^{Sun}(T_l^{Sun}) = R_s^{Sun} - R_{ll}^{Sun}(T_l^{Sun}) - H_l^{Sun}(T_l^{Sun}) \tag{3.18}$$

$$E_l^{Sh}(T_l^{Sh}) = R_s^{Sh} - R_{ll}^{Sh}(T_l^{Sh}) - H_l^{Sh}(T_l^{Sh}) \tag{3.19}$$

$$E_{soil}(T_{soil}) = R_s^{Soil} - G - R_{ll}^{soil}(T_{soil}) - H_{soil}(T_{soil}) \tag{3.20}$$

where:

- E_l^{Sun} and E_l^{Sh} are respectively the transpiration from sunlit and shaded canopy $[Wm^{-2}]$;
- E_{soil} is the evaporation from soil $[Wm^{-2}]$;
- H_l^{Sun}, H_l^{Sh} and H_l^{Soil} are the sensible heat emitted by the sunlit canopy, the shaded canopy and the soil $[Wm^{-2}]$;
- R_s^{Sun}, R_s^{Sh} and R_s^{Soil} are the shortwave radiation collected by each layers $[Wm^{-2}]$;
- R_{ll}^{Sun}, R_{ll}^{Sh} and R_{ll}^{Soil} are the net longwave radiation heat of each layers $[Wm^{-2}]$;
- T_l^{Sun}, T_l^{Sh} and T_l^{Soil} are the equilibrium temperature of each layers $[Wm^{-2}]$;
- G is the soil heat flux $[Wm^{-2}]$.

The fraction of lit and shaded canopy, as the radiation intercepted by those, is achieved using the Sun/Shade model (De Pury and Farquhar, 1997).

3.6 Sun/Shade model

In the Sun/Shade model (De Pury and Farquhar, 1997), as in the multi-layer canopy model, the canopy is represented as an absorbing medium for the shortwave radiation. The penetration of PAR inside the canopy is given by the sunfleck penetration factor, f_{Sun}, is given by:

$$f_{Sun}(L) = \exp(-k_b L) \tag{3.21}$$

where:

- k_b is the extinction coefficient [-];
- L is the leaf area index $[m^2 m^{-2}]$.

k_b depends on several factors like the solar elevation angle, the canopy albedo, the leaves orientation distribution angle and the canopy clustering (Ryu et al., 2011)

$$L_{Sun} = \int_0^{L_c} f_{Sun}(L) dL \tag{3.22}$$

$$L_{Sh} = L_c - L_{Sun} \tag{3.23}$$

where

- L_{Sh} and L_{Sun} are the fraction of leaf area index in shade and in sunlight
- L_c is the cumulated leaf area index.

$$R_{sw}^{Sun} = \int_0^{L_c} R_{sw}^{Sun} f_{Sun}(L) dL \tag{3.24}$$

$$= \int_0^{L_c} [R_{sw}^{dir}(L) + R_{sw}^{dif}(L) + R_{sw}^{sca}(L)] f_{Sun}(L) dL \tag{3.25}$$

Where:

- R_{sw}^{Sun} is the shortwave radiation intercepted by the sunlit canopy $[Wm^{-2}]$;
- R_{sw}^{dir} is the direct component of the shortwave radiation per ground area $[Wm^{-2}]$;
- R_{sw}^{dif} is the diffuse component of the shortwave radiation per ground area $[Wm^{-2}]$;
- R_{sw}^{sca} is the scattered component of the shortwave radiation per ground area $[Wm^{-2}]$.

R_{sw}^{dir} and R_{sw}^{dif} can be obtained by meteorological data measurements or using the GEOframe shortwave component (Formetta et al., 2011b). R_{sw}^{sca} is computed using the parametrization provided by Farquhar and Raschke (1978).

$$R_{sw}^{Sh} = \int_0^{L_c} R_{sw}^{Sh}[1 - f_{Sun}(L)]dL \tag{3.26}$$

$$= \int_0^{L_c} [R_{sw}^{dif}(L) + R_{sw}^{sca}(L)][1 - f_{Sun}(L)]dL \tag{3.27}$$

The multi layer models are quite useful because they allow to calculate the radiation absorbed by the various vegetation layers and the one that is not intercepted, thus allowing to describe separately the transpiration and evaporation processes. In fact, with these models is possible to compute the radiation absorbed from canopy using the previous equations.
Knowing the radiation absorbed from the canopy it is possible to compute the radiation reaching the soil:

$$R_{soil} = R_s - R_c^{sun} + R_c^{sh} \tag{3.28}$$

Where:

- R_{soil} is the shortwave radiation reaching the soil $[Wm^{-2}]$;
- R_s is the incoming shortwave radiation $[Wm^{-2}]$;

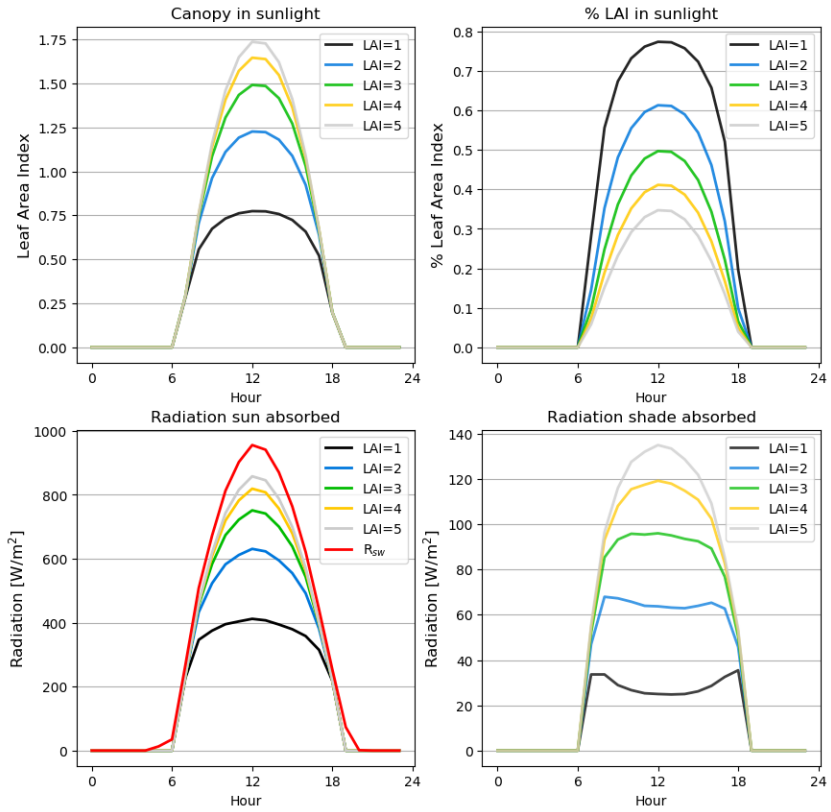

Figure 3.3: LAI and absorbed shortwave radiation with the Sun/Shade model: a) Canopy area in sunlight at the variation of the LAI; b) Fraction of canopy in sunlight with the variation of the LAI; c) Total radiation absorbed by sunlit canopy based on the LAI; d) Total radiation absorbed by shaded canopy based on the LAI.

- $R_{c,sun}$ is the shortwave radiation intercepted by sunlit canopy $[Wm^{-2}]$;

- $R_{c,sh}$ is the shortwave radiation intercepted by shaded canopy $[Wm^{-2}]$.

Consequently, using the different shortwave radiation input it is possible to compute the transpiration and the evaporation for

each layers:

$$\begin{aligned} ET &= E_c^{sun} + E_c^{sh} + EV_{soil} \\ &= E_c^{sun}(R_c^{sun}) + E_c^{sh}(R_c^{sh}) + EV_{soil}(R_{soil}) \end{aligned} \tag{3.29}$$

The Schymanski and Or (2017) equation is referred to a single leaf and the latent and sensible heat obtained is computed per area unit. To obtain the total latent heat emitted by a leaf we have to multiply the latent heat for the leaf area A_l. For sensible heat and longwave radiation is the same but we must include the coefficient a_{sH}:

$$\begin{cases} E_l = E \cdot A_l \cdot a_{sE} \\ H_l = H \cdot A_l \cdot a_{sH} \\ R_{l,ll} = R_{ll} \cdot A_l \cdot a_{sH} \end{cases}$$

Where:

- E_l, H_l and $R_{l,ll}$ are respectively the latent heat, the sensible heat and the net longwave radiation emitted by the leaf $[W]$;
- E, H and R_{ll} are respectively the latent heat, the sensible heat and the net longwave radiation per unit of surface $[Wm^{-2}]$;
- A_l is the total area of the leaf $[m^2]$.
- a_{sE} are the sides of surface exchanging latent heat, equal to 1 for hypostomatous, 2 for amphistomatous [-];
- a_{sH} are the sides of surface exchanging sensible heat or longwave radiation, equal to 1 for soil, 2 for leaves [-].

We assume the same is still valid also for the canopy, using instead A_l the canopy area A_c:

$$\begin{cases} E_c = E \cdot A_c \cdot a_{sE} \\ H_c = H \cdot A_c \cdot a_{sH} \\ R_{c,ll} = R_{ll} \cdot A_c \cdot a_{sH} \end{cases}$$

Where:

- E_c, H_c and $R_{c,ll}$ are respectively the latent heat, the sensible heat and the net longwave radiation emitted by the canopy $[W]$;
- A_c is the total area of the canopy $[m^2]$.

Furthermore some flux exchanges between the layer could happen and should be considered in order to assess the closure of the energy balance.
For example, in case of longwave radiation, the net balance for a generic layer is given by:

$$R_{ll}^n = R_{l\uparrow}^{n-1}(T_l^{n-1}) + R_{l\downarrow}^{n+1}(T_l^{n+1}) - R_{l\uparrow}^n(T_l^n) + R_{l\downarrow}^n(T_l^n) \qquad (3.30)$$

Currently, this kind of feedback is not considered and we approximate all these exchanges as based on the air temperature T_a. This is an approximation similar to that made by (Schymanski and Or, 2017) when the temperature of the objects surrounding the leaf, T_w, is assumed approximately equal to T_a.
In this version of the model the flux exchange between the layers is not considered. In fact, if fluxes exchange is allowed between layers, both if they are only two (sun/shade) or more, in the energy balance equation will compare terms depending on the leaf temperature of the other layers. In this way the system can be solved only numerically or making some assumptions.

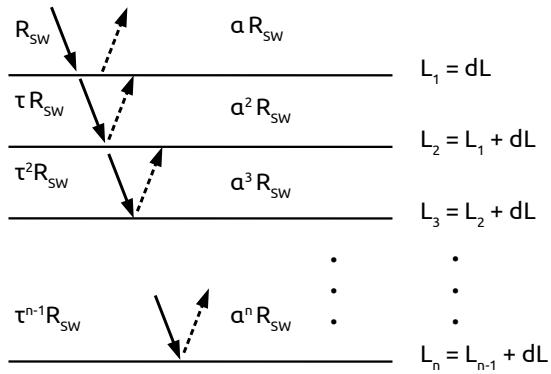

Figure 3.4: Shortwave penetration inside the canopy, assumed divided in n layers of leaf area index equal to dL, with trasmissivity τ and absorbitivity a. R_{sw} is the incoming solar radiation. The cumulated leaf area index from top of the canopy to the n^{th} layer is given by L_n, while $\tau^n \cdot R_{sw}$ and $\alpha^n \cdot R_{sw}$ represent the radiation transmitted and absorbed by the n^{th} layer.

3.7 Landscape

On the work done so far, a single type or group of trees was considered. The landscape can be though as formed by tiles, often called Hydrologic Response Units (HRU), where the parameters of the model used remain constant and the hydrological variable are uniform. These attributes, energy and water vapor exchange, forest attributes of the forest stand as LAI and canopy conductances, of which we discussed, can vary though from tile to tile. To this variation contribute (Baldocchi, 2019; Eamus et al., 2016):

- horizontal cover (usually represented by a green cover fraction;

- vertical thickness/structure
- the growth form, herbaceous or woody;
- seasonality, evergreen or deciduos;
- leaf type (broadleaf or conifer, dicot or monocotl
- photosynthetic type, C_3 or C_4;
- longevity, annual or perennial;
- type or intensity of disturbances, fire, cultivation

Therefore upscaling to landscape means mostly to subdivide the landscape in appropriate HRU and collect (characterize) properly each HRU. As in Eamus et al. (2016), remote sensing provides many of the above information and terms like, LAI (leaf area index), PAR (photosynthetically-active radiation), fAPAR (fraction of absorbed photosynthetically-active radiation), chlorophyll content, Fv (Fractional vegetation cover) are of common use in modern modelling evaporation and transpiration at catchment and large scales. These parameters and quantities are well explained in Eamus et al. (2016), section 7.4, therefore we do not repeat their treatment here.
Obviously the strictly vegetation related quantities are not the only one important for a correct modelling of transpiration. Essential is also the treatment of the variability of the meteorological forcings. Cause of this, a considerable effort was spent in developing and cleaning a system for the spatial interpolation of these quantities in rugged terrain, which is reported in Bancheri et al. (2018) and in Appendix C. Radiation itself plays a role in its own to force heterogeneously the landscape point. But we dealt with it before (Formetta et al., 2013b; 2016) and suitable radiation modelling is already included in our GEOframe system.

Finally, soil moisture is also another very relevant parameter. This quantity also comes as a product in the GEOframe system, where it can be modeled with components of various complexity that goes for the integration of Richards equation (in 1D and 3D) to classic semi-distributed lumped reservoir models, in which each HRU is treated as a group of intercommunicating reservoir, some of which provide soil moisture the the vegetation. More information about these aspects will be given in the application chapters.

3.8 Warning

There is a large variety of models and also variations in a specific model that reflect the tumultuous advance of the ecohydrological studies. Therefore we did not pretended to be comprehensive. The three books we cited, Baldocchi (2019), Eamus et al. (2016) and Bonan (2019) can serve for this scope for the interested readers. I am also aware of the fact that neglecting vegetation dynamics (especially carbon and nitrogen dynamics) can be a great limitation to any modelling type. As I already mentioned before, this modelling is not included in the present thesis, because of time constraints but it will be for sure in future version of the system described in the next chapter.

CHAPTER 4

PROSPERO DEPLOYMENT

This Chapter documents the GEOframe component Prospero which is intended to deploy the theory presented in previous thesis' chapters. GEOframe is a set modelling components that cover all the needs for simulation of the water budget at catchment scale and it is reviewed in Appendix A. As a GEOframe component is some Earth Science solution coded Java according to the OMS v3 rules. Prospero is part of a larger set of components which are intended to estimate evapotranspiration with different data requirement, including Priestley Taylor formula (Priestley and Taylor, 1972) and the FAO version of the Penman-Monteith equation (Monteith, 1965, Allen, 1986). These are collected on Github repository of Geoframecomponents and were coded mainly by Marialaura Bancheri Bancheri et al. (2018) and revised for this dissertation.

Prospero's formulas derive from the assumption that vegetation does not have great thermal capacity and the its energy budget can be simplified accordingly neglecting energy storage and implement equation 3.18 of the previous chapters 3.

To summarize some aspects detailed in Chapter 2 and 3, two main changes are made with respect to (PM):

1. It is accounted that leaves can transpire, either from one side or from two sides, according to vegetation species, while heat exchange happens from both the sides of a leaf;
2. Propero accounts for the the radiative coupling of the evaporating surface with the radiation budget through a proper linearization of the Stephan-Boltzman law. The latter two aspects are taken form a recent paper by S. Schymanski and D. Or (Schymanski and Or, 2017) and they are present, yet in a different way, in the Bonan (2019) book.

Extension from leaf to canopies is present in Prospero through a two leaf, sun-shade approach, where the canopy is subdivided in layers exposed to direct sunlight and layers in shadow, while soil is treated separately as a further layer.
The first sections of this chapter document the equations really implemented in Prospero, regarding the stresses and conductances model specification and the final solutions for the energy budget, the longwave radiation, sensible heat, temperature and, obviously, transpiration.
This Chapter, however, deals with Prospero's informatics that was designed for inclusion of various approaches to estimating the conductance by simple addition of a correspondent Java class. At present only a Jarvis (Jarvis, 1976) type of approach is implemented where environmental variables like temperature, photosynthetically active radiation, water availability in soil and vapour deficit are those that decrements transpiration as seen in Chapter 3.
A Ball-Berry type of transpiration and other formulations of transpiration reduction are under implementation. The maximum of stomata conductance is estimated by means of the procedure

suggested by Schymanski (Schymanski and Or, 2017). The Prospero component is assumed to work with the shortwave and longwave components of GEOframe at hourly scale. These are documented in Formetta et al. (2013b) and (Formetta et al., 2016). If evaporation data are present, the model can be calibrated with the LUCA (Hay and Umemoto, 2006a) and Particle Swarm calibrators, available in OMS v3 (David et al., 2013).
This Chapter is somewhat different from the other chapters of the thesis because it was designed to provide the information required to users to manage the component and to allow developers to know where to find it and modify it eventually. The information provided is a superset of the one required by the Joss journal to submit code and the delineation of the policies for the GEOframe/Prospero community, which summarize and clarify a previous long experience, should be considered part of the work of this thesis.

4.1 Prospero

During my PhD I worked on the development of an upscaled version of the Schymanski and Or formula, making it compatible with the GEOframe modeling system (Appendix A) and we decided to call this module Prospero.
Prospero borns with the purpose to be an ecohydrological and physical based model, even if currently is mainly thought to estimate evapotranspiration, it could be easily extended to the computation of photosynthesis or as the core for a lysimeter model, able to compute the water exchange between soil and atmosphere.
The idea at the base of Prospero is that the evapotranspiration is given by the sum of two different processes: evaporation from the soil and transpiration from the canopy, both the shaded and

sunlit ones.

This implies we must compute the those processed separately:

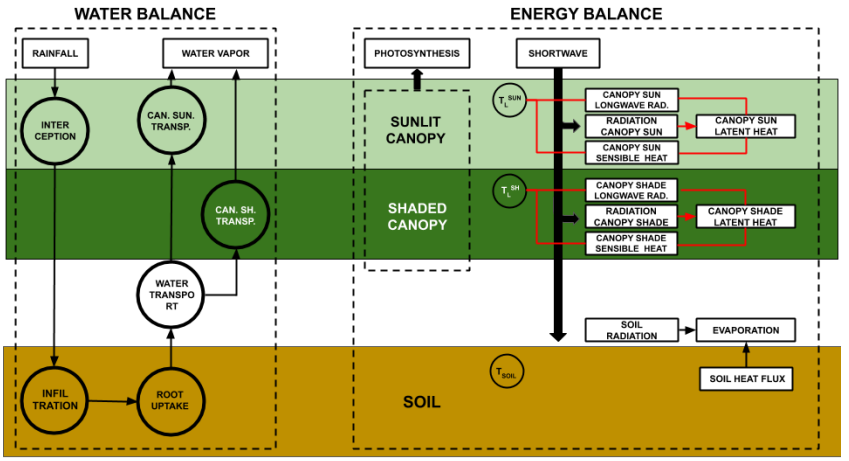

Figure 4.1: Conceptual scheme of Prospero

the evaporation from soil is computed with a Penman-Monteith FAO process (Eq. B.2, Appendix A), with specific coefficients for soil evaporation depending on the case study.

Transpiration is computed starting from the Schymanski and Or method, since it has demonstrate to ensure the best estimation of latent heat from a leaf. However, the Schymanski-Or equation has been upscaled in order to face the canopy transpiration and the mass conservation (Fig. 4.1).

We adopt a multi-layer model in order to compute the incoming shortwave radiation in each layers, and so to uncouple the evaporation-transpiration problem, as show in Eq. 3.18.

$$ET_{Ps} = EV_{soil} + E_c^{Sun} + E_c^{Sh} \tag{4.1}$$

Where:

- ET_{Ps} is the evapotranspiration computed with Prospero $[Wm^{-2}]$;

- EV_{soil} is the evaporation from the soil $[Wm^{-2}]$;
- E_c^{Sun} and E_c^{Sh} are respectively the transpiration from sunlight and shaded canopy $[Wm^{-2}]$.

This is achieved using a multi-layer canopy model: the sun/shade model.

4.1.1 Water stress & conductance model in Prospero

In Schymanski and Or (2017) the stomatal conductance is modeled using the equation 3.7. In Schymanski and Or (2017) the response of stomata to environmental forcing is not explicitly expressed through the use of stress factors but is simulated by varying the surface density and size of stomata.
This method does not provide a tool for predicting stomatal conductance, since it does not relate to the variation of stomata to the size of the forcing, whether it be climatic or related to photosynthetic activity.
Nevertheless the stomatal conductance expressed in this way and associated with the equations of Schymanski and Or (2017) gives good results therefore we have decided to include a modified version of this approach in Prospero.
Instead of using variable values for stomata size and density, we use fixed values equal to the maximum stomata radius and density ($\text{radius}_{\text{stoma}} = 22\nu m$, $\text{density}_{\text{stoma}} = 35mm^{-2}$) used in Schymanski and Or (2017). This is assumed as the maximum possible conductance value, i.e. the one that does not present stress, and therefore equal to $g_{s,max}$, in Eq. 4.3 and 4.4. Therefore, if we assume this value as the maximum value, it can be easily included in a Jarvis type formula rather than a Ball-Berry type formula. In fact, unlike Eq. 3.8 in Ball-Berry g_0 it should be equal

to zero, in order to make the stoma conductance null when the photosynthetic activity is zero (nighttime). By using it in Eq. 3.8 it is possible to reduce its value by using the stress functions. In addition Eq.4.4 is easily to be modified in order to integrate stress based on the soil water content. This is not only a variable of particular interest in hydrology but it can also be obtained from hydrological simulations and from specific components of GEOframe (Appendix).

4.1.2 Stress factors

Even if both type of conductance models (illustrated in section 3.3) can be used inside Prospero we decide to conduce all the simulation using a Jarvis-like model and in particular the one proposed by White et al. (1999).
The reason why we choose a model similar to Jarvis is given by the need to apply it on a large basin scale for hydrological applications. In fact, even if Ball-Berry still has good performance, it needs measurement of CO_2, which are not so common to find. On the contrary, models based on climatic variables use measurements easy to find in most hydro-meteorological stations. Other variables that are not available at stations can be retrieved using hydrological tools or the other GEOframe (Appendix A)components, like for example the Richards integrator for infiltration.
Specifically, Ee use a similar version of the model proposed by White et al. (1999) and by Macfarlane et al. (2004), where the conductance is respectively equal to:

$$g_s = g_{s,max} \cdot f(R_{PAR}) \cdot f(T_a) \cdot f(VPD) \tag{4.2}$$

$$g_s = g_{s,max} \cdot f(R_{PAR}) \cdot f(T_a) \cdot f(VPD) \cdot f(\Psi) \tag{4.3}$$

Where:

- $g_{s,max}$ is the conductance without any kind of stress and in well-watered conditions [ms^{-1}];
- f(R_{PAR}), f(T_a), f(VPD) and f(Ψ) are respectively the normalised stress factors induced by the PAR, the air temperature, the water pressure deficit and the leaf water potential.

The difference between the two methods is represented by the dependence of the stress factor by the water content (i.e. the leaf water potential).
We used the model proposed by Macfarlane et al. (2004), but instead of using the stress factor given by the leaf water potential, we used the one based on the soil moisture proposed by FAO approach (Allen, 1986)

$$g_s = g_{s,max} \cdot f(R_{PAR}) \cdot f(\theta) \cdot f(VPD) \cdot K_s \tag{4.4}$$

Where K_s is the normalised stress factor depending on available soil water.

$$K_s = \frac{TAW - D_r}{TAW - RAW} = \frac{TAW - D_r}{(1-p)TAW} \tag{4.5}$$

$$RAW = p \cdot TAW \tag{4.6}$$

$$TAW = 1000(\theta_{FC} - \theta_{WP}) \cdot Z_r \tag{4.7}$$

- K_s is a dimensionless transpiration reduction factor dependent on available soil water [0 - 1],
- D_r root zone depletion [mm],
- TAW total available soil water in the root zone [mm],
- p fraction of TAW that a crop can extract from the root zone without suffering water stress [-].
- θ_{FC} the water content at field capacity [m^3m^{-3}],
- θ_{WP} the water content at wilting point [m^3m^{-3}],
- Zr the rooting depth [m].

Air temperature stress The air temperature stress factor can be computed as:

$$f(T) = b(T_a - T_{low})(T_{up} - T_a)^c \tag{4.8}$$

Where b and c are defined as:

$$c = \frac{T_{up} - T_{opt}}{T_{opt} - T_{low}} \tag{4.9}$$

$$b = \frac{1}{(T_{opt} - T_{low})(T_{up} - T_{opt})^c} \tag{4.10}$$

Where:

- T_{opt} is the temperature at maximum conductance [°C];
- T_{low} and T_{up} the lower and upper temperature of the range for which a positive stomatal conductance is predicted [°C].

If $T_{low} \leq T_{air} \leq T_{up}$, f(T) = 0. White et al. (1999) assigned the values for T_{low}, T_{opt} and T_{up} equal to 0°C, 17°C and 38°C. These parameters can be set a priori or calibrated.

Total solar radiation stress The solar radiation stress can be computed as:

$$f(R_{sw}) = \left[\frac{1}{2\theta}\left(\alpha R_{sw} + 1 - \sqrt{(\alpha R_{sw} + 1)^2 - 4\theta\alpha R_{sw}}\right)\right]^{-1} \tag{4.11}$$

Where:

- α and θ are the slope and shape parameters of the stress function $f(R_{sw})$ and are set equal to 0.005 and 0.85 [-].

R_{sw} is the total solar radiation expressed in $\mu\text{mol}\,\text{m}^{-2}\,\text{s}^{-1}$. If we want to express it in Wm^{-2}we must include a conversion factor equal to $\approx 1/4.6$.

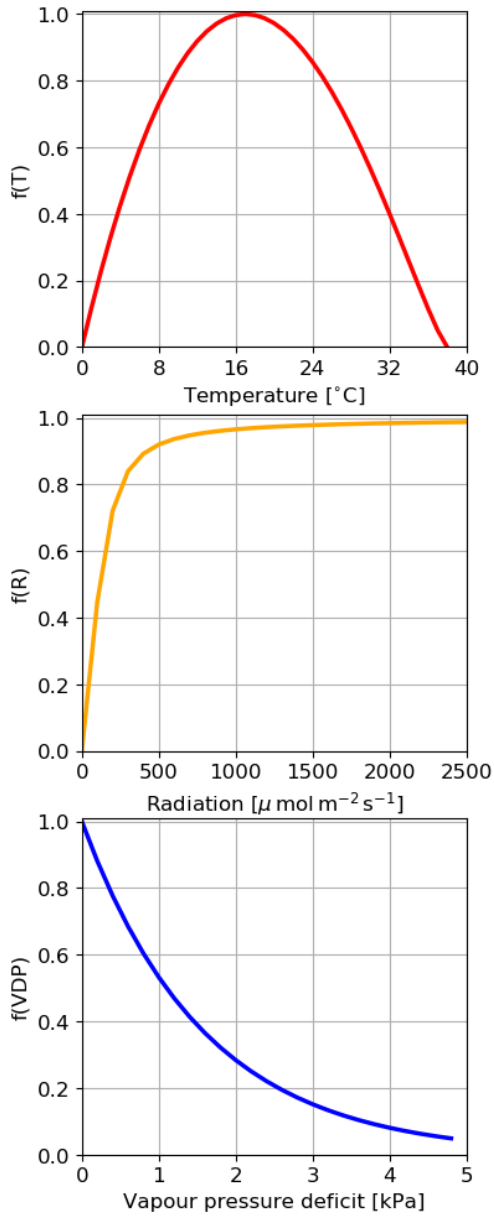

Figure 4.2: Typical values of the stress factor functions at the variation of the forcing.

Vapour pressure deficit stress The vapor deficit stress factor can be estimated as:

$$f(VPD) = 1.1 \exp[-0.63 \cdot VPD] \tag{4.12}$$

4.1.3 Maximum stomatal conductance in Prospero

In White et al. (1999) and Noe and Giersch (2004), $g_{s,max}$ (the maximum stomatal conductance) is parametrized or derived from laboratory measurements.
Since $g_{s,max}$ is the conductance of the stoma when there are no stress factors (i.e. the $f(x_n)$ are equal to 1), we assume it is equal to the stomatal conductance for water vapor (g_{tw}, Eq. 3.7) derived by Lehmann and Or (2015) and used by Schymanski and Or (2017), instead to parametrize it.

4.1.4 Prospero's equations

All the previous corrections, due to the multi-layer model and to the conductance model, are used to improve the original Schymanski-Or equation. It should be noted that in general real transpiration is calculated as the product of potential transpiration and the stomatal conductance as shown in equation 4.13.

$$ET = ETP \cdot g_s \tag{4.13}$$

In Prospero the real transpiration is obtained computing the equilibrium temperature in function of the stomatal conductance, after which it is used for the calculation of real transpiration (Eq. 4.14).

$$\begin{aligned} T_l &= T_l(g_s) \\ ET &= ETP(g_s, T_l(g_s)) \end{aligned} \tag{4.14}$$

Finally the transpiration is computed starting from the Schymanski and Or method and modified in order to include the dependence from transpiring surface, the conductance model of the stomata, other than the mass conservation. The major improvements of the Schymanski-Or model we did on Prospero are therefore the following:

- modified to use the leaf area index to obtained the **transpiring surface** (A_{tr})
- stomata opening based on radiation stress (Noe and Giersch, 2004).
- a stress function based on the **soil moisture** was added in order to ensure the water balance conservation (Allen et al., 1998)

We list here again the major of the equations of Prospero approach:

Energy budget

$$R_s = a_{sE} \cdot A_{tr} \cdot E_l(T_l) + a_{sH} \cdot A_{tr} \cdot R_{ll}(T_l) + a_{sH} \cdot A_{tr} \cdot H_l(T_l) \quad (4.15)$$

Leaf temperature (for each layer treated)

$$\begin{aligned} T_l = & \left[R_s + a_{sH} \cdot A_{tr} \cdot \epsilon_l \sigma 4 T_a^4 + c_H(a_{sH}, A_{tr}) \cdot T_a + \right. \\ & \left. + c_E(a_{sE}, A_{tr}, g_s) \cdot (\Delta_e T_a + P_w - P_{ws})\right] \cdot \\ & \cdot \frac{1}{(c_H(a_{sH}, A_{tr}) + c_E(a_{sE}, A_{tr}, g_s)\Delta_e) + a_{sH} \cdot A_{tr} \cdot \epsilon_l \sigma T_a^3} \end{aligned} \quad (4.16)$$

Longwave radiation

$$R_{ll} = a_{sH} \cdot A_{tr} \cdot \epsilon_l \sigma (T_l^4 - T_a^4) \quad (4.17)$$

Transpiration

$$E_l = c_E(a_{sE}, A_{tr}) \cdot \left[\Delta_e (T_l - T_a) + P_{ws} - P_w\right] \quad (4.18)$$

Sensible heat

$$H_l = c_H(a_{sE}, A_{tr}) \cdot (T_l - T_a) \tag{4.19}$$

The total evapotranspiration is given by:

$$ET = E_c^{sun}(R_c^{sun}) + E_c^{sh}(R_c^{sh}) + E_{soil}(R_{soil}) \tag{4.20}$$

4.2 Component Description

Prospero is written in Java, works under the OMS3 (David et al., 2013) framework and is part of the GEOframe system (Formetta et al., 2014b; Bancheri, 2017).
It has already extensively used by the students of the Hydrology class at the University of Trento for their simulations of transpiration. Main reference for understanding its theoretical foundations is this dissertation. To make it run the user must first download the OMS3 console (see section 4.3) and learn a little bit of OMS3 (information can be found, for instance, here. Tools in Python 3.* (scripting level) are also provided to treat input and output data. The execution in OMS is driven by '.sim' files and browsing them in the examples discloses most of the information a user can require. It is then clear that the reader who wants to become a user must first go through some steps of self-instruction in using those tools and understand how sim files work. This is a task to perform once forever in using OMS3/GEOframe tools, and the scope can be worthwhile for who interested in hydrology. However, the occasional reader can have most of the general information from here below.
Evapotranspiration is driven by radiation and therefore Prospero requires to run a radiation module which produces shortwave and longwave downwelling radiation. These modules are well documented theoretically at Rigon (2012), while the GEOframe modules where objects of two papers (Formetta et al., 2011c;

Formetta et al., 2014b). These modules have their own complexity that must be understood, and include two main sources of radiation modulation: the atmosphere with its transmittances (to be calibrated against some measurements) and the geometry of the terrain altering the energy flux, the angle of view and creating the shadows due to the topography. At present, terrain information is derived from a Digital Elevation Model (DEM) to be processed or from information embedded in an appropriate shapefile. GEOframe uses the Horton Machine libraries and tools to perform those geographic information analyses (Abera et al., 2014).

4.3 Licenses and policies

Prospero is provided under the General Public License version 3. All the chain of tools, libraries, are available under open source licenses and are available freely to all users. All of them, except, the codebase of OMS3 (see below) is available in Open repositories. OMS3 is distributed on an Open Source License but actual access to its code is subject to permission by OMS authors. All of this is part of an effort by the GEOframe group to develop an infrastructure allowing science replicability.

4.4 Where to find Prospero executable and how to use them

The latest executable code of this component can be downloaded from:

- Prospero on Github

and compiled following the instructions therein. A frozen version of the compiled OMS project can be found on this repository:

- Open Science Framework

Actually the repository contains a whole Object Modelling framework project, including the executable (.jar files), a set of examples, in the form of Jupyter notebooks, the simulations' scripts (.sim files) The code can be executed uploading the .sim files in the OMS3 console, which can be download and installed according to the instructions given, for instance, at the:

- website of the Winter School on GEOframe.

The code can also be executed using:

- Docker

because a "Dockerized" version of OMS3 is provided on

- Dockerhub (OMS3)

In principle is possible to run Prospero in:

- CSIP (for an oveview of the system, see also Serafin (2019), i.e. on remote platforms or services.

All of these benefits are available because of the integration of the GEOframe System in OMS/CSIP and come with the price to have to lear how to manage it. However, a few hours of training are sufficient to use the platform efficiently, as proven by the experience with the undergraduate class of Hydrology at the University of Trento. A larger amount of time should be spent in learning the basics of evaporation that allow to manage the physics of the processes involved.
For more general information regarding the use of GEOframe tools and models, please see:

- GEOframe essentials
- GEOframe Winter School

Other information is provided in Appendix A.
For who wants to compile themselves the code, they can use the appropriate Gradle script that guarantees independence from any IDE, integrated development environment as, for instance Eclipse, Netbeans or IntelliJ Idea.

4.5 Structure of the software

An example of component connection for Prospero is provided in Fig. 4.3.

4.6 Detailed description of Prospero Inputs

This information can be skipped at a first reading but it is essential to understand what Prospero does. Inputs of the Prospero components can be classified in:

- Geographical data;
- Meteorological data input;
- Evapotranspiration parameters;
- Simulation's control parameters.

Geographical data in input include:

- A DEM raster file of the catchment which contains an elevation map and the geographic coordinate system;
- A shapefile (.shp) with the geographical coordinate (latitude and longitude) of the centroid;

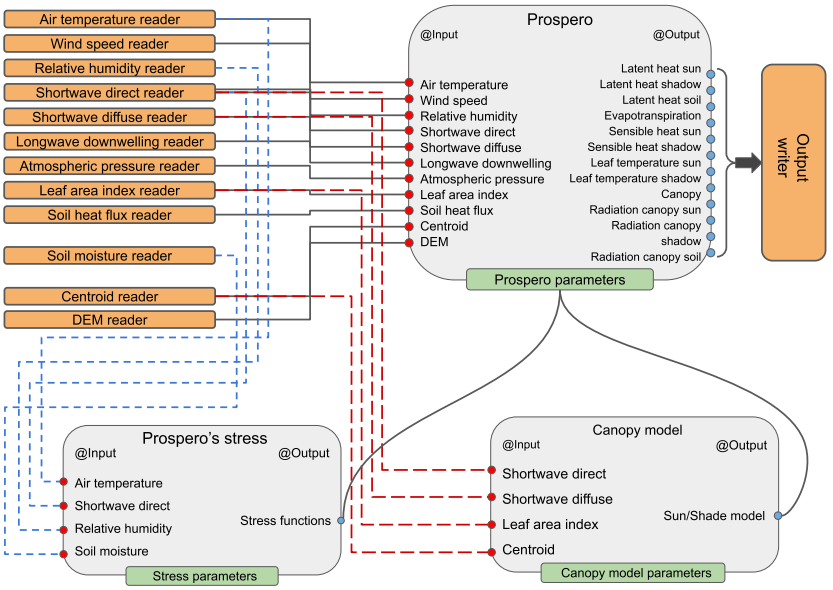

Figure 4.3: Components connection of the modelling solution of Prospero, including stress functions and the Sun/Shade canopy model.

The meteorological data include the names of the files (csv format, OMS3 format) containing:

- the air temperature [$^{\circ}C$];
- the wind velocity [ms^{-1}];
- the relative humidity [-];
- the shortwave direct and diffuse radiation [Wm^{-2}];
- the downwelling and net longwave radiation[Wm^{-2}];
- the atmospheric pressure [Pa];
- the leaf area index [m^2m^{-2}]
- the soil moisture file [m^3m^{-3}];

- the soil heat flux[Wm^{-2}].

The control parameters include for each of the meteorological data file above:

- the identification value of the location under analysis: typically the name of the basin or the site [`string`];
- the start date of simulation [string in format 'dd-mm-yyyy HH:MM'];
- the end date of simulation [string in format 'dd-mm-yyyy HH:MM'];
- the time step of simulation [minutes];
- the null value for the input and output data, typically '-9999'.

and:

- prospero.doHourly: for hourly or daily simulations [true/false];
- prospero.doFullPrint: for print all the output values on files or only the evapotranspiration [true/false];
- prospero.useRadiationStress: for using the stress deriving from radiative inputs [true/false];
- prospero.useTemperatureStress: for using the stress deriving from air temperature input [true/false];
- prospero.useVDPStress: for using the stress deriving from vapour pressure deficit [true/false];
- prospero.use WaterStress: for using the stress deriving from soil water content [true/false];
- prospero.defaultStress: a generic default value of stress (default values equal to 1).

The evapotranspiration parameters:

- *Vegetation and Canopy parameters*:

  - prospero.defaultLeafAreaIndex: default value of leaf area index if no LAI time series is available;
  - prospero.typeOfCanopy: value to select different type of canopy, currently only 'multilayer' is available;

- *Radiation Stress parameters*:
  - prospero.alpha: α parameter of eq. 4.11;
  - prospero.theta: θ parameter of eq. 4.11;
- *Vapour deficit Stress*:
  - prospero.VDP0: VDP_0 parameter of eq. 4.12;
- *Temperature Stress*:
  - prospero.Tl: T_l parameter of eq. 4.8;
  - prospero.T0: T_o parameter of eq. 4.8;
  - prospero.Th: T parameter of eq. 4.8.
- Water Stress:
- prospero.WaterWiltingPoint: θ_{WP} parameter of eq. 4.5;
- prospero.WaterFieldCapacity: θ_{FC} parameter of eq. 4.5;
- prospero.RoothDepth: Z_r parameter of eq. 4.5;
- prospero.DepletionFraction: D_r parameter of eq. 4.5.

4.7 Detailed description of the outputs

The outputs are the file names for the following variables:

- LatentHeat: the latent heat from sunlit canopy [Wm^{-2}];
- LatentHeatShade: the latent heat from shaded canopy [Wm^{-2}];
- Evaporation: the latent heat from soil [Wm^{-2}];
- EvapoTranspiration: sum of transpiration from canopy and evaporation from soil [mm];

- LeafTemperature: the equilibrium leaf temperature of sunlit canopy [K];
- LeafTemperatureShade: the equilibrium leaf temperature of shaded canopy [K];
- Radiation: the shortwave radiation intercepted by sunlit canopy [Wm^{-2}];
- RadiationShade: the shortwave radiation intercepted by shaded canopy [Wm^{-2}];
- RadiationSoil: the shortwave radiation reaching the ground [Wm^{-2}];
- Canopy: sunlit leaf area index [m^2m^{-2}];
- SensibleHeat: the sensible heat from sunlit canopy [Wm^{-2}];
- SensibleHeatShade: the sensible heat from shaded canopy [Wm^{-2}].

4.8 Examples of usage

The component cannot work alone, to get the input and the output it has to be coupled with reader and writers in a modelling solution. A working, simple example, is given at OMS ProjectET. Examples can be found in form of Python Notebooks in the directory Notebooks/Jupyter and simulations of the Component Project. Data can be found in data.

4.9 Known bugs and limitations

The code depends of the radiation inputs. It was found, during the extensive use made of the component that radiation is not returned properly in some particular cases. This bug has to be fixed but it is actually not a bug of the Prospero component. At present Prospero uses just one strategy for determining the stresses, according to Jarvis (Jarvis, 1976) and what written in

the previous Chapter 3. The code, however, is prepared to be extended to Ball-Berry-Leuning type of stresses, dependent on the photosynthesis processes.

4.10 Developments proposal

In this section we mostly discuss improvements of the informatics. Improvements from the point of view of the Physics treated are instead in Conclusions. Overcoming the above limits on the type of stresses implemented is the first step forward in the implementation of future versions of Prospero. Some other refactoring is ongoing to connect Prospero with the various version of the Richards equation (1D, 2D) integration in GEOframe available on the Github website. This task is called provisionally "Broker project". Future versions of the code will decouple the type and forms of inputs variable from the one actually used by the algorithm solving the equation. Stresses will be the appropriate classes that implement a common interface and the Strategy Pattern (Gamma, 1995) will be used to select among the different ones (Prospero 2.0 Project). This would make more transparent the addition of new stresses function, encapsulating each strategy in its own classes. The present version, as presented in the previous Chapters, implements a "two leaves" model. The structure of Prospero can be made more flexible to represent a multi-layers model by parsing the radiation contribution among the layers separately from Prospero itself (Prospero 2.5 Project).

4.11 Support

Support for users can be obtained by writing at the:

- GEOframe Users Group

Developers should write to the:

- GEOframe Developers Mailing List

4.12 Policies of the GEOframe (Prospero) community

Anyone is free to contribute. However, the suggestion is to start with branching our code, modifying it and eventually call issue a pull request. Giving appropriate credits for the intellectual input through coauthor ships or citations should be the proper functioning of the community. The formal, legal conditions that govern the use of GEOframe at present are given by the G.P.L. v 3. Any new GEOframe component can have its own license though. A **developer** is any person whose expertise has either significantly

- influenced the design of GEOframe code or
- who has written code,

with no distinction between scientific and technical inputs.

- Financial support alone is **not enough** to claim for being a code author. This should be recognized in Acknowledgments (see below)
- For being added as co-author of an existing code, modifications have to be substantial, not simply a bug fixing which is recognized in Acknowledgment. Essentially this status is discussed upon a pull request.

When contributing to Prospero, or any other GEOframe piece, developers should consider the following:

- Provide a brief description of what their contribution does.

- Recognize the previous authors of the code and the following modifiers.
- Describe the input required by their contribution and its output.
- Add some notes concerning the limitations, and the algorithms used within the component. A wish-list for the future version and/or information (as done in this Chapter).
- Mention articles or books which have inspired the codex or justified its necessity. Users are encouraged to cite these papers in their own work.

Which is what this Chapter is about.
The contributors, please see also: The GEOframe publication policy 1.0 document.

4.13 Acknowledgements

- Michele Bottazzi and Riccardo Rigon developed the theoretical aspects of Prospero (Authors).
- Michele Bottazzi designed the first version of the code (Authors)
- Michele Bottazzi implemented and deployed it (Authors)
- Riccardo Rigon provided financial support
- Concetta D'Amato made bug fixing regarding some aspects of beta version of the Prospero code
- Michele Bottazzi and Concetta D'amato wrote the documentation of the Notebooks

CHAPTER 5

POINTWISE ESTIMATES

In this section we compare the results obtained with the Prospero component with those obtained with the other components present in the GEOframe system, that is PM FAO and PT.
These methods are applied to two case studies. The performances are compared at plot scale, using direct latent heat measurements provided at hourly, monthly and annual timescale. The two case studies are represented by two alpine pastures: the Torgnon site, in the Val d'Aosta, and the Viote del Monte Bondone site, in Trentino (Italy). Pastures were chosen as they present a simpler canopy structure and therefore considered more suitable for validating the method. Both are FLUXNET sites and therefore equipped with eddy covariance stations, which provide a direct measure of latent heat. The data provided by FLUXNET stations are first analyzed and corrected to close the energy budget. All the models are driven by the same hydro-meteorological forcings, and no parameters calibration was performed. All the model behave surprisingly well, at least when the data are aggregated at the monthly time-scale but Prospero outperforms all of

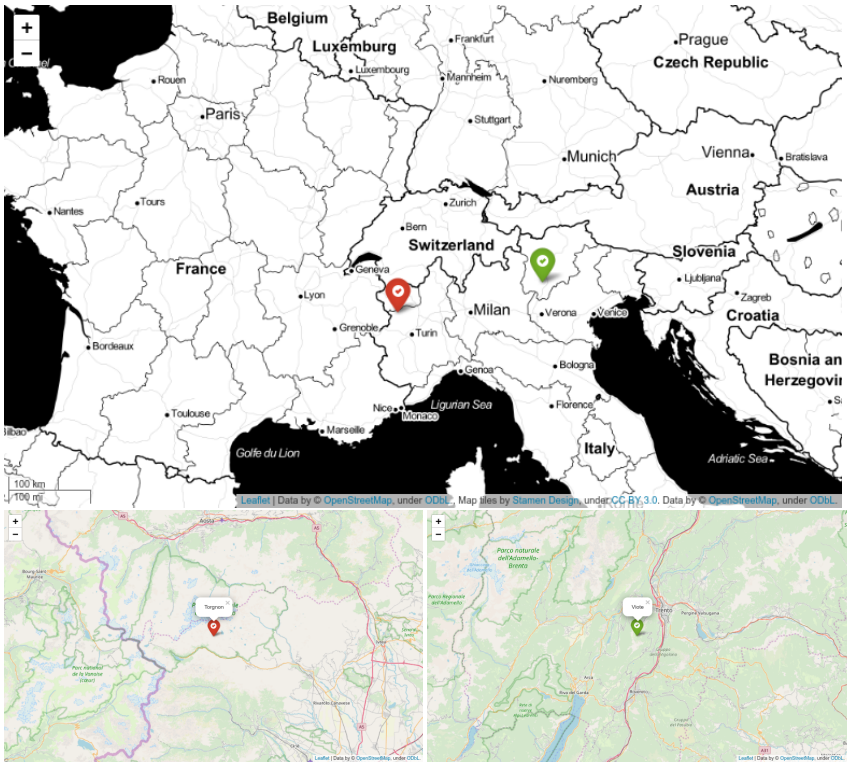

Figure 5.1: Map of the case studies, Torgnon (red marker) and Viote (green marker).

them. PT is shown usually to overestimate evapotranspiration, while FAO usually underestimated it. Also Prospero, on average, slightly underestimate evapotranspiration but much less than FAO and it is almost bias-free.

Obviously Prospero, besides providing evapotranspiration also returns the surfaces temperature and the sensible heat flux from the transpiring surface, which are reported and commented. We could not exploit the value of this variables here but they can be the occasion for future comparison and assessments.

5.1 Torgnon

The Torgnon site, active since June 2008, is an unmanaged subalpine grassland located a few kilometers from the village of Torgnon in the northwestern Italian Alps (Aosta Valley, 45° 48'25.6" N 07°34'15."2 E) at an elevation of 2160 m asl. In the past the site was used for domestic livestock grazing and was abandoned in late 1990s (Cremonese et al., 2010). Vegetation is mainly composed by matgrass with other graminoids and forbs as co-dominant species. The site is characterized by an alpine climate with strong seasonality. The mean annual temperature is 3.1°C and mean annual precipitation is about 880 mm, however growing season cumulative precipitation can show huge variations (from 160 to 630 mm). On average, the site is covered by a thick snow mantle (90-120 cm) from the end of October to late May, which limits the growing season length to four-five months. The peak value of leaf area index (LAI) is on average 2.2 $m^2/m^2$and maximum canopy height is 0.2 m. Continuous eddy covariance (EC) measurements of CO_2 and H_2O fluxes are carried out since June 2008, additionally, a weather station provided 30-min averaged records of different meteorological parameters, including air and soil temperature, soil water content, soil heat flux, net radiation, photosynthetically active radiation, snow height, precipitation, wind speed. Radiometric indexes like NDVI and PRI and greenness timeseries are collected by different unattended sensors.
Soil is mainly composed by silt and sand (40-50% silt, 50-60% sand, 4-6% clay, Galvagno et al., 2013).
This site is managed by the Arpa Valle d'Aosta.

5.2 Viote

The Viote site is located at 1550 m a.s.l. on a mountain plateau in the Italian Alps (Viote del Monte Bondone, 46° 01' 46.8" N; 11° 04' 58.3" E). The mean annual air temperature is 5.5^oC with monthly averages ranging from -2.7^oC in January to 14.4^oC in July. The mean annual precipitation is about 1189 mm, with peaks in June (132 mm) and October (142 mm); snow cover occurs between November and April.
The area is managed as an extensive meadow. The maximum canopy height at the peak of the growing season (mid June to early July) can reach up to 30 cm. Meadows represent the main land use on this plateau ($2km^2$) and are traditionally managed for hay production with low mineral fertilization and one cut per year in mid-July. (Papale et al., 2015).
Also in this site a continuous eddy covariance (EC) measures CO_2 and H_2O fluxes, and a weather station provided 30-min averaged records of different meteorological parameters, including air and soil temperature, soil water content, soil heat flux, net radiation, photosynthetically active radiation, snow height, precipitation, wind speed.
The soil is mainly composed of silt, sand and clay (Papale et al., 2015).
This site is managed by the Edmund Mach foundation of San Michele all'Adige.

5.3 Data on Evapotranspiration

FLUXNET sites are considered as case studies because they provide complete data sets of meteorological measurements and heat fluxes. In fact, eddy covariance observations are ones of the few ones that allow a direct measurement of evapotranspiration.

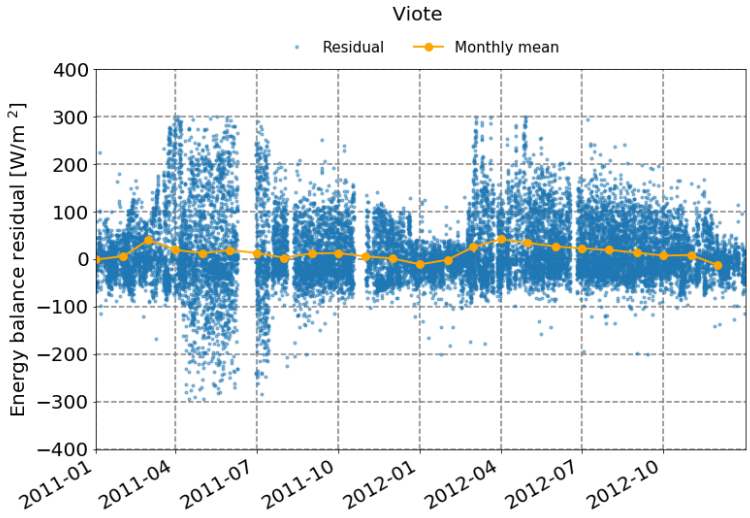

Figure 5.2: Energy balance residual on Viote.In orange the monthly mean and in blue the hourly deviations.

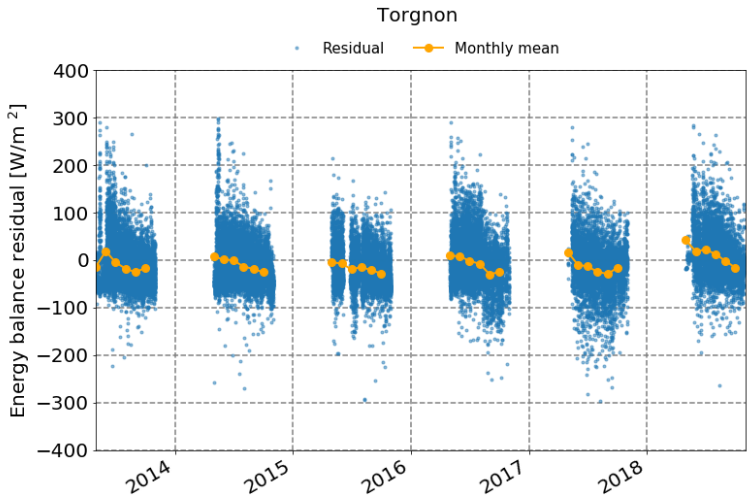

Figure 5.3: Energy balance residual on Torgnon. In orange the monthly mean and in blue the hourly deviations.

However, the turbulent fluxes measured by eddy covariance stations are often underestimated (Castelli et al., 2018). Therefore, to validate Prospero, we first check the closure of the energy balance in data. To guarantee this, the energy balance at the station is calculated as the sum of the fluxes (Eq. 5.1) and it is verified that the energy balance is closed (Wohlfahrt et al., 2009).

$$R_s - R_{ll} - G - E_l - H_l = \Delta E \tag{5.1}$$

where ΔE is the residual of energy budget. If there is no underestimation and assuming the internal energy variation negligible or instantaneous, as explained in Chapter 2, ΔE should be zero or close to zero. However, this does not occur in most cases and the energy balance returns a non-zero residual. Often, instead, the residue obtained results to be of the same order of magnitude as the observed value. Of course, also radiation and soil heat flux measurements can be affected by an instrumental errors, but most frequently a systematic bias is given by eddy covariance measurement of turbulent fluxes, which do not include advective fluxes and large-scale eddies (Twine et al., 2000).
As we can see in the Fig. 5.2 and 5.3 the energy balance is almost never closed. The mean error, represented in orange is close to zero, but the hourly error can be as large as 300 W m^{-2}.

This problem is well known in the scientific community and widely treated Twine et al. (2000), Wohlfahrt and Widmoser (2013) and a detailed analysis is presented by Foken (2008).
Although it is clear that the hypotheses behind the eddy covariance method (Aubinet et al., 1999) are more likely to be violated in orographically complex terrain than flat and homogeneous ones,the lack of closure of the energy balance in this the study falls well within the range of values observed in a wide range of FLUXNET sites (Stoy et al., 2013) and that the closure of the energy balance is generally not worse than for mountain grasslands

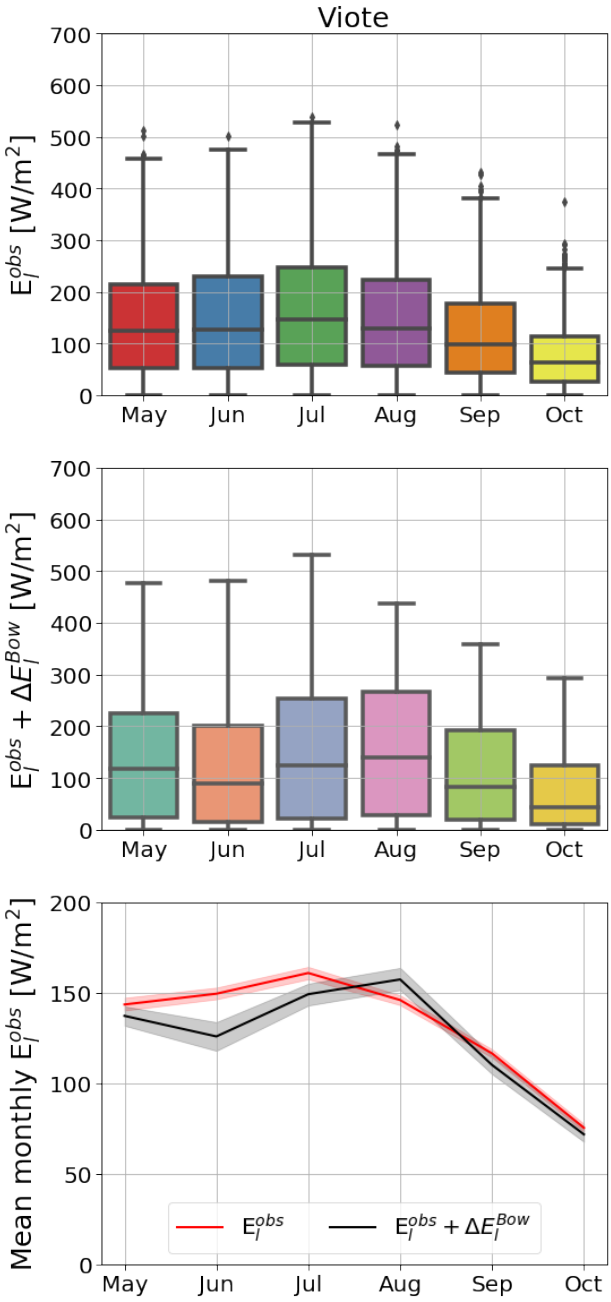

Figure 5.4: Monthly distribution of latent heat in Viote site before and after the correction of the energy balance based on the Bowen ratio (boxplot) and the mean monthly value (band represent the 95% of the confidence interval)

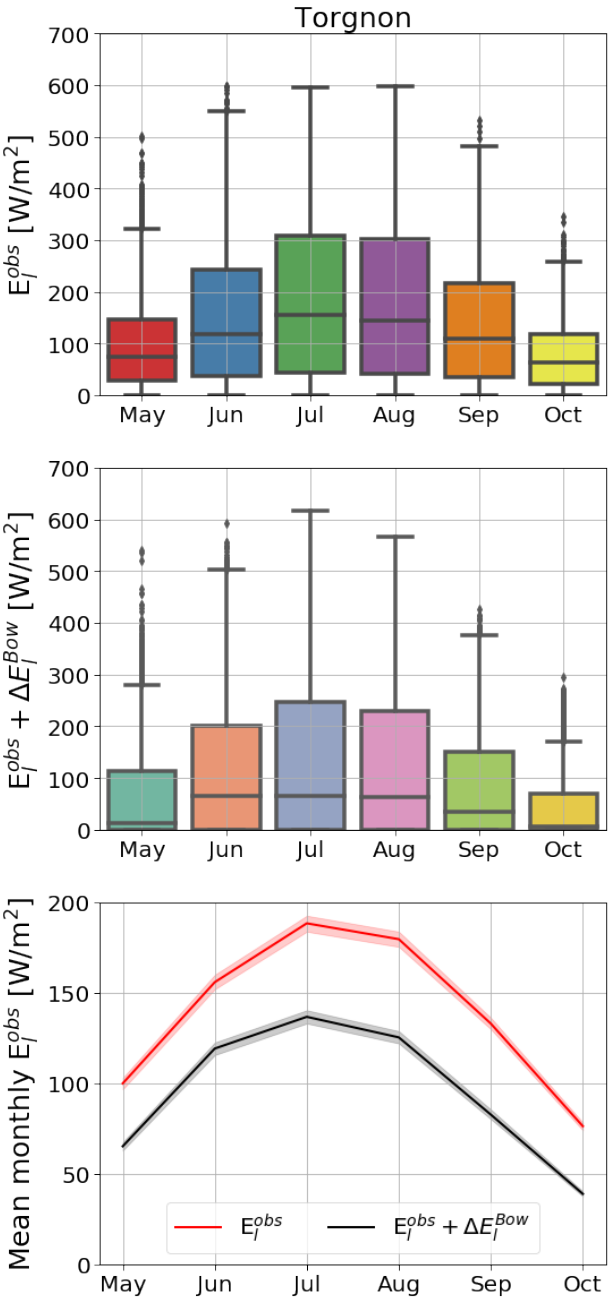

Figure 5.5: Monthly distribution of latent heat in Torgnon site before and after the correction of the energy balance based on the Bowen ratio(boxplot) and the mean monthly value (band represent the 95% of the confidence interval)

in complex topography (e.g. Hammerle et al., 2007; Hiller et al., 2008).

In any case, it was decided to discard the data when the error on the closure of the energy balance is too high and the usefulness of E_l and H_l for the validation of the model is significantly reduced. The same criteria used successfully by Castelli et al. (2018) were also used in another alpine pasture, the Val di Mazia site (LTSER, long-term socio-ecological research), also present in the Trentino Alto-Adige region, not far from the Viote site.

We therefore excluded the measurements from our analyzes when the ΔE exceeds 300 Wm^{-2}:

$$R_s^{obs} - \delta R_{ll}^{obs} - G^{obs} - E_l^{obs} - H_l^{obs} \geq 300 W m^2 \tag{5.2}$$

and when the relative closure exceeds 0.4, i.e. when there is a strong imbalance between the fluxes, the radiative ones and heat ones:

$$\frac{R_s^{obs} - \delta R_{ll}^{obs} - G^{obs} - E_l^{obs} - H_l^{obs}}{R_s^{obs} - \delta R_{ll}^{obs}} \geq 0.4 \tag{5.3}$$

Furthermore, only dates when all the measures of the energy fluxes and environmental forcings are available, are considered. In addition, due to the snow cover during the winter, the analysis is limited to the period from early May to late October. This involves a large reduction in the initial data set.

Once the residual has been calculated, it is used to force the closure of the energy balance. This is done using two commonly adopted approaches (Twine et al., 2000; Wohlfahrt et al., 2009; Wohlfahrt and Widmoser, 2013).

In the first case, which represents the 'worst case scenario', the residual ΔE is used to correct only the latent heat, therefore we assume that all the error is committed on it.

$$\Delta E = R_s^{obs} - \delta R_{ll}^{obs} - G^{obs} - E_l^{obs} - H_l^{obs} \tag{5.4}$$

Where:

- ΔE is the residual of the energy budget [W/m^2];
- R_s^{obs} is the observer value of the shortwave radiation [W/m^2];
- δR_{ll}^{obs} is the observed value of the net longwave radiation, i.e. the difference between downwelling and upwelling [W/m^2];
- G^{obs} is the observed value of the soil heat flux [W/m^2];
- E_l^{obs} is the observed value of the latent heat flux [W/m^2];
- H_l^{obs} is the observed value of the sensible heat flux [W/m^2].

And:

$$E_{l,cor}^{obs} = E_l^{obs} + \Delta E \tag{5.5}$$

while all the other quantities remain unchanged. In the second case is based on the Bowen ratio and it uses the residue to correct both the latent heat and the sensitive one:

$$B_{ratio} := \frac{E_l^{obs}}{H_l^{obs}} \tag{5.6}$$

Therefore, the sensible heat results:

$$\Delta H_l^{Bow} = \Delta \cdot \frac{1}{1 + B_{ratio}} = \Delta \cdot \frac{H_l^{obs}}{|H_l{}^{obs}| + |E_l{}^{obs}|} \tag{5.7}$$

and the correction to the latent heat is

$$\Delta E_l^{Bow} = \Delta - \Delta H_l^{Bow} \tag{5.8}$$

resulting finally in:

$$E_{l,cor}^{obs,Bow} = E_l^{obs} + \Delta E_l^{Bow} \tag{5.9}$$

$$H_{l,cor}^{obs,Bow} = H_l^{obs} + \Delta H_l^{Bow} \tag{5.10}$$

Soil composition	Viote	Tognon	θ_{fc}	θ_{wp}
Sand	17%	45%	0.07-0.17	0.02-0.07
Silt	74%	55%	0.28-0.36	0.12-0.22
Clay	9%	5%	0.32-0.40	0.20-0.24

Table 5.1: Soil composition in Viote and Torgnon site.

	Viote	Tognon
θ_{fc}	0.289	0.248
θ_{wp}	0.153	0.124

Table 5.2: Values of field capacity and wilting point obtained for the two sites based on the soil composition

Since it is generally calculated on daytime, i.e. when both E_l and H_l are positive, there are no problems at the denominator. To avoid these problems, we consider the absolute value of the heat fluxes.
After this correction, the residual is recalculated to verify that the energy balance is correctly closed.
The corrected values of the latent heat estimation is reported in Figure 5.4 for the Torgnon site and in Figure 5.5 for the Viote site. In both Figures are reported: on top the boxplot of the original measurements, in center the corrected measures, and on the bottom the correction. All the figures are shown at the monthly time scale.
LAI data for Torgnon are provided as mean monthly values over the entire period. For Viote, the leaf area index values are not available and so they are derived from satellite Terra MODIS. Terra MODIS data (MOD15A2H) have a 8-days frequency and a resolution of 500m. Massive data download was done using the Pymodis package.
The values of water field capacity(θ_{fc}) and wilting point (θ_{wp}) for the two sites are calculated by means of weighted averages

on the soil composition (Tab. 5.1 and 5.2).

5.4 Models, their setup and parameterisation

To model evapotranspiration, we used, besides Prospero, the Priestley Taylor (Priestley and Taylor, 1972) formulation and the FAO version of the Penman-Monteith equation (Penman, 1948). Their equations can be found in Appendix A, while Prospero was extensively presented in the previous Chapter 4.1. In the following we briefly describe their requirements in term of parameters and setup. All the models require to be fed by radiation measurements or their estimation. These estimations has been performed by using the shortwave and longwave component GEOframe. The hydrometeorological parameters do not have to be elaborated, since they are measured in site. The configuration of components for both the PT and FAO models inside the GEOframe framework are represented in Figure 5.6 and 5.7. Components connection for Prospero is presented in Figure 4.3.

Priestley-Taylor In this component the only parameter present is α, which links potential to real evapotranspiration. We set α equal to the average value reported in literature (1.26, Priestley and Taylor, 1972; Cristea et al., 2013).

Penman-Monteith FAO In the Penman-Monteith FAO component there are two sets of parameters: those related to vegetation and those related to soil.
We know that both Viote and Torgnon are pastures, so we can use the parameters for grazing pasture reported by (Allen et al.,

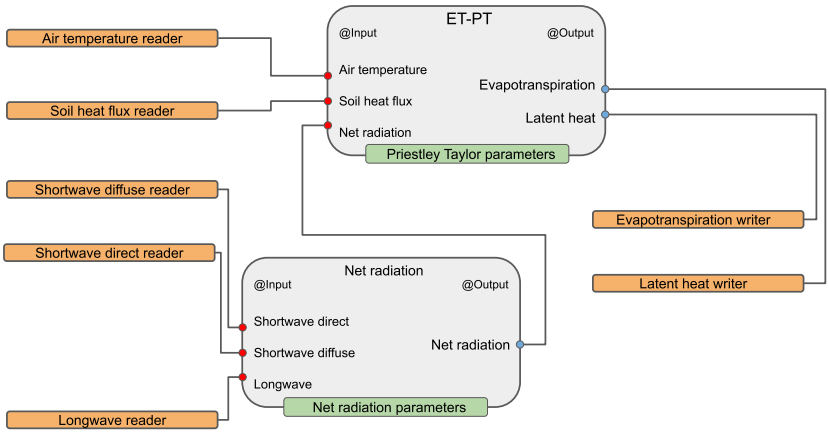

Figure 5.6: Components connection for Priestley-Taylor evapotranspiration.

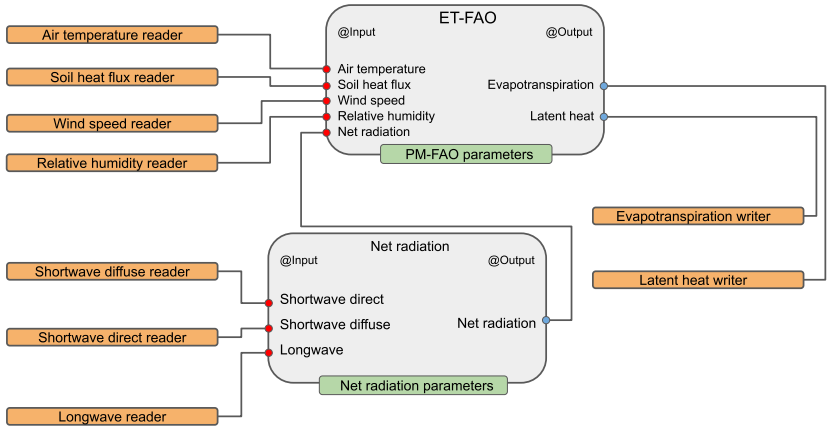

Figure 5.7: Components connection for Penman-Monteith FAO evapotranspiration.

Pasture	Viote	Torgnon
Vegetation		
crop coefficient ($K_{c,mid}$)	0.75	0.75
roots depth	0.75	0.75
depletion fraction	0.55	0.55
canopy height	0.2	0.2
Soil		
water wilting point	0.153	0.124
water field capacity	0.289	0.248

Table 5.3: Values for PM-FAO component for the two sites.

1998) and reported in the table 5.3.
The crop coefficient, K_c, is the ratio of the crop ET_c to the reference ET_0, and it represents an integration of the effects of crop height, albedo, canopy resistance and the evaporation from soil that distinguish the crop from reference grass.
Currently there is no possibility of set the crop coefficient (K_c) with multiple values, i.e. for the initial stage ($K_{c,ini}$), for the mid-season stage ($K_{c,mid}$) and for the end of the late season stage ($K_{c,end}$), so we decide to use $K_{c,mid}$ (Allen et al., 1998).
The soil parameters are set by knowing the composition of the soils in the two sites. The values of θ_{fc} and θ_{wp} are calculated with a weighted average on the composition.

Prospero The stomatal conductance in Prospero is computed using equation 4.4 and g_{sw} is obtained using equation 3.7. In this component the parameters for stress and soil are fixed (Tab. 5.4). For the parameters relating to soil and water stress, the same parameterization used for the FAO component (Tab. 5.3) is used (Allen et al., 1998).
The parameters of the other stresses are set equal to the values found in the literature, there is no reference range (Jarvis and

Parameters	Viote	Tognon
Vegetation		
canopy height	0.2	0.2
roots depth	0.75	0.75
depletion fraction	0.55	0.55
Stress		
α	0.005	0.005
θ	0.85	0.85
VPD_0	5.0	5.0
T_l	0.0	0.0
T_o	18.0	18.0
T_u	35.0	35.0
Soil		
water wilting point	0.153	0.124
water field capacity	0.289	0.248

Table 5.4: Parameters used for Prospero simulations in Viote and Torgnon.

Mcnaughton, 1986; White et al., 1999; Noe and Giersch, 2004). The simulations are carried out on all complete periods, (2011-2012 Viote, 2013-2018 Torgnon). Simulations' parameters are not calibrated.

5.5 Results

The performances of the three components are evaluated by calculating the *mean absolute error* and *root mean square error* calculated on the whole periods are reported in table 5.5. RMSE and MAE calculated on the results of Prospero are almost equal on both sites. On the contrary, FAO's performances show a variation of more than 50%, at the same time being the model that

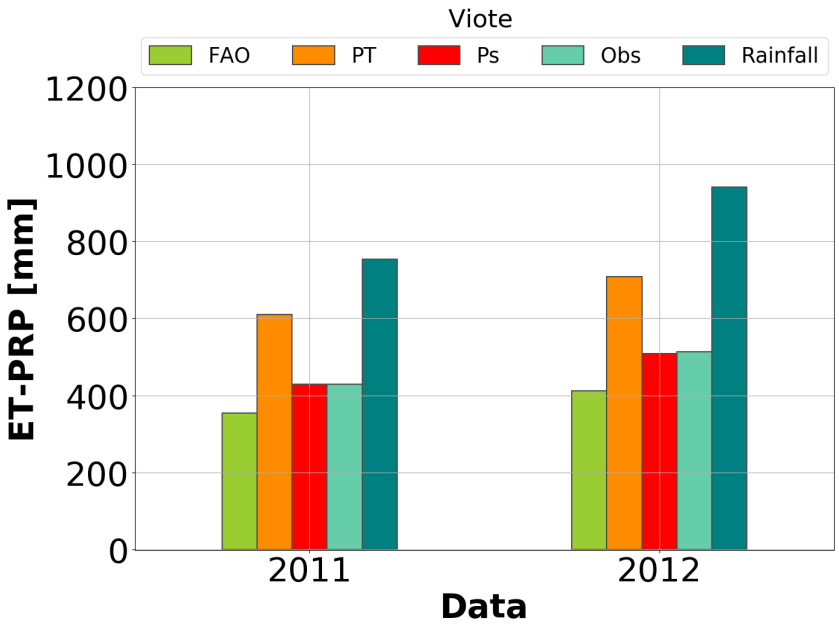

Figure 5.8: Total annual evapotranspiration simulated and observed on Viote.

Viote	MAE	RMSE
Prospero	44.8	58.2
FAO	38.7	49.1
PT	67.4	88.9
Torgnon	MAE	RMSE
Prospero	42.9	53.6
FAO	62.6	75.7
PT	52.3	70.2

Table 5.5: *Root mean square error* and *mean absolute error* obtained on Viote and Torgnon simulations

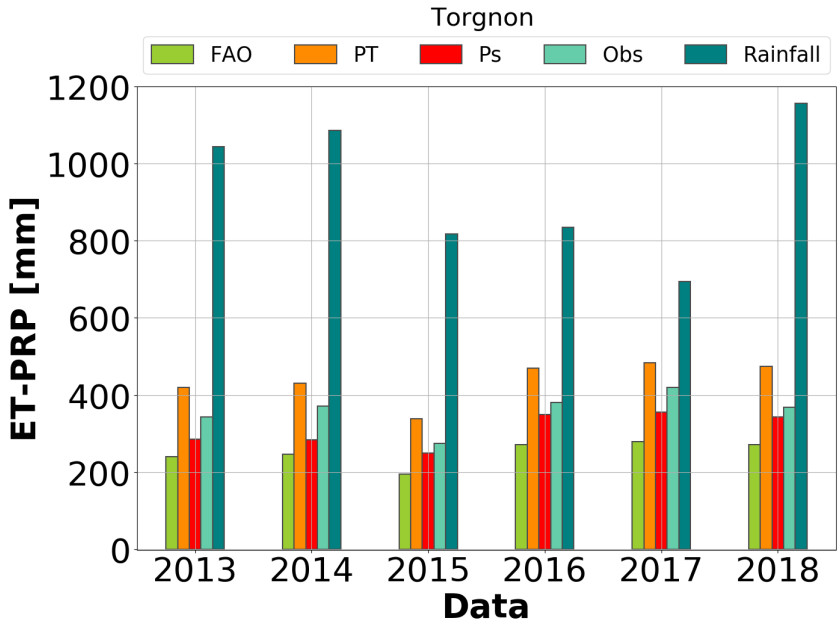

Figure 5.9: Total annual evapotranspiration simulated and observed on Torgnon.

provides the best results on Viote and the worst on Torgnon.
The results are represented by scatter plots in Figures 5.16 and 5.17. We can see that there is an underestimation of the FAO method compared to the observed, more marked for the Torgnon site, while for the Viote site this underestimation is more linked to the maximum values of E_l, not returning values of E_l greater than 400 W m^{-2}.
In fact, almost all the simulated values are below the secant (black line). This underestimation can be easily noticed by observing the regression of the calculated-observed data, represented by the orange line, which shows a lower trend compared to the ideal one, represented by the black line.
The results obtained through the Prospero component show a trend more coherent with the theoretical one but with a greater dispersion. This dispersion is further accentuated for the min-

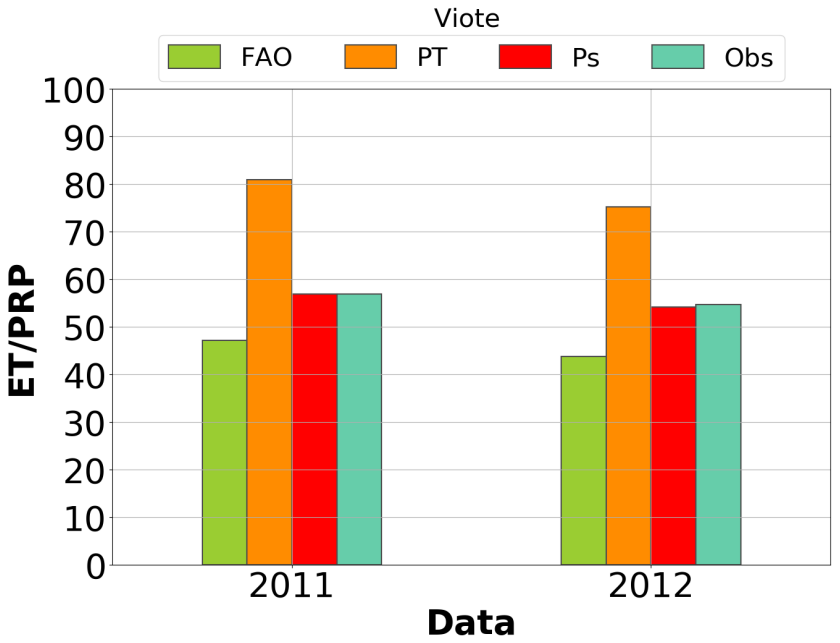

Figure 5.10: Ratio between the total annual evapotranspiration, both simulated and observed, and precipitation on Viote.

imum values of Viote. This is reflected in a higher RMSE (Tab. 5.5) on Viote than the one obtained with the FAO method. These errors are however comparable with those typically obtained in estimating latent heat (Blyth et al., 2010; Ershadi et al., 2014; Zhu et al., 2014).

Observing also the hourly scale MAE (Fig. 5.15) it can be seen how Prospero gives a more constant trend during the 24 hours, unlike FAO and PT, which show a bias due to the daily cycle, thus demonstrate that they are not able to represent well the daily evolution of evapotranspiration. This type of bias is not present even in the monthly MAE and it can be seen that Prospero's performance is substantially better (Fig. 5.5 and 5.5). Probably Prospero performances at hourly scale are better because it assess the closure of the energy balance and it also includes a time-dependent

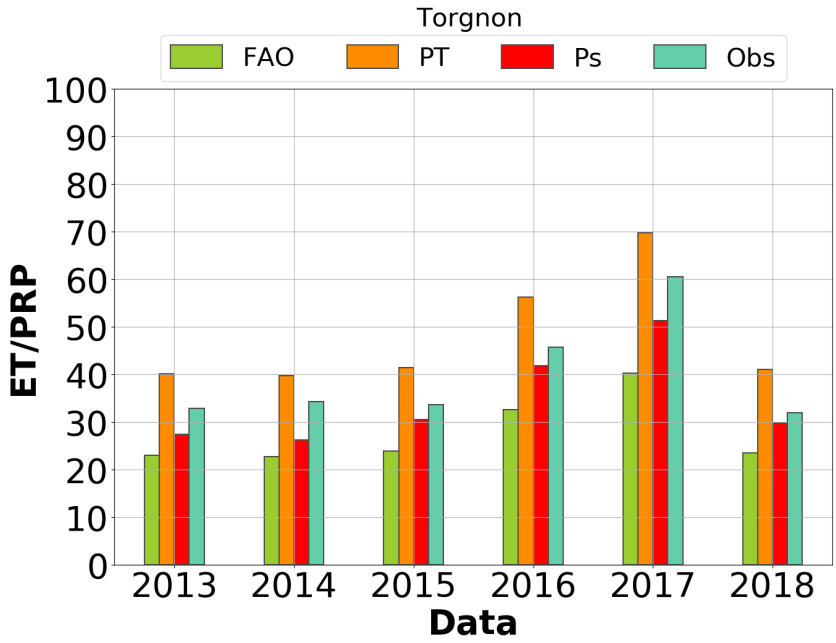

Figure 5.11: Ratio between the total annual evapotranspiration, both simulated and observed, and precipitation on Torgnon.

stomatal conductance model, in addition to canopy model that depends on the sun angle.

By comparing the estimated values on an annual scale with the observed values we can see that PT has a strong overestimation compared to the observed evapotranspiration, representing about 75-80% of the observed rainfall, while the real evapotranspiration turns out to be approximately 55% annual rainfall. This value is certainly well represented by the Prospero, while FAO underestimates it.
Evapotranspiration in the Torgnon site is slightly lower than in the Viote, probably because it is higher and colder.
In Torgnon evapotranspiration accounts from 30 to 60% of precipitation. This variation is due to the strong variation of annual precipitation, which can reach 400 mm/year. FAO's perfor-

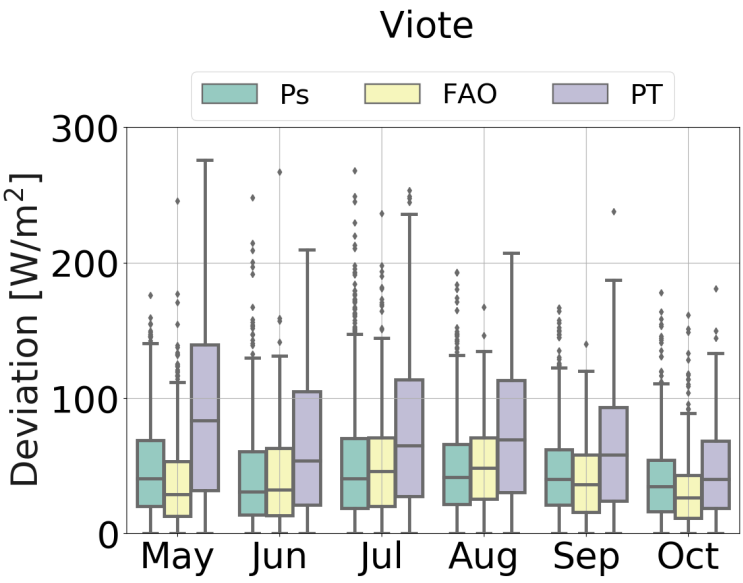

Figure 5.12: Boxplot of the difference between simulated and observed grouped at monthly timescale for Viote site.

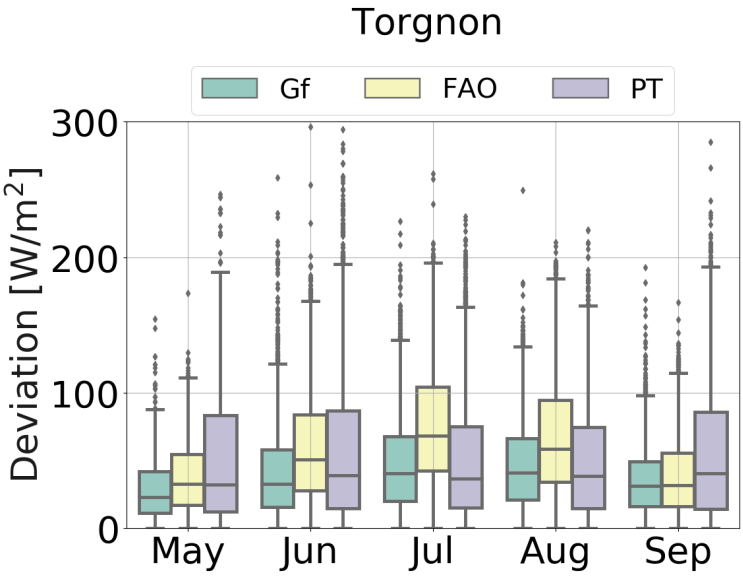

Figure 5.13: Boxplot of the difference between simulated and observed grouped at monthly timescale for Torgnon site.

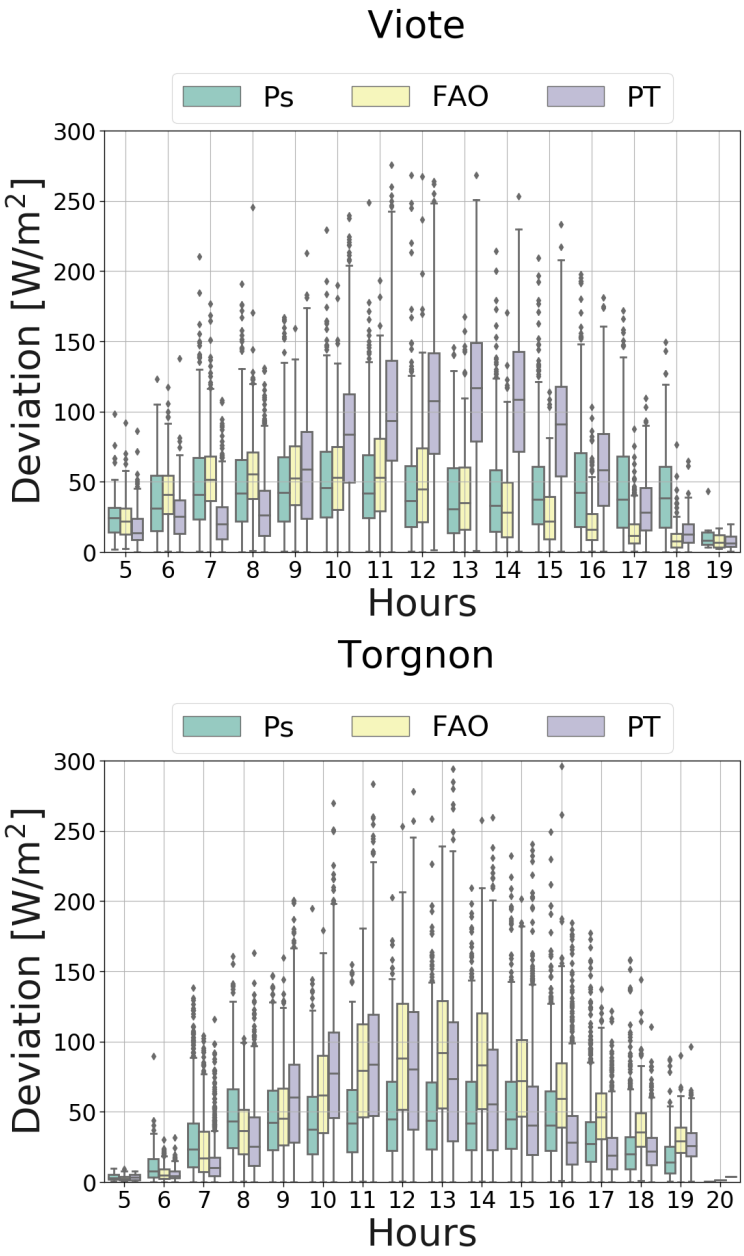

Figure 5.14: Boxplot of the difference between simulated and observed grouped at daily timescale.

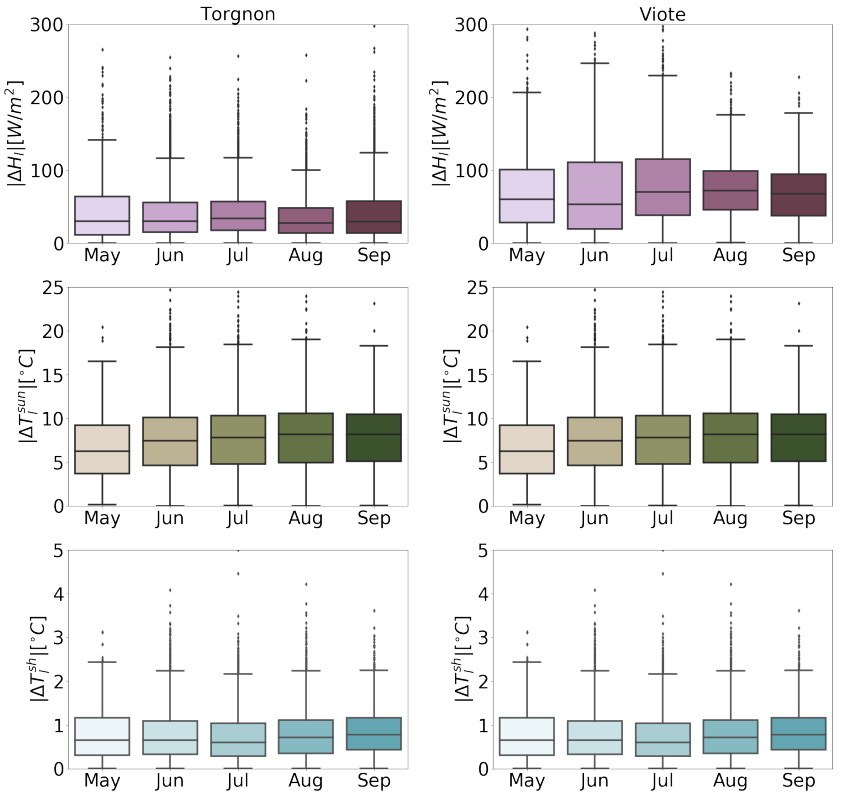

Figure 5.15: Absolute deviation between the observed sensible heat and the estimated sensible heat ($|\Delta H_l|$). Estimated sensible heat is obtained as the sum of the one generated by the sunlit and the shaded canopy (Eq. 4.19). Absolute deviation between the measured air temperature and the equilibrium temperature (Eq.4.16) of the sunlit canopy ($|\Delta T_l^{sun}|$) and the shaded equilibrium temperature ($|\Delta T_l^{sh}|$).

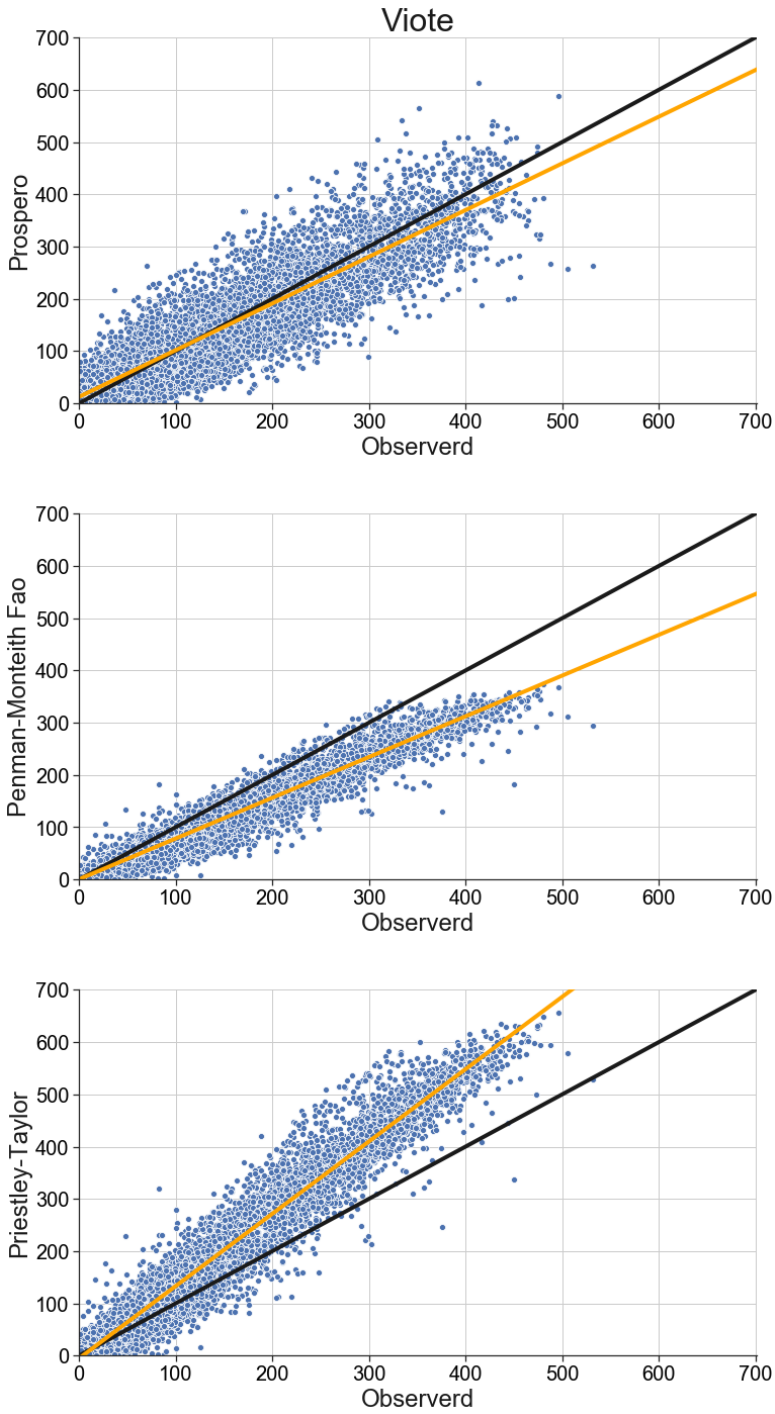

Figure 5.16: Scatter plot simulated vs observed.

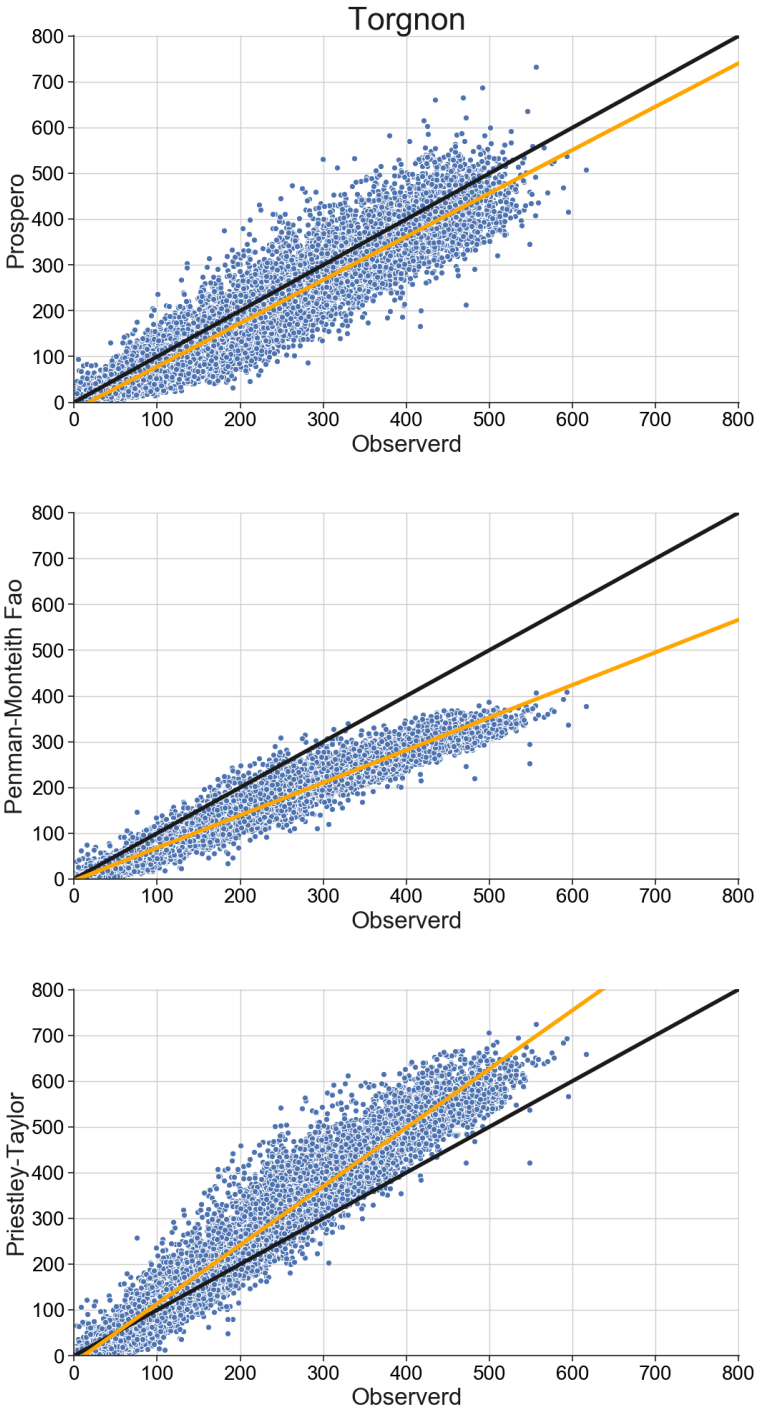

Figure 5.17: Scatter plot simulated vs observed.

mances are good on the Viote case study, while on the contrary they show a big difference on the Torgnon site, especially at an hourly rate (Fig. 5.5 and 5.5).
In general it can be said that the performances provided by Prospero at plot scale are better than the other methodologies and that even without calibration they capture the measured evapotranspiration pattern well, causing an error comparable with that obtained from other studies carried out on alpine grasslands (Blyth et al., 2010, Ershadi et al., 2014, Zhu et al., 2014).

5.6 Conclusions

In this Chapter we verified the pointwise behavior of the Prospero model component against FLUXNET data and the behavior of other two well known evaporation formulas. The results can be considered highly satisfactory, considering that no parameter was calibrated. The behavior of the traditional method by Priestley-Taylor and FAO (based on the Penman-Monteith equation) give also good results, on average, but they are outperformed by the Prospero model. It should be noted that in Torgnon PT generally overestimates the total evapotranspiration, while FAO underestimates it, viceversa on Viote site.
Additionally Prospero provide an estimation of the leaf temperature and sensible heat. The canopy temperature is compared with air temperature and shows a deviation among 5-10°C, is in accord with the classic range of variation find in literature (Andrews et al., 1992, Martin et al., 1994, Duffkova et al., 2006), while the latter gives an error comparable with the one on latent heat.
Lastly this chapter highlights how difficult it is to have reliable and accurate measurements of evapotranspiration and how important it is therefore to have models available physically based models that can provide good performance even in the absence

of calibrations.

CHAPTER 6

CATCHMENT-BASED ESTIMATES

This case study is part of the SILVA research project (***S**cambi **I**drici tra suo**L**o, **V**egetazione e **A**tmosfera: un'analisi comparativa in due bacini forestati italiani - Water exchanges between soil, vegetation and atmosphere: a comparative analysis in two Italian forested basins*). This project was done in collaboration with Giulia Zuecco, Ph.D (university of Padova) and Alessandro Errico, Ph.D (university of Firenze), presented at the Italian Hydrological Society and winning the 'Florisa Melone' award. The SILVA research project has as its main objective the improvement of the understanding of the hydrological response in two forested basins in the Pre-Alpine and Apennine area characterized by different climatic conditions, identifying the fundamental hydrological mechanisms that regulate the seasonal-event-scale inflow-runoff on forest basins and the impact of evapotranspiration on the generation of outflow, analyzing the hydrological response also in different scenarios of land use and modification of evapotranspiration flows. During the year of the SILVA research project, the collection of hydro-meteorological and veg-

etation data was carried out by Giulia Zuecco and Alessandro Errico at the experimental basins of Rio Ressi (Vicentine Prealps) and Re della Pietra (Tuscan-Emilian Apennines), they also elaborated and analyzed the hydrological response of the two basins on a monthly scale and of the identified inflow-outflow events. I dealt with the geomorphological analysis of the two experimental basins, the preparation of the data to be used as input in the GEOframe-NewAGE modelling system, the calibration of the hydrological model and the analysis of the results given by the simulation. Unfortunately it was not possible to use the data collected on Re della Pietra due to problems with the instruments caused by frost. In fact, the timeseries of data on this basin is less than one year, making the calibration and validation of the model not possible. Therefore the Re della Pietra basin will be excluded from the subsequent analysis and will be re-proposed in future works if it will be possible to obtain a sufficient amount of data. The subsequent analysis is an investigation of the Rio Ressi hydrological functioning, based on the available measures and the modelling with Prospero of the evapotranspiration fluxes, otherwise not available, to obtain a credible perceptual model of the catchment. The sun-shade modality of Prospero was also used to discuss a little about the vegetation energy budget, as an initial step to be further investigated in the field. A preliminary modelling of the discharges is also pursued with the use of the ERM modelling solution, available within GEOframe.

6.1 Rio Ressi

Rio Ressi is an experimental basin located in the southern part of the Posina river basin (116 km^2) at the foot of the central-eastern Alps (45°47'11.79" N; 11°15'54.12" E), with an area of 0.02 km^2. The Posina river is a tributary of the Astico river that flows into

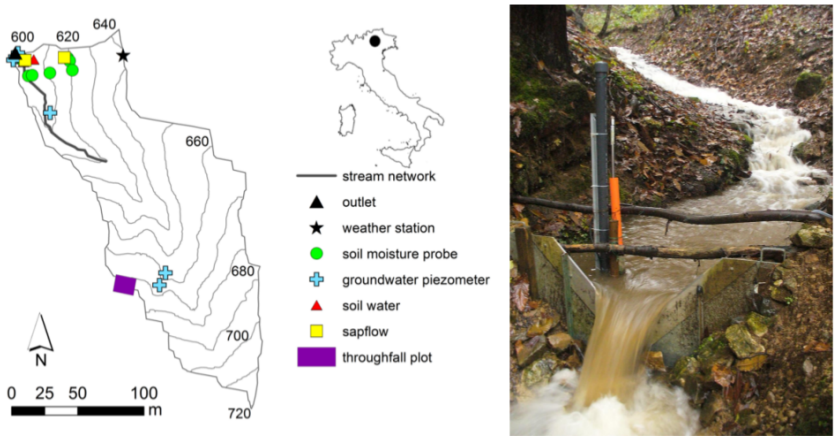

Figure 6.1: Experimental basin of Rio Ressi with gauges indicated. At the weir in figure the discharge is measured. Its position correspond to the outlet labeled in figure.

the Adriatic sea. About 74% of the Posina basin is densely vegetated (Norbiato et al., 2009), partly due to the marked expansion of deciduous forests in the last fifty years following the abandonment of agricultural practices. The basin is completely covered by the forest and the dominant species are beech, chestnut, hazel and mountain maple. Starting from July 2017, during the vegetative period, the sapflow rate in three beeches and one chestnut has been measured, while the quantity, spatial and temporal variability of the throughfall precipitation was monitored during the years 2013 and 2014 (Zuecco, 2016). All the gauges are shown in Figure 6.1. The climate is humid temperate and the average annual precipitation (1992-2007) recorded by a meteorological station in the central part of the Posina basin (at 597 m a.s.l., about 4.5 km in a straight line from Ressi) is 1695 mm. The average annual temperature is 9.7° C; average monthly temperatures fluctuate between 1.2° C in January and 18.7° C in July. Precipitation is concentrated in spring (150 mm and 159 mm on average, respectively in April and May) and in autumn (236 mm

and 246 mm on average in October and November, respectively). The altitudes in the study basin range from 609 to 725 m a.s.l. The average slope is 26°; the appearance is mainly north-west. The canal is about 150 m long. The frequently saturated channel and near-flat near-flow zone comprise about 1.5% of the basin area. Since August 2012, Rio Ressi experimental basin (Fig. 6.1) is subject to hydro-meteorological monitoring. Starting from May 2018, sensors were installed in the basin for the continuous measurement of air temperature, wind speed and direction, global solar radiation and relative humidity. For the period 2012-2017, data provided by the Regional Agency for Environmental Prevention and Protection of Veneto from four meteorological stations located a few km away from the Rio Ressi basin were used.
The meteorological variables are available with a frequency of 5 or 10 minutes, they are subsequently resampled on an hourly scale to be consistent with the flow measurements. The flow stage it was measured at an interval of 5 minutes by a pressure transducer behind a V-shaped dam. Flow was measured under different flow conditions using the volumetric method to verify the dam equation. Groundwater levels were monitored with 5 minute resolution in two riparian wells (GW1 and GW2) and in a well at the bottom of the slope (GW3). They are marked with a light blue cross in Figure 6.1. The depth of the wells was 2.04, 1.04 and 0.68 m respectively for GW1, GW2 and GW3. Another well (GW4, 1.80 m deep) was used for manual sampling of groundwater. For the examined period, only data of depth of water table of GW1 and GW4 are available. The soil moisture near the surface (0-30 cm) was measured at 10 minute intervals using four reflectometers. The probes were installed in different positions along a transect: SM1 was positioned in the riparian zone, about 1 m from the torrent, SM2 when passing between the riparian zone and the slope (footslope), SM3 in the central part of the slope and

SM4 in the upper part of the slope. They are represented with a green circle in Figure 6.1. These data can be requested to the group of Professor Marco Borga of university of Padova who manages the catchment. In addition, there are flow measurements detected by the hydrometer located in the closing section.
LAI is derived from throughfall measurements (Zuecco, 2016). Given the small size of the sub-basin, no interpolation of the meteorological data is considered necessary since the measurements are collected directly in the basin.
The geomorphological analysis of the basin used a digital elevation at resolution of 1 m and served to delineate the drainage directions, the network and the sky-view factor. Due to the small size of the Rio Ressi basin (about 21930 m^2), the homogeneity of the lithology and soils and the unbranched hydrographic network it was decided to use a single hydrological response unit for the pre-Alpine basin. Starting from the digital elevation model, the geomorphological analysis is carried out using the HortonMachine integrated into GEOframe (Abera et al., 2014; Formetta et al., 2011a; Formetta et al., 2013b; Rigon et al., 2011).

6.1.1 Data Analysis

Rainfall data provided by the measurements can be seen in Figure 6.2. The detailed analysis of the rainfall data, reveals that precipitation is spread throughout all the months but it's very irregular across the years. The average yearly precipitation along the record is 1797 mm but with a minimum of 1138 mm in 2015 and a maximum of 2965 in 2014, as it follows from figure 6.3. Monthly grouping of precipitations, in figure 6.4 shows that minimum precipitation occurs during January and December, while the maximum is during February and November. Runoff is con-

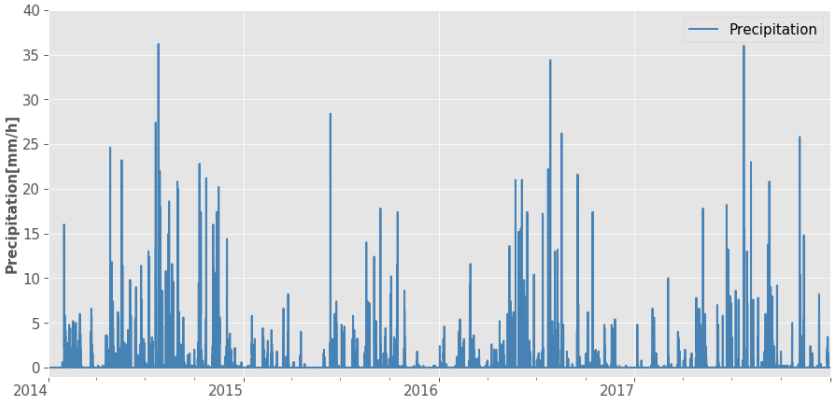

Figure 6.2: Hourly precipitation on Rio Ressi basin.

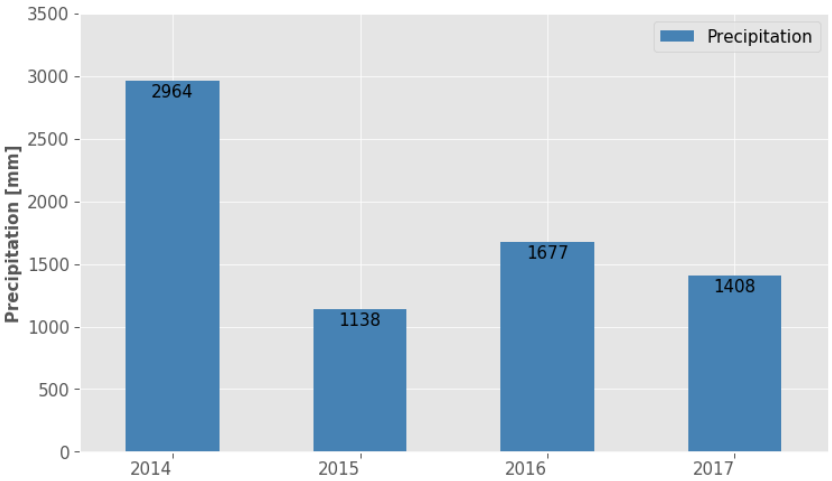

Figure 6.3: Yearly precipitation is highly variable among the years, with variation from 1138 to 2965 mm.

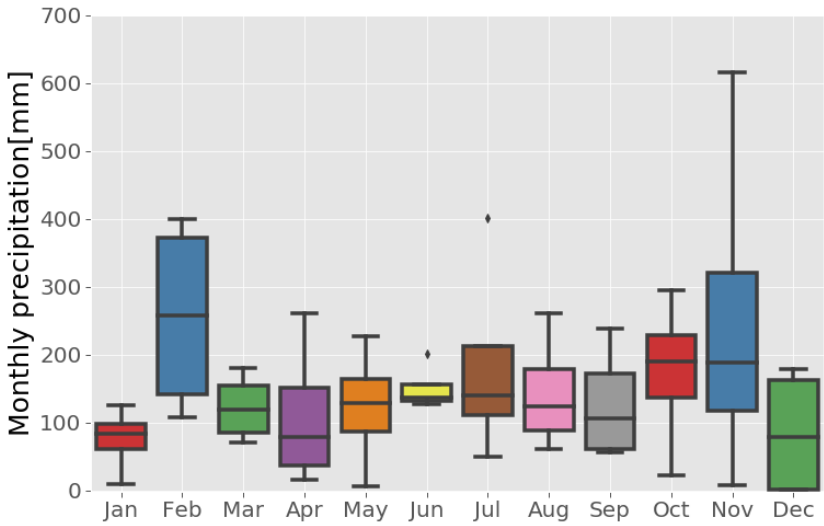

Figure 6.4: Boxplot with monthly distribution of precipitation.

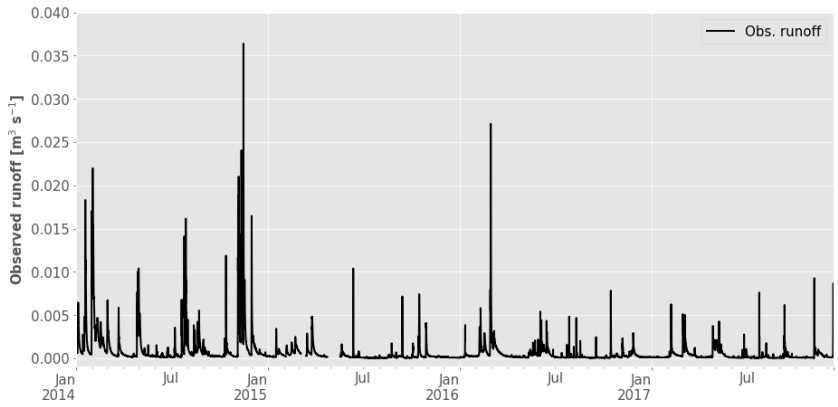

Figure 6.5: Measured runoff between 2014 and 2017 included.

sequential to the rainfall variation. It is represented in Figure 6.5 along the same years where rainfall was recorded. Figure 6.6 compares the runoff and precipitation volumes with interesting results. The figure shows that after an initial time in which precipitations fallen in years before than 2014 have an effect, the precipitation tends to be twice the runoff, meaning that, in the hydrological budget the sum of soil-moisture, groundwa-

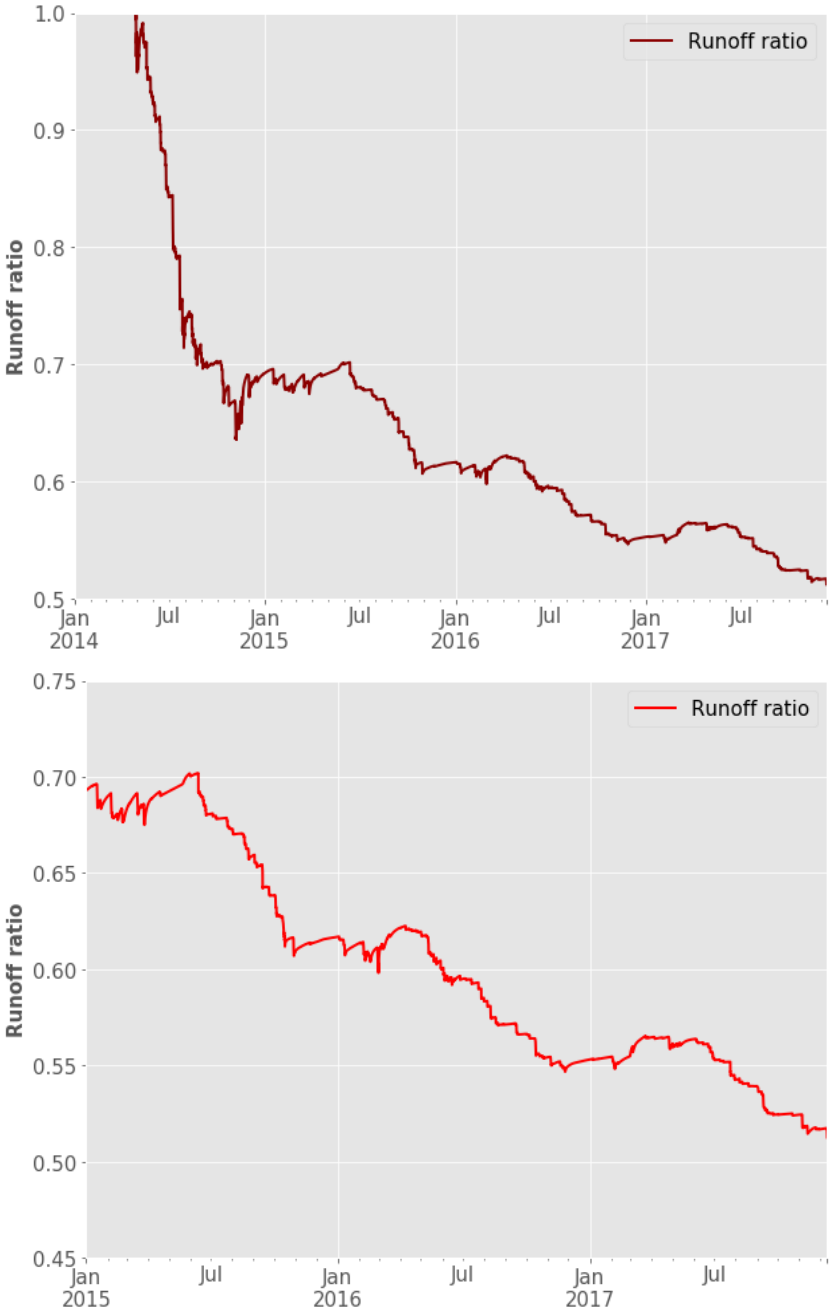

Figure 6.6: Runoff coefficients between 2014 and 2017, both included and between 2015-2017. Clearly the figure shows a decline of their ratio to 0.5.

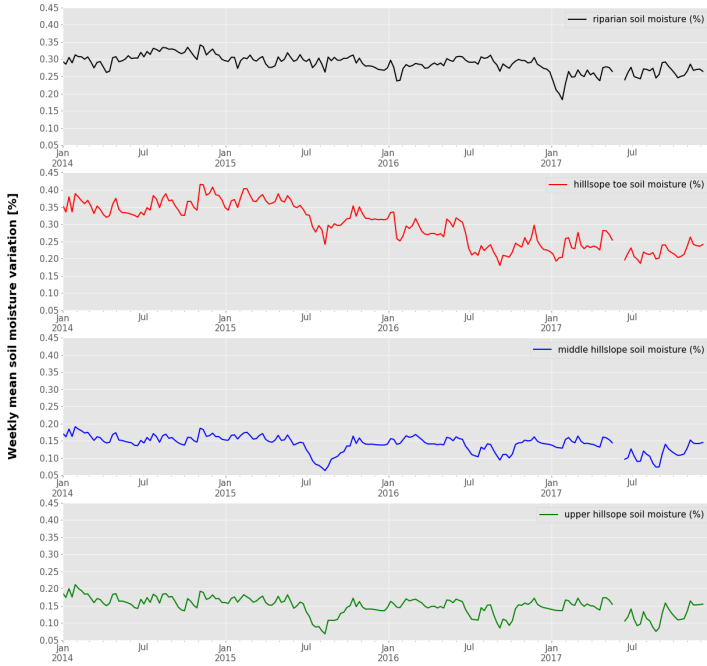

Figure 6.7: Mean weekly soil water content, expressed in $m^3\ m^{-3}$.

ter (recharge) and evapotranspiration is at least fifty per-cent of the budget. A second fact that it is important to remark is that the catchment seems to never be in some stationary equilibrium, with shorter cycles visible as humps during the seasons superimposed to a the main decreasing trend. This is by itself an important result, since it is generally believed that the dynamics of such small basins is easily captured in stationary behaviors, which is clearly not true for the Rio Ressi.

The data available also allowed us to analyze soil moisture and groundwater. Soil moisture can be derived from measuring the volumetric soil moisture content, as shown in Figure 6.7. It can be noticed that the measurements cluster into two groups. One

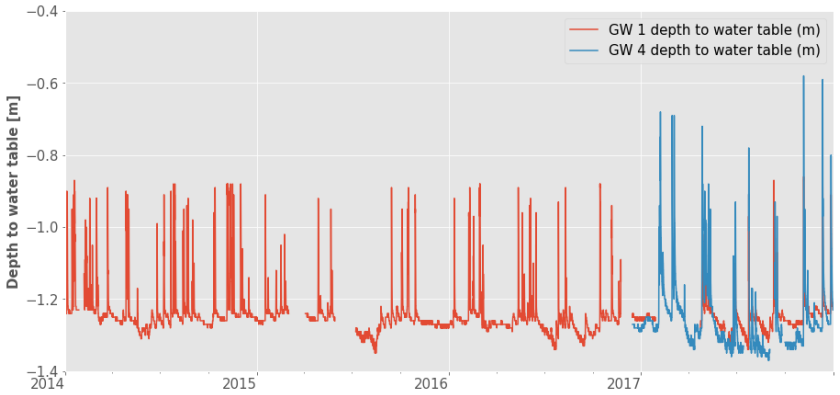

Figure 6.8: Measured depth to water table in the riparian zone, expressed in meters.

including hillslope toe and riparian gauge with a mean soil moisture around 0,29 and the other including the upper hillslope and the middle hillslope sites which measure an almost identical water content, around 0,14. Soil moisture water equivalent in mm can be estimated by using the measured soil moisture as a proxy of the mean volumetric water content and multiplying it by the groundwater depth. The latter, in turn, can be obtained by the measure performed in the GW1 and GW4 wells. The measured groundwater data are reported in Figure 6.8. From the previous data it can be estimated that the variation of the sum of soil moisture and groundwater is often bigger than the difference between measured precipitation and runoff. Therefore the soil moisture and groundwater data cannot be used to close the water budget at the wells. Locally, at the wells, in fact the water is:

$$ET = P - Runoff_n - \frac{\Delta S}{\Delta t} \tag{6.1}$$

where ET is evapotranspiration, P is precipitation, R_n the net outflow from the well and $\Delta S/\Delta t$ the variation of the soil-ground water amount. Unfortunately, as made evident from data, Runoff$_n$ must be negative (giving therefore a positive contribution in Eq.

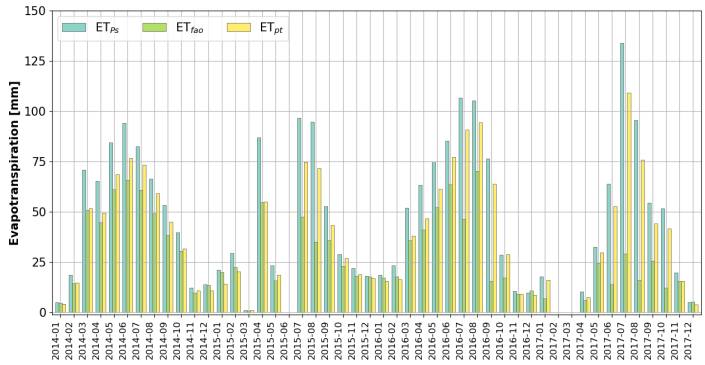

Figure 6.9: Total monthly evapotranspiration, simulated using the different GEOframe ET components. In dark green the Prospero estimation, in light green the FAO estimates and in yellow, the Priestley-Taylor ones.

6.1) at the weir because some accumulation of lateral flow can be present. The hypothesis that Runoff$_n$ is actually null, because inflow compensates with outflow at the well, is not sustainable because the groundwater variation alone is often larger than P.

6.2 Analysis of the water budgets

The results of ET simulations and can be observed in Figure 6.9. Evapotranspiration was aggregated at monthly scale form in order to make the differences among the various models more evident. Usually Prospero model provides more evapotranspiration than other models, but by aggregating them at a monthly scale all models seems to perform analogously. The fact that Prospero shows more evaporated water is not a linear consequence of its equations because, on the contrary, Prospero embeds more stress factors than the other models, and therefore in principle, it is expected to give less evapotranspiration that the others. The

cumulated evapotranspiration is shown in 6.10 where, from top to bottom, we have the measured runoff, the evapotranspiration modelled with Prospero, the evaporation modeled with Priestley-Taylor and the evaporation modeled with FAO. At the bottom, there is also the simulated variation of soil moisture that, as logic suggests, oscillates close to the zero level. The modelled evapotranspiration estimates oscillate from 37% percentage of the water budget for the Prospero one, to 30% for the Priestley Taylor, and to 21% for the FAO, as reported in Table 6.4. These values, considered on the whole period, are in agreement with previous analysis by Bancheri et al. (2018) and Abera et al. (2017) on the entire area of Posina catchment. However they are strongly influenced by the 2014 wet season which caused an increase in runoff and a decrease in evapotranspiration. Another observation we can draw is that any estimation of evapotranspiration (we remind that is an estimation based on literature parameters but which gave good results in the point wise analysis), is well below the P-R level (Figure 6.10, as typical of humid areas. This difference, green line minus the violet line for the case of Prospero, can be possibly intended as the quantity of precipitation that goes to recharge.

At the light of the latter considerations, one possible conceptual model for the Ressi catchment behavior is represented in Figure 6.11. The circles represent conceptual reservoirs. Therefore we have three of them, one describing an upper reservoir S_u, one a lower reservoir, S_d, close to the weirs and the third representing groundwater storage, S_g. The upper storage is required, according to what shown before, for giving to S_d the water quantity that exceeds the precipitation volumes, through the flux Q_{ud}. S_d is providing the stormflow subsurface discharge, in the assumption of having negligible runoff. S_g is required to control the water table level and provide the baseflow, Q_g. The groundwater is con-

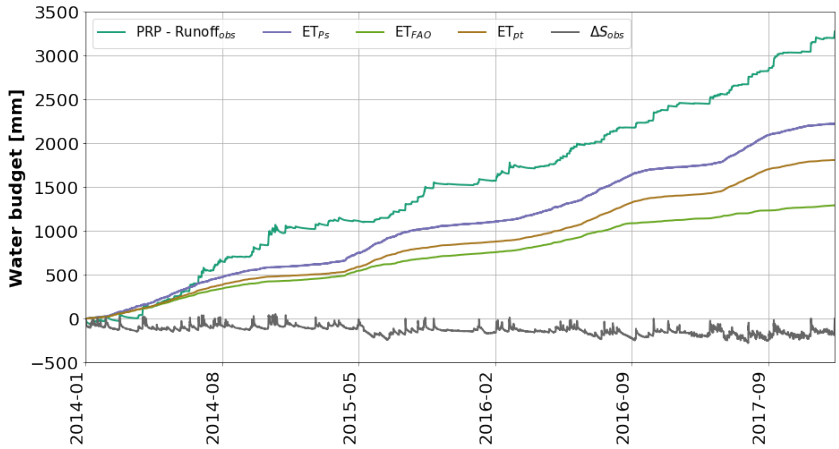

Figure 6.10: Cumulated ET volumes estimated with PS, FAO and PT components, compared with the precipitation minus the runoff and the variation of water storage.

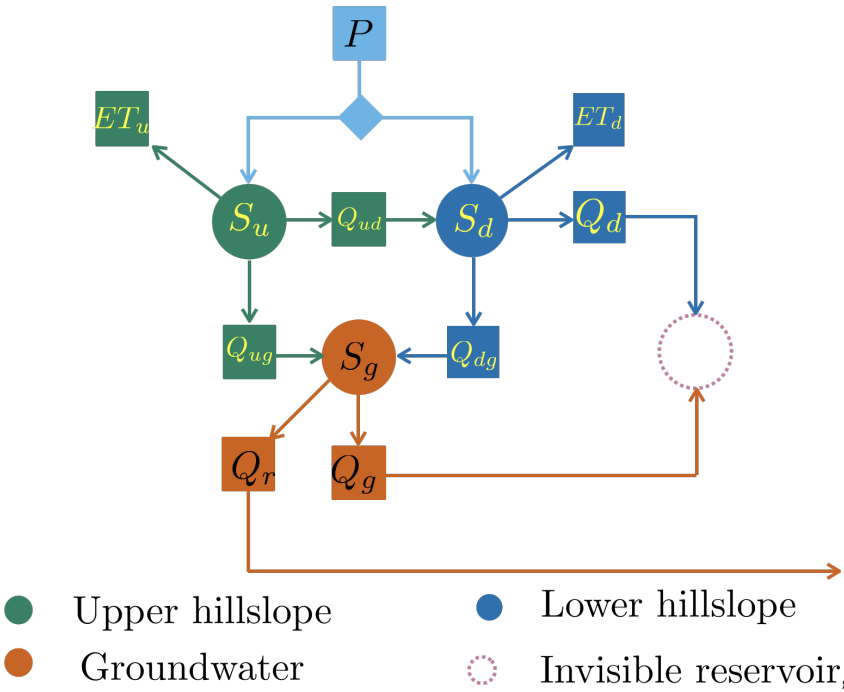

Figure 6.11: A first hypothesis on the conceptual model for the water budget of Rio Ressi Symbols are explained in the text.

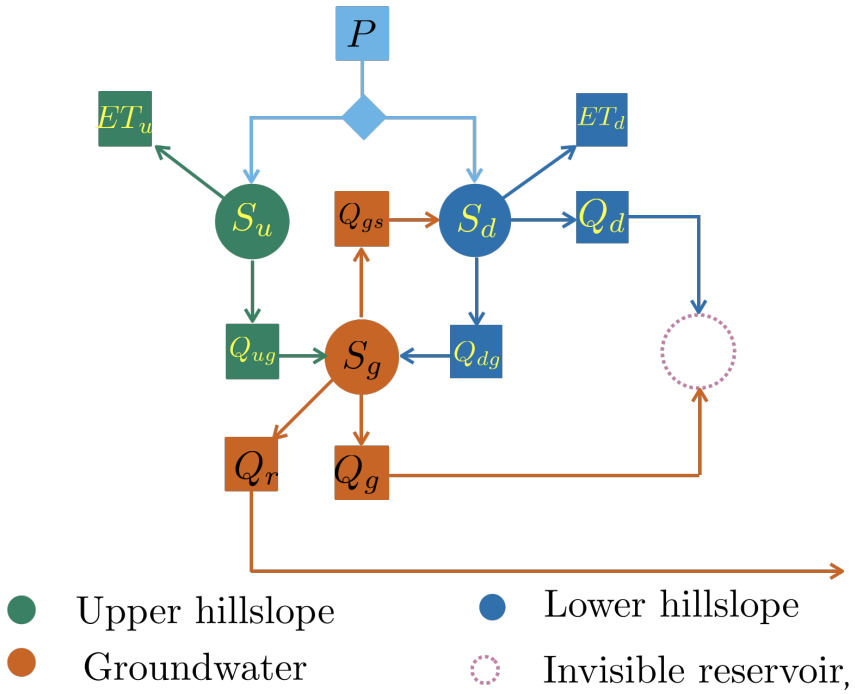

Figure 6.12: A second hypothesis on the conceptual model for the water budget of Rio Ressi Symbols are explained in the text.

tributed by both the upper and the lower reservoirs, through the fluxes Q_{ug} and Q_{dg}. The dashed ball indicates that the soil water stormflow is simply added to the baseflow to obtain the total discharge. Evapotranspiration ET derives from both the upper and the lower reservoirs, and precipitation, P, is partitioned among them. According to Bancheri et al. (2019) these graphics can be transformed in equations and solved, once the functional form of the fluxes is assigned. However, this is not the only modelling structure compatible with the gauged data. Another possibility is represented by Figure 6.12. The relevant difference between Figure 6.11 and Figure 6.12 is that in the second model structure, groundwater S_g and the lower domain S_d can exchange water in one direction or in the opposite, accordingly to controls that remain, at present, unspecified. The question as which of the two

modelling structure is more adequate to describe the real system, is intriguing but it is out of the scopes of the present thesis. In the following we discuss the energy budget and, subsequently, for getting a model of runoff, we will consider an acceptable compromise to use the ERM model (Bancheri, 2017).

6.3 Analysis of the energy budget

Prospero, unlike the other evapotranspiration formulas, provides solutions for the energy budget and, therefore, by using it, we gain information about the sensible heat exchanges and the temperature of the evaporating surfaces. This information is provided in synthesis by Figures 6.13 to 6.16. Besides, being a dual-layer model, solution of the energy budget can be obtained both for the illuminated (sun) layer and for the ones in shadow. The Figure 6.13 summarizes the daily and the annually behavior of the sensible heat exchange for the sunlit canopy. Figure 6.14 is the latent heat exchange due to the shade layer. The median is slightly negative but the distribution is quite skewed to negative values, meaning that the shade layer, as it is logical to think, is heated by exchange with the surrounding. This last consideration calls for a rethinking of the present Prospero scheme which does not include feedbacks among the temperature of the layers. Since the shade layer gets heat from air temperature, it should be absorbed also by the sun light canopy. This will be certainly an aspect to account in the next versions of the model.

The behavior of the sensible heat is not reflected trivially in the behavior of leaves temperature. The temperature of leaves is, in fact increasing faster than air temperature, since the early morning, as shown in Figure 6.15a and, at the annual scale, in Figure 6.15b the largest differences in temperature are recorded in winter months. The total difference in temperature can be very

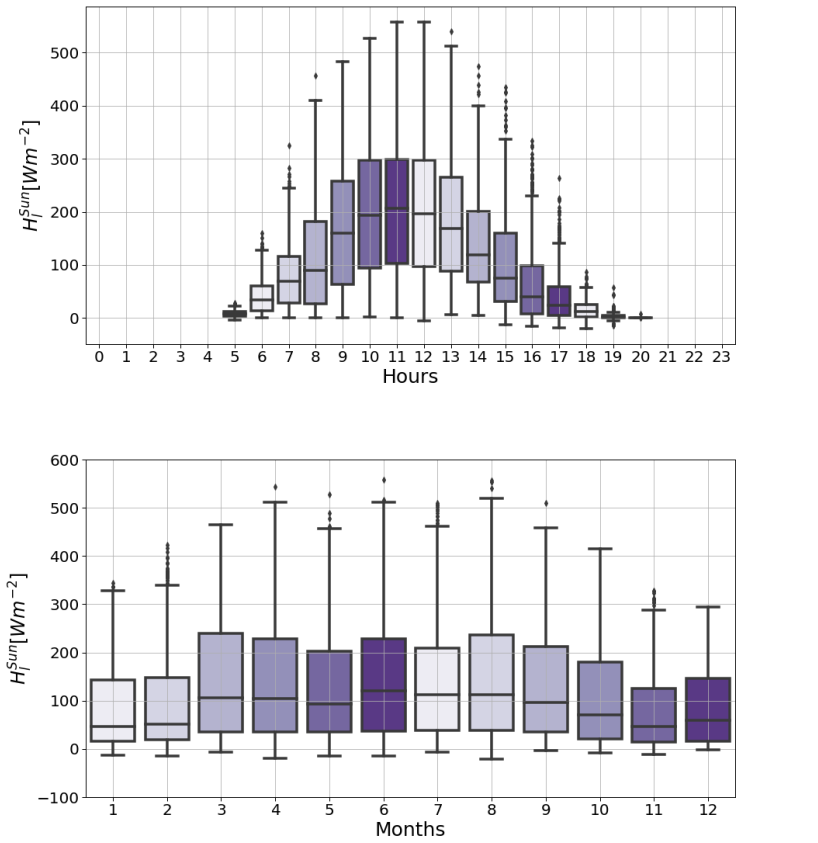

Figure 6.13: Estimated sensible heat fluxes from sunlit canopy, at daily and annual scale.

large, and if the larger differences has to be marked as nonphysical behaviors, due to an incorrect closure of the stomata due to the radiation stress function, since the median differences that can be still very large and of the order of 20 Celsius degree for the hourly gaps, can be acceptable according to some reference (Andrews et al. 1992, Martin et al. 1994, Duffkova et al. 2006). Obviously the monthly statistics involve less pronounced temperature gaps. All of these behaviors has certainly to be further investigated. Shadows leaves manifest, with respect to temperature

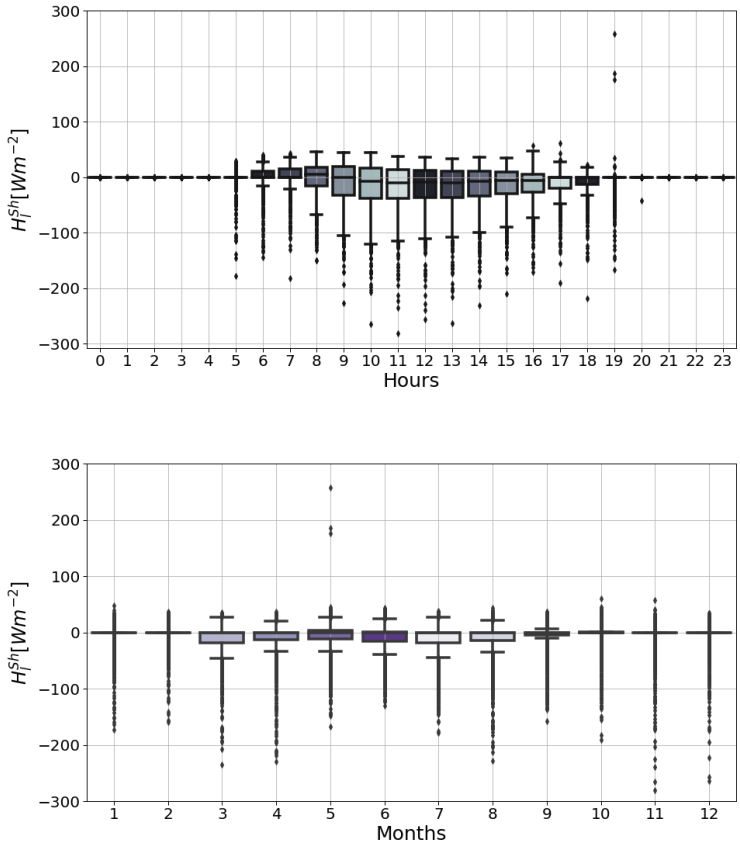

Figure 6.14: Estimated sensible heat fluxes from shade canopy, at daily and annual scale.

a different pattern than sun leaves. The mean monthly pattern of temperature seems completely in counter-phase respect to the behavior of the sun leaves, by showing that the larger gap between leaves and air temperature is in the summer months. However, the behavior is reversed if this gap is normalized to the actual temperature. I.e. we have a larger gap in summer because we have larger temperatures. This consideration, however, reveals, that, instead, the gap in temperature for the sun light leaves in Figure 6.15b is much more emphasized in winter months. Un-

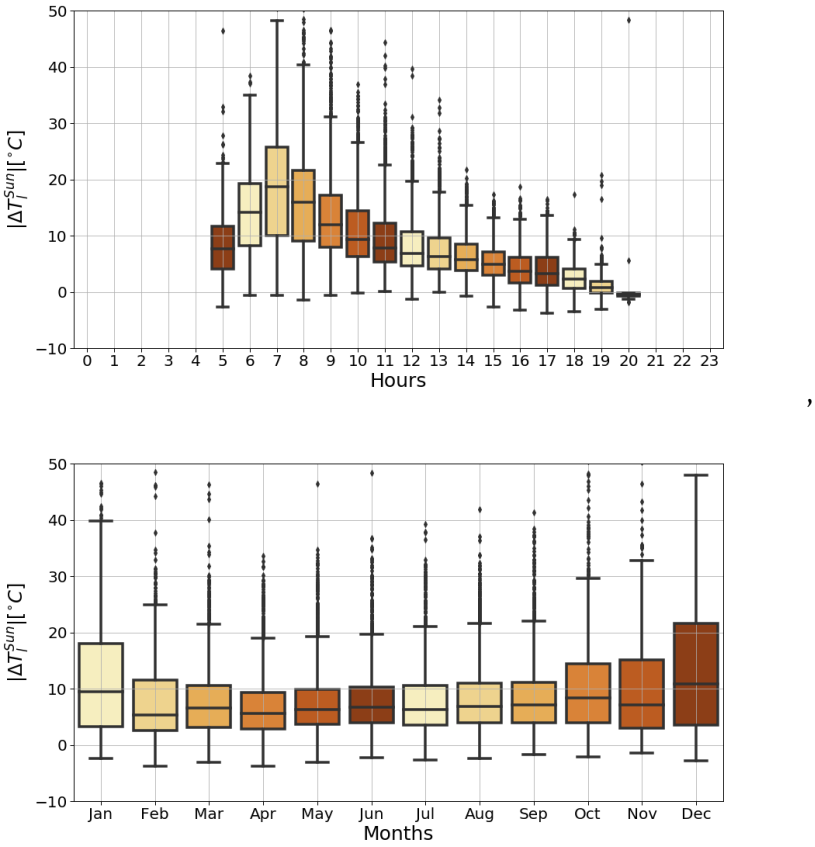

Figure 6.15: Daily and annual deviation between sunlit leaves temperatures and air temperature.

derstanding this behavior and understanding if it is a byproduct of modelling or a real characteristics of canopies, will be certainly argument of future studies.

6.4 The Embedded reservoirs model (ERM)

In order to simulate the discharge of the Rio Ressi, the Embedded reservoir model (Bancheri, 2017) has been used, as a first

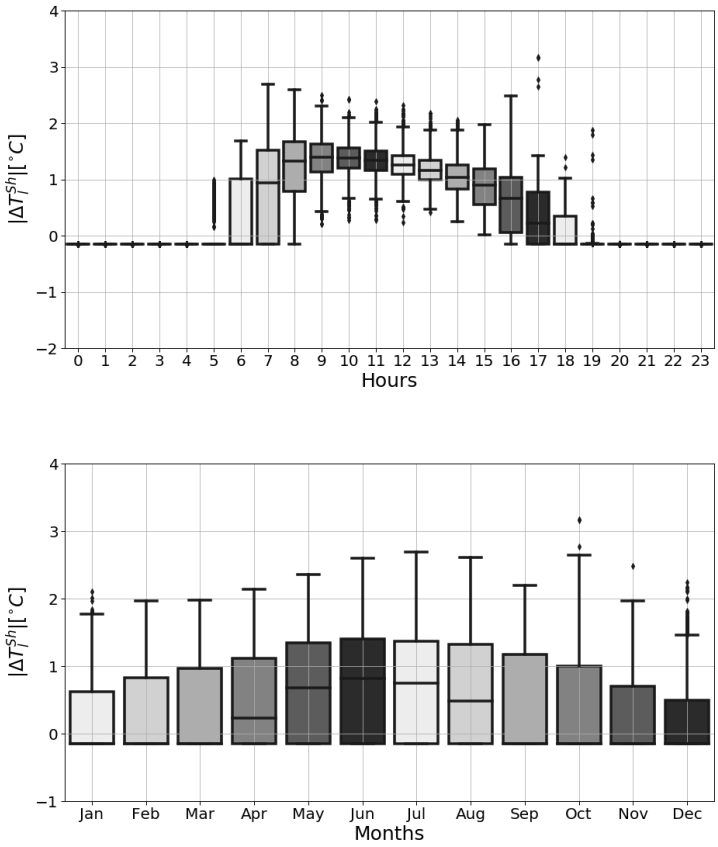

Figure 6.16: Daily and annual deviation between shaded leaves temperatures and air temperature.

approximation of the Ressi perceptual model. A detailed description of ERM is presented in Bancheri (2017). The ERM is a semi distributed model for runoff, which describes each HRU with five coupled storages:

- Snow pack;
- Canopy;
- Root zone;
- Surface flow;

- Groundwater.

These storages are represented in Figure 6.17 using the extended Petri Nets graphics (Bancheri et al., 2019). The detection of the

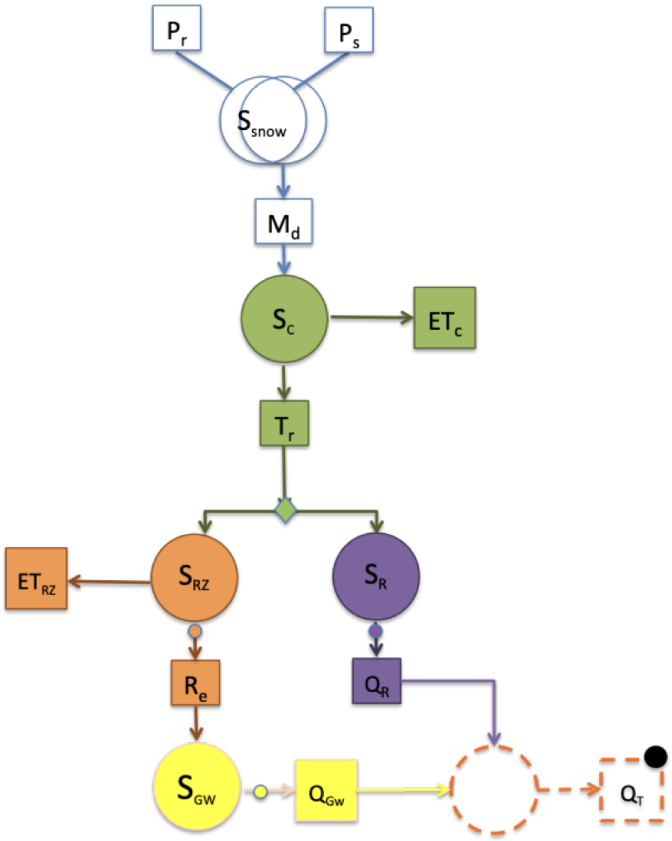

Figure 6.17: Representation of the ERM Model

rainfall and the snowfall from the total precipitation is integrated in the snow component of GEOframe-NewAge (Formetta et al., 2013a), and used to simulate snow melting and snow water equivalent with the Hock model (Hock, 1999). The snow melting and the rainfall are the inputs of the canopy layer.
If there is a canopy, precipitation is intercepted, otherwise it reaches directly the soil and so the root zone.
The precipitation exceeding the root zone capacity becomes sur-

face runoff, modeled using a non-linear reservoir model. Water from the root zone can be extracted through evapotranspiration or as a recharge of the groundwater. Evapotranspiration in the root zone describes both the evaporation from the soils and the transpiration from the canopy. Baseflow from the groundwater is modeled using a non-linear reservoir. Total runoff is the sum of the direct runoff and of the baseflow. The parameters of

Reservoir	**Parameter**	**Range**
Snow	α_m	[0.01 - 1.0]
Snow	α_f	[0.0001 - 0.1]
Snow	α_e	[$1.0{\cdot}10^{-5}$ - $1.0{\cdot}10^{-4}$]
Snow	α_l	[0.3 - 0.9]
Canopy	k_c	[0.1 - 0.3]
Root zone	$S_{rz_{max}}$	[100 - 400]
Root zone	a	[0.0001 - 0.01]
Root zone	b	[1.0 - 2.0]
Root zone	B	[0.1 - 0.8]
Direct runoff	p_{Sat}	[20.0 - 80.0]
Direct runoff	c	[0.0 - 0.1]
Direct runoff	d	[1.0 - 3.0]
Groundwater	$S_{gw_{max}}$	[500 - 1000]
Groundwater	e	[100 - 600]
Groundwater	f	[1 - 10]

Table 6.1: Parameters range of the Embedded Reservoir Model.

the above components are summarised in Table 6.1. As a consequence of using ERM, we are going to simulate all the principal compartments of the hydrological cycle. Whilst evapotranspiration parameters can be set using literature data, the parameters of the ERM runoff model must be calibrated to obtain reasonable results. Since the channel is very short, the routing is not considered.

6.5 Methods

The analysis of the Rio Ressi hydrology was conducted for the period from the beginning of 2014 to the end of 2017. There are also precipitation data for the two-year period 2012-2013, which precipitations were interpolated from nearby stations, but we preferred to exclude them from the analysis.
The year 2014 was found to be very rainy with almost 3000 mm of annual precipitation but we also decided to exclude them for what concerns the calibration of the discharge. We kept it for other analysis.
It was therefore decided to calibrate the model only for the year 2015 and subsequently validate the entire period. Three discharge simulations were conducted, each using a different GEOframe component for estimating evapotranspiration, i.e. the Priestley-Taylor Model, the Penman-Monteith-FAO, both in Appendix B, and the Prospero model, presented in Chapter 4.1 of this dissertation. The calibration of the ET components is not carried out as for the case of the previous chapter, as there is no direct measurement of the evapotranspiration. At each simulation the ERM model was calibrated, using the OMS internal calibrator, LUCA (Let Us CAlibrate, Hay and Umemoto, 2006b), comparing the simulated runoff with the observed one, optimizing the Kling-Gupta Efficiency coefficient (KGE, Gupta et al., 2009).
For these simulations the value of Priestley-Taylor α (please see Appendix A) was taken equal to the average value (1.26, Priestley and Taylor, 1972), while for the FAO Penman-Monteith method the parameters for forest trees, was used (Tab. 6.2).

For Prospero simulations only parameters about water stress were changed (Eq. 4.5) using the ones reported in Tab. 6.5. Others Prospero's parameters are the same of previous simulations (Tab.

Forest trees	Value	Unit
crop coefficient ($K_{c,mid}$)	1.00	[-]
roots depth	1.25	[m]
depletion fraction	0.7	[-]
canopy height	10	[m]
water wilting point	0.15	$[m^3 m^{-3}]$
water field capacity	0.27	$[m^3 m^{-3}]$

Table 6.2: FAO's vegetation parameters used for the Rio Ressi simulation.

5.4).

6.6 Calibration of the ERM model and runoff simulations resuls

Runoff calibration is performed (Tab. 6.1) for the year 2015, validation is done on the remaining years.
The model is calibrated in order to maximize the KGE of the simulated runoff compared with the observed one. The parameters used for FAO are those of the forest trees (Testa et al., 2011) and reported in Tab. 6.2. For PT the value of α is always kept equal to 1.26. The parameters of Ps, also in this case, are kept equal to those used in the literature and not calibrated.

Figure 6.19 shows the reproduction of the calibrated runoff (in red in the Figure) and using Prospero for estimating Evapotranspiration. The differences among this estimate and the one obtained using the other ET models is not very large, from the one obtained by using the other models of ET, even if the goodness of fit indicators in Table 6.5, show that Prospero perform a little better than the other models. The differences are somewhat apparent when presenting the water budget aggregated at the monthly scale, as in Figure 6.18 where it is shown that usually

Reservoir	Parameter	Ps	Pt	FAO
Snow	α_m	0.40	0.60	0.43
Snow	α_f	0.05	0.07	0.04
Snow	α_e	7.85E-05	3.57E-05	4.77E-05
Snow	α_l	0.84	0.46	0.57
Canopy	k_c	0.37	0.52	0.49
Root zone	$S_{rz_{max}}$	223.0	307.7	261.2
Root zone	a	8.9	3.6	6.8
Root zone	b	49.6	26.4	67.7
Root zone	B	0.20	0.32	0.26
Direct runoff	c	0.12	0.18	0.14
Direct runoff	d	12.1	14.8	10.3
Direct runoff	p_{Sat}	49.9	60.5	48.4
Groundwater	e	6.5	3.6	7.5
Groundwater	f	7.4	6.9	6.6
Groundwater	$S_{gw_{max}}$	531	571	904

Table 6.3: Calibrated parameters of the Embedded Reservoir Model using the different GEOframe ET components.

Year	%Runoff$_{obs}$	%ΔS_{obs}	%ET$_{Ps}$	%ET$_{FAO}$	%ET$_{pt}$
2014	61%	-4%	23%	17%	19%
2015	39%	-4%	59%	36%	45%
2016	39%	-1.4%	43%	26%	36%
2017	25%	12%	45%	14%	36%
2014-17	46%	-0.5%	37%	21%	30%

Table 6.4: Percentage of the observed runoff, observed variation of water storage and estimated ET with Prospero, FAO and PT components compared to the annual precipitation.

the runoff simulated with the evaporation provided by Prospero are slightly larger than the other estimates. All the simulations, however, show a negative bias, that is a consistent under estimation of the runoff volume. This is apparent in Figure 6.19 where the runoff volumes cumulated over the period are reported. Un-

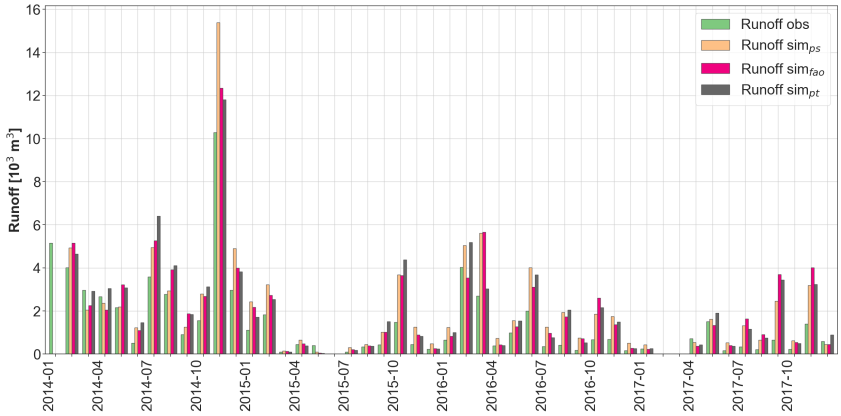

Figure 6.18: Total monthly runoff, observed and simulated, generated using the different ET component in the ERM.

	Prospero	*PM-FAO*	*PT*
$\mathbf{KGE}^{2015}_{cal}$	0.76	0.75	0.76
$\mathbf{KGE}^{2014/2018}_{val}$	0.67	0.63	0.54
$\mathbf{NS}^{2015}$	0.67	0.60	0.60
$\mathbf{NS}^{2014/2018}$	0.43	0.45	0.39
$\mathbf{Pbias}^{2014/2018}$	-16.0	-26.5	-34.6
$\mathbf{R^2}^{2014/2018}$	0.74	0.45	0.65

Table 6.5: Performances of the ERM using different components for the evapotranspiration. Coefficients are computed both on year of calibration (2015) and on the whole period. Only KGE was calibrated.

fortunately, after various trial, we were not able to get better volume estimates, and we can lead back this partial failure to the structure of the ERM model not being different to the perceptual models we introduced in the previous sections. Further investigations could not be pursued due to time constraints, but will be performed in the next future.

6.7 Conclusions

In this chapter we extended the application of the Prospero model to a small sub-catchments where many data were available. Overall the performance of Prospero, that could not be calibrated also in this data-rich case, is in general agreement with the behavior of the other quantities taken into consideration. Evapotranspiration was shown to vary from 21% to 37%, of the total budget, a result, in agreement with previous analysis of the Posina catchment by Abera et al. (2017) and Bancheri (2017). A detailed analysis of the data, led to the hypothesis that the lower part of the Ressi catchment receives a large amount of storm-water flow from the upper hillslope. Besides a consistent part of the rainfall is seen to contribute to recharge. The closure of the budget was made possible by the estimation of evapotranspiration, otherwise some of the pieces of the water budget would have remained unknown. Even if the precise quantities can be dispute, we think that the overall qualitative behavior of the catchment is based on solid foundations. Prospero allows to compute the energy budget of the canopy, other than the water budget, and distinguishes between the canopy at sun light and the one in shadow. The results in this direction must be considered preliminary due to the missing feedback among the parts. However, interesting patterns were shown in the dedicated section to allow further advancement to more robust and reliable

models.

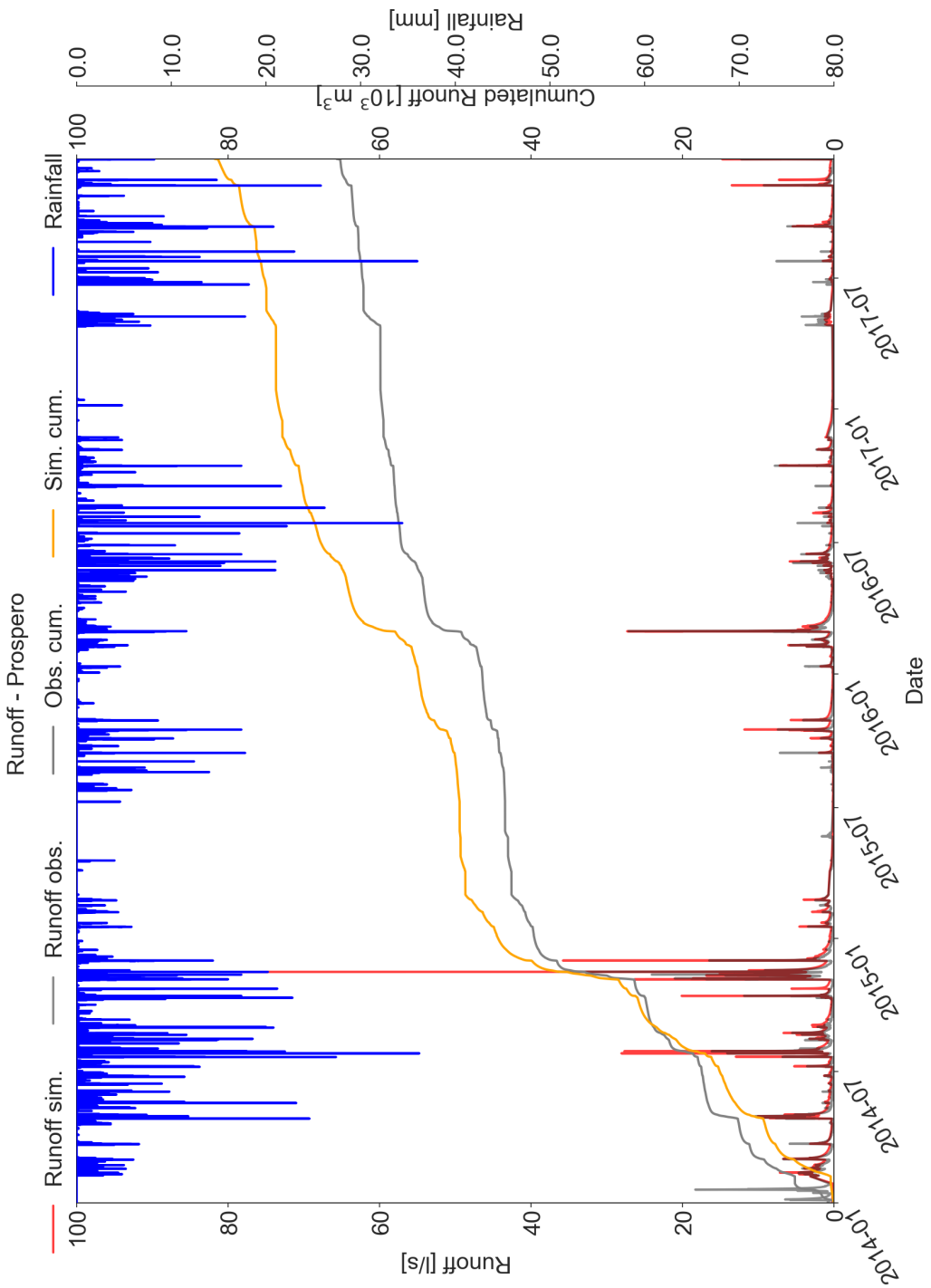

Figure 6.19: Observed and simulated hydrogramm and cumulated runoff, compared with precipitation, obtained with the ERM model and the Prospero component.

CHAPTER 7

CONCLUSION

In this thesis work we have discussed about the evaporation and transpiration theory and presented a new model, Prospero, to estimate the latter.

In the chapter 2 we have presented the transpiration theory starting from the milestones until to the newest works. In particular the physics of transpiration has been analyzed, defining the energy balance and its components. Some omissions made evident from recent studies (Schymanski and Or, 2017) have been highlighted. We have emphasized that the derivation promoted by Penman is not only providing a formula for evapotranspiration but is a resolution of the coupled simplified energy budget with the Dalton law and the sensible heat transfer in turbulent atmosphere. This results in giving the temperature of the evaporating surface, the air humidity and the sensible heat exchange as prognostic variables. This results is absolutely clear but have not been highlighted enough in literature. Based on the work by Lehmann et al. (2008) we have also provided a theoretical framework that clearly distinguishes soil evaporation from plant

transpiration, even if we could not deploy it in software because of time constraints. In the third chapter we have faced the problem to constrain transpiration to water availability by defining the leaf conductances and how they vary with atmospheric or physiological plants conditions.
During the thesis we have applied a Jarvis type of strategy for the stress factor but the implementation was left open to easy extensions with other strategies (like the Ball-Berry-Leuning one) through an appropriate work on the informatics. In the trade-off between adding the BBL formulas or checking the correctness of the overall model functioning, we have decided for the latter option.
In chapter 3 we have analyzed some strategy commonly used to adapt the transpiration's equations at the canopy scale and at the catchment scale, and have introduced a multi-layer canopy model based on a variation of Lambert-Beer's radiation extinction law. The role of leaves in shadow has been discussed.
In chapter 4.1 has been presented the Prospero GEOframe component and how it combines with the other GEOframe tools. A comprehensive information about the code availability has also been given, in an optic of users. The other GEOframe components used to estimate the evapotranspiration, and the GEOframe hydrological model have been reported in Appendix A.
Finally in chapter 5 and 6 Prospero has been applied to two different type of case studies, at point-wise scale and catchment scale as a stand-alone tool. Prospero's Performances are compared with previous GEOframe's tools for evapotranspiration and with observed measurements.
To be specific, in chapter 5, Prospero results have been compared with data of latent heat collected by eddy covariance stations and in presence of simple canopy structures, in two sites. On both sites Prospero have given good performances, comparatively bet-

ter than the results obtained by the other evapotranspiration estimator included in GEOframe. The errors (i.e. RMSE and MAE) respect to the observed measurements obtained on Torgnon and Viote case studies have been in line with the results found by Blyth et al. (2010), Ershadi et al. (2014), Zhu et al. (2014), and the total annual evapotranspiration observed has been well fitted by Prospero.

In chapter 6 have been analyzed the case of the Ressi catchment. This subcatchments has been instrumented with wells, soil moisture probes, hydrometeorological stations and, therefore, an accurate analysis of its hydrological behavior has been possible. According to this analysis, the catchment is always far from equilibrium and all of the components of the hydrological budget has be shown to vary. Some seasonal effect on soil moisture has been detected but an overall trend has been found as inherited by the 2014 wet season. Runoff has been resulted larger that 50% of the rainfall. Soil and groundwater variations, as measured, have been found to be larger that the rainfall inputs, bringing to consider that the lateral flow are an essential component of the budget and that the Ressi catchment cannot be modeled as a single reservoir, notwithstanding its small extension. We have not had the possibility to calibrate the evapotranspiration models, since no data allowed this operation. However, the results of chapter 5 have made us confident that our estimated obtained through literature parameter were not going to be exceedingly imperfect.

Using Prospero and the other evapotranspiration models included in GEOframe, it has been possible to assess, that Ressi is also recharging the water table for an amount which is varying from 17.5% to 24.5%, according to the different estimate of evapotranspiration.

Prospero has been also used to discuss the effects of the energy

budget on the canopies using the sun-shade scheme. The relevant aspects of the energy budget, is the well known fact that leaves temperatures are usually higher than the temperature of the surroundings. The behavior of the leaves in shadows, however, has to be further investigated to understand if it is simply a byproduct of the model structure and assumptions, or reflects reality.
As a proof of concept of the application of the whole GEOframe machinery jointly with the Prospero (and the others) model of evapotranspiration, the ERM model has been used to simulate the runoff. ERM depends upon the estimation of evapotranspiration and, therefore, runoff estimates differ when use different models.
We observed that using Prospero component plug into ERM gave good performances on a so small catchment, especially for the values of Nash-Sutcliffe and Kling-Gumpta efficiency. Performances obtained using Prospero on the calibration period were similar or a little better than the ones obtained with pre-existing evapotranspiration components but a clear improvement on the uncalibrated period in GEOframe performances was obtained when Prospero component was used.

In conclusion, we can say that this thesis explored some theoretical aspects of evapotranspiration, its implementation in an “open science" framework, a successful verification of the models at a station, and the application of the model to dissects the hydrological budget of a small catchment in the Prealpine region. Any of these topics have left room for subsequent improvements. The theoretical part, streamlined the models and can be improved, for instance, by adding more complex treatments of turbulent boundary layer. A subsequent natural expansion of the theory introduced would be also the coupling of evapotranspi-

ration with the carbon budget and photosynthesis. Many of the theoretical aspects already explored still requires an implementation, starting from different conceptualisation of vegetation resistances. The latter could require to move from water content indicators to suction estimations. Pointwise applications regarded essentially grasslands, where the importance of canopies is minimal. Canopies modelling in fact has to be pushed forward and made more reliable. At that point new verifications could be obtained, for instance for forest sites. The work on Ressi catchment itself, requires further thinking and implementations. To the perceptual models we envisioned other could be added in a way that field measurements could be used to calibrate part of the modelling machinery with multiple objective function. I am listing all of these possibilities because the informatics on which the GEOframe system is based and that the present thesis contributed to consolidate, already have implemented part of these possibilities, which just need to be exploited. Therefore I hope that the reader of this thesis can understand that I was not only in search for immediate results but to open pathways for others who will follow.

CHAPTER 8

PERSPECTIVE WORKS

The first future step would be integrating all the various strategies to estimate the stomatal resistances either dependent on the water content or the suction. This could require a refactoring of the present code for encapsulating the code parts that can change. Then a sequence of studies could be done, including an expansion of what was already done in the local places and in Rio Ressi along the lines of what Dewar (2002a) did. With respect to his finding, we can make available data and codes that together with our GEOframe environment, allows for a fair comparison among the parameterization, since only them will be changed along the modelling chain. The new emerging theory of soil evaporation, which includes a treatment of the energy budget containing the thermal capacity of the soil is another next step. It can be accomplished in various ways. The most direct is probably to use the existing Richards1D/2D codes, coupled with the energy budget implemented by Niccolo Tubini and extend it with the explicit introduction of evaporative fluxes. Actually this is going to be accomplished by another dr. Rigon Ph.D student, Concetta

D'Amato. Differentiating the codes between evaporation and transpiration, will mean to differentiate the response of plants and soil and help separating the stories of the two evaporative fluxes (no more evapotranspiration, but soil evaporation and plant transpiration). Finally. the theory of water travel times, as developed after Botter et al. (2011), and presented, for instance, in Rigon et al., 2016 can be placed side by side with the water fluxes computation performed with the GEOframe evaporation tools, to allow the exploting of tracers analysis. In this perspective, the new platform aims to give contribution to resolve the question posed by Evaristo et al. (2015) regarding the different fate of soil and streamflow waters.

Unfortunately there was not enough time to prepare papers on the topics covered in this thesis. The intention is to prepare them in the near future, I will certainly try to frame Chapter 2 and 3 in a review paper for which we should possibly add some theory about renewal models of turbulence and their impact on simulation of vapor and heat transport. Chapters 10, 11 and 12 of the recent Bonan book, can serve as an overview. However, they are missing a convincing treatment of water-limited environment and situations, and the possible use of renewal theories just mentioned. Besides, overlooking the non stomatal resistances, could hamper the estimation of the stomatal resistance, and this aspect is completely neglected in the book. The book is also not treating soil evaporation properly. Then there are other two possible publications: one regarding the code itself with target a journal like Geoscientific Model Development and a possible submission of the software, once refactored, in Journal of Open Source Software. Work on Ressi catchment, once completed the measure campaigns University of Padua is pursuing, is certainly another target, presently pushed away by the spread of Covid-19.

APPENDIX A

GEOFRAME

GEOframe-NewAGE (previously known as JGrass - NewAge, Formetta et al., 2011c) is an open-source system for designing modeling solutions for semi distributed hydrological modeling. GEOframe is not a model in the classic sense of the term but it is more a system of components that can be joined together at run-time for obtaining "modeling solutions" customized for the application in exam. In a modeling system like GEOframe each component represents a physical process and it is constructed as a standalone component that can be connected with the others via the input/output (Fig. A.2). In this way each user can easily build-up and modify its own set of components and connect it with the rest of the system provided by the work of other PhD students and researchers. GEOframe components are connected on the Object Modelling System v3.0 (OMS3, David et al., 2013). OMS3 is a Java-based framework for the environmental modeling, able to support multiple programming languages (Fortran, C/C++, Python and R). Very often the models are represented by a monolithic code, built in a specific

environment (for example Linux or Windows) and using a certain language (Fortran, Python, C, etc.). This generally creates compatibility problems when the model is run or must be compiled under different operating systems. In addition, the models are often made for specific case studies, which makes them difficult to apply to other case studies. This is further complicated by the fact that the models are written by few researchers and if the code is not well documented, it is difficult to read for new users. A modeling solution in GEOframe is made by selecting the components that best describe the physics of the problem, after which the components are combined together in a `.sim` file using the OMS3 framework. The connection of the components takes place through the management of the inputs / outputs of the components themselves.
The main components of interest for this work are briefly summarized below. An exhaustive list can be found in table A.1 and an accurate description can be found in the relative works (Bancheri, 2017, Formetta et al., 2014b).

A.1 GEOframe: a system to obtain science replicability

Probably the phrase that best represents the thinking of our research team was provided by Leek (2013): "I have been frustrated often with statisticians and computer scientists who write papers where they develop new methods and seem to demonstrate that those methods blow away all their competitors. But then no software is available to actually test and see if that is true. Even worse, sometimes I just want to use their method to solve a problem in our pipeline, but I have to code it from scratch![...]In my mind, new methods/analyses without software are just vapor ware."

Figure A.1: The GEOframe universe and its component.

Vaporware and software well express the fundamental idea that science must be reproducible and possibly replicable (Bancheri, 2017).

Replicable science means that reproducing the original results using the same tools should be possible for any user. Reproducibility offers the possibility of obtaining results from scratch, starting only from the description of the text and using different tools in different contexts.

However, a theoretically reproducible model may not be reproducible in practice, since non-trivial programming and computer skills are often required and this takes time to be acquired. We have therefore outlined some practices to improve the reproducibility and replicability of our results, creating a reproducible research system (RRS), (e.g. Formetta et al. (2014b)).

First, the methods should be shared and any source code made public, under a copyleft license (e.g. GPL v 3.0), allowing every-

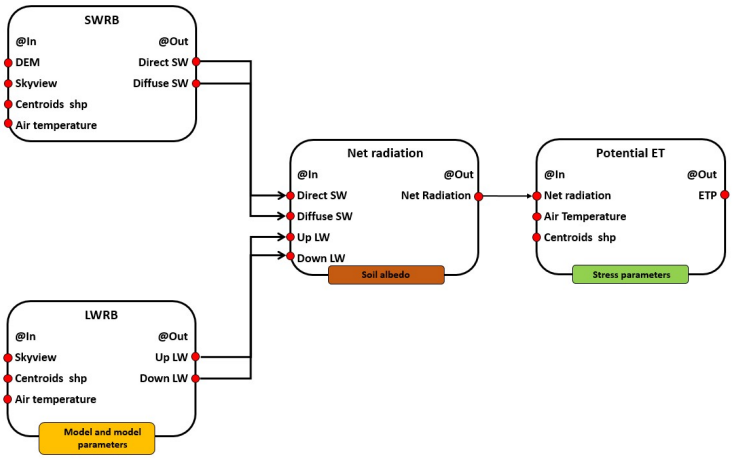

Figure A.2: Example of modelling solution for ET in GEOframe

one to have free access to the code. This allows other users to use our tools and possibly improve them. Building something "quick and dirty", assuming indefinitely delayed cleaning, is something that could easily be avoided by adopting an open source code approach. However, working with open source tools does not only mean sharing codes, but also doing it in the right way, in order to create interest among users, who can also become active collaborators.

A.2 GEOframe community

This is further encouraged by creating a community of sharing ideas, questions, doubts and support. Trying to follow all the previous steps, the GEOframe organization was founded.
The organization is conceived as a system for computer hydrology, a sharing community for researchers and users. The idea of this community dates back to 2008 but, from an operational point of view, the organization was born in 2016 and received the

logo in Figure A.1, with this research project. The need to share our efforts in the scientific community has led us to think about how to do it efficiently, easily and with some basic standards for collaborators and users.

To support the idea of reproducibility and replicability of the research, certain tools are used to track the evolution of the code, documentation and construction system.

GitHub has been chosen as a public repository both for the source codes and for the GEOframe projects. GitHub is a web-based git, a version control repository and an Internet hosting service. GitHub takes care of the development history of changes to the registration and version of the source code (git), storing these changes in a public repository (GitHub). In particular, the GEOframerepository is created for the development of the source code. In addition to sharing the code, GitHub provides test and data cases (possibly open source).

However, during the development of a code it is normal that changes are made that can affect the test case or worse, that no test is performed. For this reason it was decided to use a tool that guarantees continuous integration, that is, that guarantees the test of the source code at each commit.

Using GitHub as a web-based git repository hosting service, Travis CI, is the best choice for a continuous integration service. The continuous integration service, automatically creates executable codes, checks if the tests are performed correctly and returns a positive response if everything is performed correctly. To facilitate the assembly of the Java project, with all dependencies on external classes and / or libraries resolved automatically and updated to the latest versions, Gradle, (Berglund and McCullough, 2011) was chosen as the construction system but valid alternatives are represented by Maven or IVY.

Gradle allows for a more concise representation of tasks and

uses a Groovy-based Domain Specific Language (DSL), (Groovy). Gradle allows you to create a short, clean script that is relatively easy to write and maintain. It is also compatible with the Ivy and Maven repositories. Collecting a source code in a project managed by a construction system is the key to making it independent of the IDE, allowing developers not to modify their favorite development tool. Zenodo was previously used as a filing system. Zenodo is a research data repository. It was created by OpenAIRE and CERN to provide a place for researchers to deposit data sets. "Then, once a new version of the software is produced, it is uploaded to Zenodo, a DOI (Digital Identification Object) number is assigned to the version and the code is stored, recoverable and permanently quoted. Recently, for the storage space, it was decided to use OpenScienceFramework (OSF).

Since 2019, The GEOframe group organize yearly a Winter School at the beginning of January to disseminate the content of the system whose lecture are available on the GEoframe blog.

A.3 GEOframe structure

Even if GEOframe is mainly oriented to the hydrological modeling, it includes also components for data processing, like spatial interpolation or geomorphological analysis. The complete list of components is specified in table A.1 but they can grouped in six categories:

- geomorphic and DEM analyses;
- spatial extrapolation/interpolation of the meteorological tools;
- estimation of the radiation budget;

- estimation of evapotranspiration;
- estimation of runoff production;
- channel routing;

The DEM analysis is performed using the Horton Machine (aka JGrasstools), (Rigon et al. 2006; Abera et al. 2014; Formetta et al. 2014a), that allows, starting from a DEM, to extract several hydrological information like the drainage directions, the total contributing areas, the slopes, the river network, the sub-basin partitioning and the topographic characteristics required by computation. Different tools are available to interpolate data collected to the meteorological stations to the centroids subbasin interpolation. Both geostatistic, (Kriging techniques Bancheri et al., 2018) and deterministic, (Inverse Distance Weighting, IDW, Cressman, 1959) and Just Another Model Interpolator (JAMI)) methodologies are available. The radiation budget model has been presented and validated in Formetta et al. (2013b) and Formetta et al. (2016) and includes both shortwave and longwave radiation.
Before this thesis work, evapotranspiration was estimated using two different formulations: the FAO model (Allen et al., 1998), and the Priestly-Taylor model (Priestley and Taylor, 1972).
Snow melting and snow water equivalent is treated in a component which includes three models, as described in Formetta et al. (2013a).
Two different runoff generation models are implemented, the Duffy's model (Duffy, 1996) and the Hymod model (Moore, 1985), even if Duffy model was never really tested.
The discharge, generated at each hillslope, is routed to each associated stream link according to Mantilla et al. (2006).

Typical input/output data files are represented by csv file but GEOframe is also able to manage different data structures

Process	Component	Reference
Geomorphological model setup	Horton Machine	Formetta et al. (2014a) Rigon et al. (2006)
Meteorological interpolation tools	Kriging IDW, JAMI	Bancheri (2017) Formetta et al. (2014a)
Energy balance	Shortwave radiation Clearness index Longwave radiation	Formetta et al. (2013b) Formetta et al. (2016) Formetta et al. (2016)
Evapotranspiration	Penman-Monteith FAO Priestley-Taylor	Formetta et al. (2014a) Formetta et al. (2014a)
Snow melting	Rain-snow separation Snowmelt and SWE	Formetta et al. (2013b) Formetta et al. (2013b)
Runoff production	Adige Embedded reservoirs	Formetta et al. (2014a) Bancheri (2017)
Travel times description	Backward travel times Forward travel times	Bancheri (2017) Bancheri (2017)
Routing	Cuencas Muskingam-Cunge	Formetta et al. (2014a) Bancheri (2017)
Calibration	LUCA Particle-swarm Dream	Formetta et al. (2014a) Formetta et al. (2014a) Formetta et al. (2014a)

Table A.1: List of the current components of GEOframe (Bancheri, 2017)

like rasters (ASCII and geotiff) or shapefile (.shp), commonly used within the GIS and managed with the Geotools library, Turton (2008). Starting from 2015 a refactoring of the code was performed by Bancheri (2017), even if it was more at design level than to the algorithmic one, with the introduction of the design patterns (DP) (Gamma et al., 1994; Freeman et al., 2008).
I contributed to the maintenance of the components of GEOframe. Furthermore, in addition to having worked on the development of Prospero and updating the other evapotranspiration components, I have contributed directly to the development and testing of the Kriging component (Bancheri et al., 2018, see Appendix C).

APPENDIX B

EVAPOTRANSPIRATION

The evapotranspiration module includes three components:

- Priestley-Taylor model
- Penman-Monteith FAO
- Prospero

All these component can compute the process both at daily or at (sub)hourly time-step.

B.1 Priestley-Taylor

The Priestley-Taylor model is one of the most diffused equation for the evapotranspiration. It is based on the relation between evapotranspiration-net radiation, since at middle latitude the evapotranspiration in mainly energy limited. The equation is

governed by the α parameter.

$$ET_{PT} = \alpha \frac{(R_n - G) \cdot \Delta}{(\Delta + \gamma)} \tag{B.1}$$

- α is an empirical coefficient relating actual evaporation to equilibrium evaporation,
- Δ is the slope of the saturation vapor pressure and air temperature curve (kPa $^{\circ}C^{-1}$),
- γ is the psychrometric constant (kPa $^{\circ}C^{-1}$),
- R_n is net radiation (Wm^{-2}),
- and G is ground heat flux (Wm^{-2})

Based upon a number of experiments at mid-latitude environments and in different climates over both land and water surfaces, Priestley and Taylor (1972) established the mean value of α= 1.26 (e.g., McNaughton and Black, 1973; Mukammal and Neumann, 1977; Parlange and Katul, 1992).
The extensive use of this formula is given by the simplicity of the method and the small amount of input needed. Although the physical representation is relatively simplified, it provides good performance (Abera et al., 2017, Bancheri, 2017).
It is also easy to calibrate, making it suitable for use in hydrological models.

B.2 Penman-Monteith FAO

The PM FAO is the approximation for the PM, defined for a reference crop as a hypothetical crop with an assumed height of 0.12 m, having a surface resistance of 70 s m^{-1} and an albedo of 0.23. It is widely used especially in agricultural field.

The FAO approximation for a grass reference surface For a wide range of crops the zero plane displacement height d, and the roughness length governing momentum transfer, z_{om}, can be estimated from the crop height h by the following equations:

Variable	**Value**	**Unit**
h	0.12	[m]
z_{om}	$0.123 \cdot h$	[m]
z_{oh}	$0.1 \cdot z_{om}$	[m]
LAI	24 h	[-]
LAI_{active}	$0.5 \cdot$ LAI	[-]
r_l	≈ 100	[s m^{-1}]

Assuming these values, the aerodynamic and surface resistance are:

$$r_a = \frac{208}{u_2} \tag{B.2}$$

$$r_s \approx 70 \tag{B.3}$$

The equation for the reference evapotranspiration becomes:

$$ET_0 = \frac{1}{\lambda} \frac{0.408\Delta_{eTa}(R_n - G) + \gamma \frac{900}{T+273} u_2 (P_{was} - P_{wa})}{\Delta + \gamma(1 + 0.34u_2)} \tag{B.4}$$

The reference evapotranspiration can be converted in the reference latent heat multiply it for the latent heat constant λ:

$$E_0 = ET_0 \cdot \lambda \tag{B.5}$$

Actual evapotranspiration can be obtained using the water stress coefficient K_s and the single crop coefficient K_c:

$$ET_{FAO} = ET_0 \cdot K_s \cdot K_c \tag{B.6}$$

Values for K_c are given by FAO. K_s can by derived as:

$$K_s = \frac{TAW - D_r}{TAW - RAW} = \frac{TAW - D_r}{(1-p)TAW} \tag{B.7}$$

$$RAW = p \cdot TAW \tag{B.8}$$

$$TAW = 1000(\theta_{FC} - \theta_{WP}) \cdot Z_r \tag{B.9}$$

- K_s is a dimensionless transpiration reduction factor dependent on available soil water [0 - 1],
- D_r root zone depletion [mm],
- TAW total available soil water in the root zone [mm],
- p fraction of TAW that a crop can extract from the root zone without suffering water stress [-].
- θ_{FC} the water content at field capacity [$m^3 m^{-3}$],
- θ_{WP} the water content at wilting point [$m^3 m^{-3}$],
- Zr the rooting depth [m].

APPENDIX C

THE DESIGN, DEPLOYMENT, AND TESTING OF KRIGING MODELS IN GEOFRAME WITH SIK-0.9.8

The purpose of this study was to create and present a geostatistical software for the spatial interpolation kriging (SIK) of climatological variables, such as temperature and precipitation.

This package was built in order to easily coupled with the GEOframe hydrological model. Additionally our aim was to provide a practical example of an accurately designed software from the perspective of reproducible research, to demonstrate the goodness of the results of the software and have a reliable alternative to more traditional tools.

More than 10 types of theoretical semivariograms and four types of kriging (ordinary, detrended, local ordinary and local detrended kriging) were implemented and gathered into Object Modeling System-compliant components. This, the package provides a real-time optimization for semivariogram and kriging parame-

ters.

Some practices were delineated in this paper and implement in the SIK building in order to make it a reproducible research system(RRS) (e.g.Formetta et al., 2014a).

First of all the kriging's code is available from a control version system under a GPL v3.0 license, using a collective GEOframe organization repository created under GitHub, using Git, and can be found at the following link.

Building tools can be considered a modern evolution of the UNIX make and take care of gathering the various concurring libraries and linking them to form the final executable file.

There are possible choices for Java projects: Apache Ant, Maven, and Gradle.

All of these provide ways to solve the software dependencies. Both Maven and Gradle can download and update the remote resources needed. We choose Gradle since it uses a more concise syntax, thanks to the use of the Groovy language, compared to the XML used by Maven. Using building tools also allows abstraction from the use of integrated development environments (IDEs). Main IDEs for Java are NetBeans, Eclipse, and IntelliJ and all of them support both Gradle and Maven, and Ant and can import a Gradle or Maven (or Ant) project seamlessly.

These tools can help researchers to use and improve others' codes, especially if they are open source. For this reason, we adopted a proper building tool in order to promote collaborative work and open science.

Another important step in the management of the code was the implementation of a continuous integration system Jenkins.It ensures the building and testing of the source code a teach commit, forcing the good practice of preparing tests for each software module developed. Continuous integration (Meyer, 2014) is the practice of merging all developer working copies to a shared

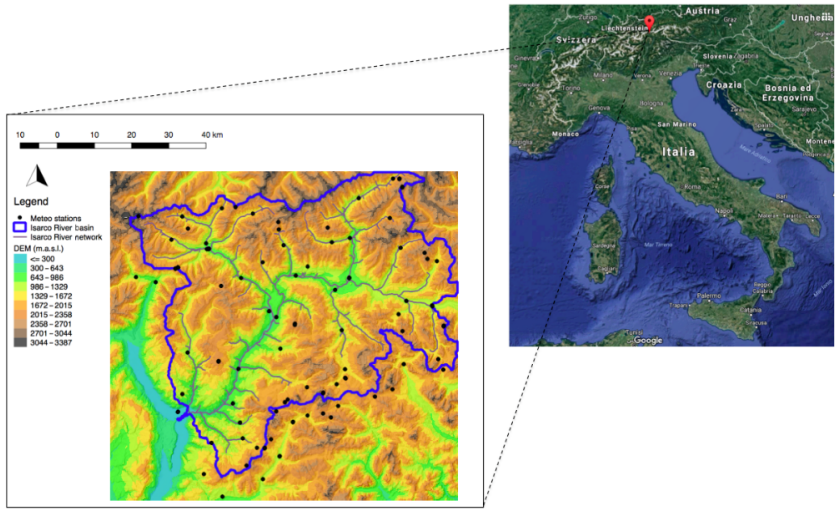

Figure C.1: Geo-location of study area and position of meteorological stations.

mainline several times a day. Unit tests (Beck, 2003) are built with the code and run each time the merging is performed. The continuous integration service automatically builds the executable codes, checks if the tests are performed correctly, and returns a positive answer if all is carried out properly. For this purposes, we chose to use TravisCI, which uses GitHub as a web-based Git repository hosting service, which is a good choice for a continuous integration service. Since GitHub is a repository and not an archival system,we decided to use Zenodo to provide our products with a Digital Object Identifier (DOI) and then we put the entire project, as used to obtain the results presented in this work, on Open Science Framework. The assignment of the DOI allows researcher peers to retrieve exactly that code in the foreseeable future

The component was tested on the interpolation of a year of hourly temperature measurement rainfall and a rain storm event (11 hours) recorded in 2008, measurements collected from 97 stations located in the Isarco River Valley (Fig. C.1). The Isarco River

is a left tributary of the Adige River, in the Trentino-Alto Adige region, northern Italy. The catchment area is about 4200km^2 and the altitude ranges from 210 to 3400 m a.s.l.

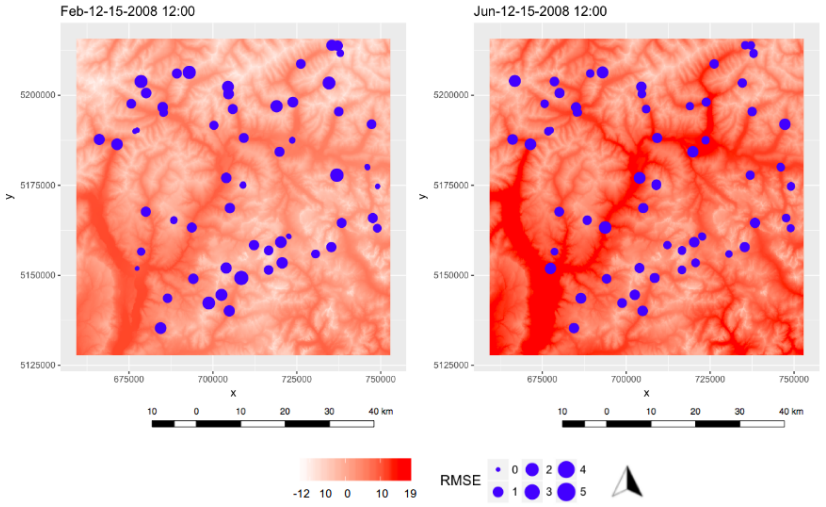

Figure C.2: Maps of spatialized temperature for 15 February 2008 and 15 June 2008. Two bubble plots are overlapped, which represent the RMSE between the measured and interpolated values.

Semivariance analysis was performed and the experimental semivariograms were fitted using all 11 theoretical models in order to use the one that gives the best result. Both local and detrended simulations were performed.
Results obtained from the interpolation of the temperature dataset were compared to the results obtained with R gstat, in order to assess the differences between the two packages, their easiness of use, and their performances. Kriging performances were also assessed using the leave one out cross validation.
The interpolations of both the temperature and the rain-fall gave very good results, with a high agreement between the measured and the interpolated variables. The tests also showed how it is possible to choose between 11 variograms and four kriging alternatives and to compare the outcomes easily. Conversely, the

single rainfall event did not show trend with elevation.In comparison with gstat, the SIK package proved to be a good alternative, regarding both the easiness of use and the accuracy of the interpolation.

APPENDIX D

MORE GREEN AND LESS BLUE WATER IN THE ALPS DURING WARMER SUMMERS

Below a short summary of our work published on Nature Climate Change. In this study it was evaluated how the partition of water between the hydrosphere (streams and runoffs, the blue water) to biosphere (evapotranspiration, the green water) can change in different climatic conditions in the alps (Falkenmark and Rockström, 2006; Orth and Destouni, 2018).

Although relatively small, the European Alps contribute a disproportionally large amount of water, especially during summer, to four major European rivers (Weingartner et al., 2007), and in these rivers' basin reside more than 170 million people. Even if they are referred to as 'the water towers of Europe' (Viviroli et al., 2007), water scarcity and droughts in central Europe are becoming more frequent (Briffa et al., 2009).

In fact due to climate change relative humidity is generally decreasing, temperature and evapotranspiration are increasing,

snow distribution is shifting to higher elevation with a relative shrink of glaciers and climatic extremes are becoming more frequent (Brunetti et al., 2009;Fatichi et al., 2015; Duethmann and Blöschl, 2018;Beniston et al., 2018;Samaniego et al., 2018). Additionally climate change can reduce surface-water supply by enhancing evapotranspiration in forested mountains, especially during heatwaves.

We investigated this phenomenon ("drought paradox") for the European Alps using a database with more than one thousand stations and a hyper-resolution ecohydrological simulations to quantify blue (runoff) and green (evapotranspiration) water fluxes. The study was carried out throughout three years (2001-2003) where two of those were extremely wet and dry (2001 and 2003). During the 2003 heatwave, evapotranspiration in large areas over the Alps was above average despite low precipitation, amplifying the runoff deficit by 32% in the area between 1300 and 3000 masl, which is the most important for the runoff production. We also simulated an increase of 3°C air temperature that could enhance annual evapotranspiration up to 100 mm (45 mm on average), which would reduce annual runoff at a rate similar to a 3% precipitation decrease. This suggests that green-water feedbacks (which are often poorly represented in large-scale model simulations) pose an additional threat to water resources, especially in dry summers. Despite uncertainty in the validation of the hyper-resolution ecohydrological modelling with observations, this approach allows more realistic predictions of mountain region water availability.

Simulations were carried out using a physical based ecohydrological model (Tethys-Chloris (T&C) Mastrotheodoros et al., 2019) that resolves water, carbon and energy budgets at the hourly timescale. To account for the high spatial heterogeneity of the region, analysis was performed with massively parallel simulations

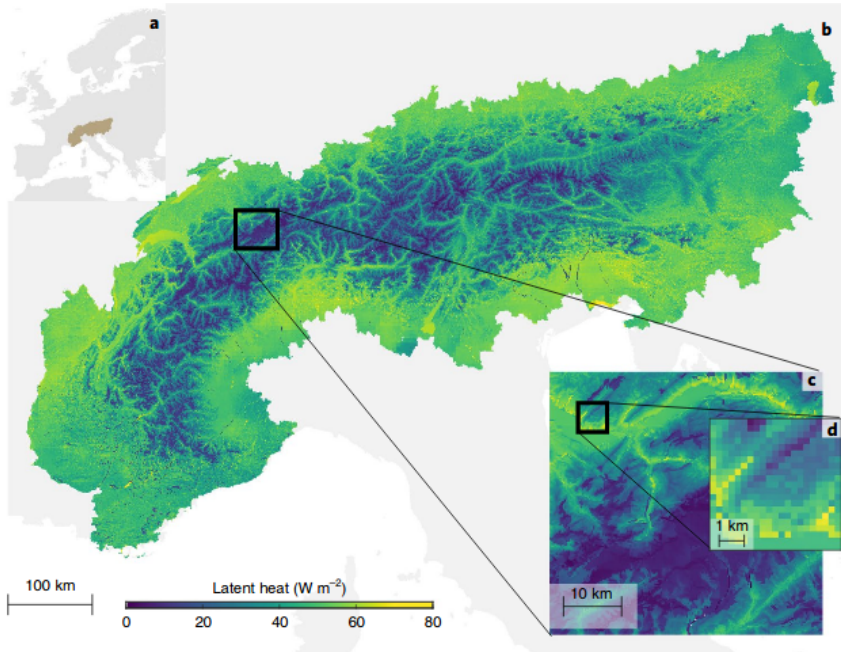

Figure D.1: **Simulation results highlight the spatial heterogeneity in latent heat (ET in energy units)**.a, The spatial extent of the European Alps. b, November 2000-October 2003 average latent heat flux for the entire 257045 km^2 domain simulated with Tethys-Chloris. c,d, Zoom on the Bernese highlands, Switzerland, and illustration of the small-scale spatial heterogeneity captured with the hyper-resolution simulation (250 m × 250 m pixels).

($6.1 \cdot 10^5$ CPU hours) at an unprecedented high resolution (250 m grid) for the entire Alpine arch ($\approx 260 \cdot 10^3 km^2$).

Results confirms that energy is the dominant driver of ET in the alpine area, obtaining the maximum latent heat in the wetter areas while in the drier regions, such as in the upper Rhone valley, latent heat is overall lower because precipitation ($\approx$ 500 mm yr^{-1}) becomes the critical constraint for annual ET.

Average precipitation - ET (P - ET) was used as a proxy for runoff (Goulden and Bales, 2014) since changes in soil and snow water storage over three hydrological years could be considered small, and ice melt only marginally contributed to the total water

budget (less than 3%) at the annual scale at a rate of roughly $4km^3yr^{-1}$. The Alpine water budget also displays high temporal variability; P - ET in 2001 was 53% higher than in 2003, which can be explained by both higher precipitation and lower ET. More specifically, the Alps received 225 mm more precipitation in 2001 compared with 2003 (1363 and 1138 mm,respectively, averaged over the entire domain) while ET was 30 mm lower on average.
We focused on analyzing runoff deficits, computing how much ET contributed to amplifying the effect of precipitation deficit on runoff during the 2003 May-September period (the growing season). This is the period with active vegetation and when green-water feed-back can be pronounced. We found that in 75% of the catchments, ET amplified the drought impact on runoff. The remaining 25% of the catchments-mostly located in the south-west and northeast of the pan-Alpine domain-experienced dry conditions with water-stressed vegetation and reduced ET.
On the whole alpine domain, ET increased during the drought in an area covering more than $144000km^2$.
The increase in green-water flux amplified the precipitation-driven deficit by roughly 22%. In the areas between 1300 and 3000 m a.s.l., enhanced ET created an additional water loss of almost $4km^3$ during the 2003 growing season compared with the 2001-2003 growing season average, amplifying the runoff decrease due to precipitation by 32%.
Our results, which derived from a single mechanistic model, indicate that ET considerably contributed to reduce water yield during the 2003 growing season because vegetation benefited from the unusually warm and sunny conditions in a large part of the Alpine region at higher elevations.
Another important result is that at the annual timescale the temperature-driven ET feedbacks on runoff are less important than the direct effect of changes in precipitation; a 3% reduction

in annual precipitation would affect runoff production over the entire pan-Alpine domain similarly to a hypothetical increase in mean annual air temperature of 3°C, even if the scenario of a +3°C change in air temperature is simply based on a space-for-time analysis.

Combined with the expected decrease in ice melt and earlier snow melt (Beniston et al., 2018), our results demonstrated that blue water could be considerably reduced in the European Alps during warmer summers, but green water will continue to increase (Duethmann and Blöschl, 2018), leading to the oxymoron 'lush vegetation-drier rivers'.

Alternatively, the expected increase in plant water use efficiency with higher levels of CO_2 concentration (Mastrotheodoros et al., 2017) as well as large-scale disturbances (for example, forest mortality Dupire et al. 2017), species changes and plant acclimation, which are not considered in this study, may partially offset this ET feedback during warmer summers in the long term, but they will probably not have a major role in the near future.

Furthermore, in certain regions of the Alps, vegetation management is intense, and past disturbances such as wildfires or forest logging may have influenced vegetation composition and function in ways that are not accounted for in the model initialization. While the presented concepts are general, the extension of the results to other mountain regions strongly depends on the relative magnitude of precipitation and ET at the annual scale and during summer. Important factors are also the elevation at which P - ET shifts from positive to negative during warm and dry summers and the areal extent covered by different elevation bands and vegetation types. Nevertheless, results from the Sierra Nevada (Gilbert and Maxwell 2018, Bales et al. 2018) largely agree with our findings. Understanding the partitioning of green- and blue-water fluxes and their spatial distribution from a few square

kilometers to the entire Alps is essential to manage the European water resources under current and future climatic conditions (Orth and Destouni, 2018) . This partition has implications for ecosystem functioning, energy production and water supply.
We showed that ecohydrological simulations driven by high - resolution hydrometeorological forcing improve the quantification and understanding of the water budget in mountainous areas and its vulnerability to climate, providing insights into processes that coarser-scale approaches fail to reproduce (Fan et al. 2019, Wood et al. 2011, Maxwell and Condon 2016). This highlights the urgent need of more realistic, high-resolution quantifications of water availability (Barnett et al., 2005) . Our study demonstrates that recent advances in ecohydrological modelling, combined with large-scale datasets and new computational capabilities, offer the possibility to address this urgent need, thus helping to define strategies to counteract or adapt to climate change impacts on water resources.

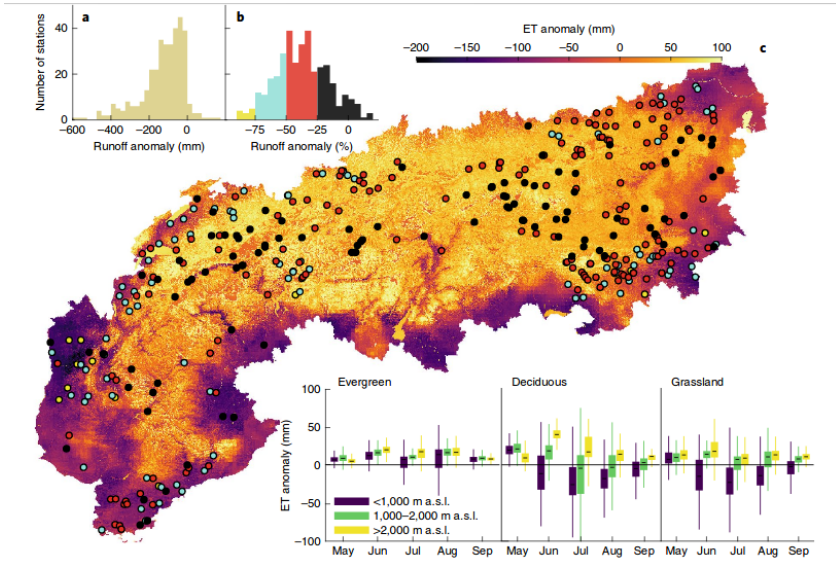

Figure D.2: Analysis of anomalies in blue-and green-water fluxes during the 2003 drought.a, Histogram of observed May-September 2003 total runoff anomalies (mm) for 381 locations. b, Histogram of observed May-September 2003 runoff anomalies (%) for the same locations coloured according to the magnitude of the anomaly (<-75%: yellow, -50 to -75%: cyan, -25 to -50%: red and >-25%: black); growing season 2003 is compared with the mean of each station for the period 2001-2003. c, Spatial distribution of the simulated ET anomaly (mm) during the 2003 growing season (May-September; the reference period for ET is also 2001-2003). The dots represent the 381 locations with hydrological measurements and are coloured as described in b. The three insets in the lower right panel show the box plots of simulated ET anomaly in May-September 2003 for three vegetation types in three elevation classes. The box length provides the interquartile range (IQR), the bottom of the box is the 25^{th} percentile (first quartile, q_1), the top of the box is the 75^{th} percentile (third quartile, q_3) and the horizontal line within the box is the median. The lower whisker corresponds to q_1 - $1.5I_{QR}$, and the upper whisker corresponds to q_3 + $1.5I_{QR}$.

APPENDIX E

ACKNOWLEDGEMENTS

We thank ARPA Valle d'Aosta ARPA Aosta and in particular Paolo Pogliotti for Torgnon data.
We thank Edmund Mach Foundation of San Michele all'Adige and in particular Damiano Gianelle for Viote data.
A special thanks to the Italian Hydrological Society and to the family of Florisa Melone for establishing the Florisa Melone award and to Giulia Zuecco (university of padova) and alessandro errico (university of Florence) for the collaboration in the SILVA project born within this award.
We thank the projects EcoHydro and LTER financed by Eurac Research, and the PRIN WATZON

BIBLIOGRAPHY

W. Abera, A. Antonello, S. Franceschi, G. Formetta, and R. Rigon.
The udig spatial toolbox for hydro-geomorphic analysis.
Geomorphological Techniques, 2(4.1):1–19, 2014.

W. Abera, G. Formetta, M. Borga, and R. Rigon.
Estimating the water budget components and their variability in a pre-alpine basin with JGrass-NewAGE.
Advances in Water Resources, 104:37–54, 2017.
ISSN 03091708.
doi: 10.1016/j.advwatres.2017.03.010.

R. G. Allen.
A penman for all seasons.
Journal of Irrigation and Drainage Engineering, 112(4):348–368, nov 1986.
ISSN 07339437.
doi: 10.1061/(ASCE)0733-9437(1986)112:4(348).
URL http://ascelibrary.org/doi/10.1061/{%}28ASCE{%}290733-9437{%}281986{%}29112{%}3A4{%}

R. G. Allen, L. S. Pereira, D. Raes, M. Smith, et al.
Crop evapotranspiration-guidelines for computing crop water requirements-fao irrigation and drainage paper 56.
Fao, Rome, 300(9):D05109, 1998.

P. B. Alton, P. R. North, and S. O. Los.

The impact of diffuse sunlight on canopy light-use efficiency, gross photosynthetic product and net ecosystem exchange in three forest biomes.
Global Change Biology, 13(4):776–787, jan 2007.
ISSN 13541013.
doi: 10.1111/j.1365-2486.2007.01316.x.
URL http://doi.wiley.com/10.1111/j.1365-2486.2007.01316.x.

P. K. Andrews, D. J. Chalmers, and M. Moremong.
Canopy-air temperature differences and soil water as predictors of water stress of apple trees grown in a humid, temperate climate.
Journal of the American Society for Horticultural Science, 117 (3):453–458, 1992.

T. Anfodillo, V. Carraro, M. Carrer, C. Fior, and S. Rossi.
Convergent tapering of xylem conduits in different woody species.
New Phytologist, 169(2):279–290, 2006.

P. Aphalo and P. Jarvis.
Do stomata respond to relative humidity?
Plant, Cell & Environment, 14(1):127–132, 1991.

P. Aphalo and P. Jarvis.
An analysis of ball's empirical model of stomatal conductance.
Annals of Botany, 72(4):321–327, 1993.

M. Aubinet, A. Grelle, A. Ibrom, Ü. Rannik, J. Moncrieff, T. Foken, A. S. Kowalski, P. H. Martin, P. Berbigier, C. Bernhofer, et al.
Estimates of the annual net carbon and water exchange of forests: the euroflux methodology.
In *Advances in ecological research*, volume 30, pages 113–175. Elsevier, 1999.

D. Baldocchi.
Espm 228, advanced topics in biometeorology and micrometeorology.
Instructor, 2019.
URL https://nature.berkeley.edu/biometlab/index.php?scrn=espm228.

D. Baldocchi and P. Harley.
Scaling carbon dioxide and water vapour exchange from leaf to canopy in a deciduous forest. ii. model testing and application.
Plant, Cell & Environment, 18(10):1157–1173, 1995.

R. C. Bales, M. L. Goulden, C. T. Hunsaker, M. H. Conklin, P. C. Hartsough, A. T. O'Geen, J. W. Hopmans, and M. Safeeq.
Mechanisms controlling the impact of multi-year drought on mountain hydrology.
Scientific reports, 8(1):690, 2018.

J. T. Ball, I. E. Woodrow, and J. A. Berry.
A Model Predicting Stomatal Conductance and its Contribution to the Control of Photosynthesis under Different Environmental Conditions.
In *Progress in Photosynthesis Research*, pages 221–224. Springer, 1987.
doi: 10.1007/978-94-017-0519-6_48.

M. Bancheri.
A flexible approach to the estimation of water budgets and its connection to the travel time theory.
PhD thesis, University of Trento, 2017.

M. Bancheri, F. Serafin, M. Bottazzi, W. Abera, G. Formetta, and R. Rigon.
The design, deployment, and testing of kriging models in geoframe with sik-0.9. 8.

Geoscientific Model Development, 11(6):2189–2207, 2018.

M. Bancheri, F. Serafin, and R. Rigon.
The representation of hydrological dynamical systems using extended petri nets (epn).
Water Resources Research, 55(11):8895–8921, 2019.

T. Banerjee, F. De Roo, and M. Mauder.
Explaining the convector effect in canopy turbulence by means of large-eddy simulation.
Hydrology and Earth System Sciences (Online), 21(LA-UR-17-22651), 2017.

G. G. J. Bange.
On the quantitative explanation of stomatal transpiration.
Acta Botanica Neerlandica, 2(3):255–297, 1953.

T. P. Barnett, J. C. Adam, and D. P. Lettenmaier.
Potential impacts of a warming climate on water availability in snow-dominated regions.
Nature, 438(7066):303–309, 2005.

G. K. Batchelor.
An introduction to fluid dynamics. 1967.
Cambridge,: UP xviii, 615, 1967.

A. Beer.
Bestimmung der absorption des rothen lichts in farbigen flussigkeiten.
Ann. Physik, 162:78–88, 1852.

M. Beniston.
Impacts of climatic change on water and associated economic activities in the swiss alps.
Journal of Hydrology, 412:291–296, 2012.

M. Beniston, D. Farinotti, M. Stoffel, L. M. Andreassen, E. Coppola, N. Eckert, A. Fantini, F. Giacona, C. Hauck, M. Huss, et al.
The european mountain cryosphere: a review of its current state, trends, and future challenges.
Cryosphere, 12(2):759–794, 2018.

M. Berger, J. Moreno, J. A. Johannessen, P. F. Levelt, and R. F. Hanssen.
Esa's sentinel missions in support of earth system science.
Remote Sensing of Environment, 120:84–90, 2012.

T. Berglund and M. McCullough.
Building and Testing with Gradle.
O'Reilly Media, Inc., 1st edition, 2011.
ISBN 144930463X.

G. Bertoldi, J. Albertson, W. Kustas, F. Li, and M. Anderson.
On the opposing roles of air temperature and wind speed variability in flux estimation from remotely sensed land surface states.
Water resources research, 43(10), 2007.

E. Blyth, J. Gash, A. Lloyd, M. Pryor, G. P. Weedon, and J. Shuttleworth.
Evaluating the jules land surface model energy fluxes using fluxnet data.
Journal of Hydrometeorology, 11(2):509–519, 2010.

G. Bonan.
Climate change and terrestrial ecosystem modeling.
Cambridge University Press, 2019.

G. Bonan, M. Williams, R. Fisher, and K. Oleson.

Modeling stomatal conductance in the earth system: linking leaf water-use efficiency and water transport along the soil–plant–atmosphere continuum.
Geoscientific Model Development, 7(5):2193–2222, 2014a.

G. B. Bonan, M. Williams, R. A. Fisher, and K. W. Oleson.
Modeling stomatal conductance in the earth system: Linking leaf water-use efficiency and water transport along the soil-plant-atmosphere continuum.
Geoscientific Model Development, 7(5):2193–2222, 2014b.
ISSN 19919603.
doi: 10.5194/gmd-7-2193-2014.

G. B. Bonan, E. G. Patton, I. N. Harman, K. W. Oleson, J. J. Finnigan, Y. Lu, and E. A. Burakowski.
Modeling canopy-induced turbulence in the earth system: A unified parameterization of turbulent exchange within plant canopies and the roughness sublayer (clm-ml v0).
Geoscientific Model Development, 2018.

G. Botter, E. Bertuzzo, and A. Rinaldo.
Catchment residence and travel time distributions: The master equation.
Geophysical Research Letters, 38(11), 2011.

I. S. Bowen.
The ratio of heat losses by conduction and by evaporation from any water surface.
Physical Review, 27(6):779–787, jun 1926.
ISSN 0031899X.
doi: 10.1103/PhysRev.27.779.
URL https://link.aps.org/doi/10.1103/PhysRev.27.779.

K. Briffa, G. Van Der Schrier, and P. Jones.

Wet and dry summers in europe since 1750: evidence of increasing drought.
International Journal of Climatology: A Journal of the Royal Meteorological Society, 29(13):1894–1905, 2009.

T. J. Brodribb, N. M. Holbrook, M. A. Zwieniecki, and B. Palma.
Leaf hydraulic capacity in ferns, conifers and angiosperms: impacts on photosynthetic maxima.
New phytologist, 165(3):839–846, 2005.

M. Brunetti, G. Lentini, M. Maugeri, T. Nanni, I. Auer, R. Boehm, and W. Schoener.
Climate variability and change in the greater alpine region over the last two centuries based on multi-variable analysis.
International Journal of Climatology: A Journal of the Royal Meteorological Society, 29(15):2197–2225, 2009.

W. Brutsaert.
Catchment-scale evaporation and the atmospheric boundary layer.
Water Resources Research, 22(9S):39S–45S, 1986.

W. Brutsaert.
History of the Theories of Evaporation.
Kluver Academic Publisher, 2013.
ISBN 978-90-481-83651-4.
doi: 10.1007/978-94-017-1497-6.
URL http://link.springer.com/10.1007/978-94-017-1497-6.

T. Buckley, K. Mott, and G. Farquhar.
A hydromechanical and biochemical model of stomatal conductance.
Plant, Cell & Environment, 26(10):1767–1785, 2003.

T. N. Buckley.
Stomatal responses to humidity: has the 'black box'finally been opened?
Plant, cell & environment, 39(3):482–484, 2016.

F. Carswell, P. Meir, E. Wandelli, L. Bonates, B. Kruijt, E. Barbosa, A. Nobre, J. Grace, and P. Jarvis.
Photosynthetic capacity in a central amazonian rain forest.
Tree Physiology, 20(3):179–186, 2000.

M. Castelli, M. C. Anderson, Y. Yang, G. Wohlfahrt, G. Bertoldi, G. Niedrist, A. Hammerle, P. Zhao, M. Zebisch, and C. Notarnicola.
Two-source energy balance modeling of evapotranspiration in Alpine grasslands.
Remote Sensing of Environment, 209(2):327–342, 2018.
ISSN 00344257.
doi: 10.1016/j.rse.2018.02.062.

J. Chen, J. Liu, J. Cihlar, and M. Goulden.
Daily canopy photosynthesis model through temporal and spatial scaling for remote sensing applications.
Ecological modelling, 124(2-3):99–119, 1999.

J. M. Chen and J. Cihlar.
Retrieving leaf area index of boreal conifer forests using landsat tm images.
Remote sensing of Environment, 55(2):153–162, 1996.

J. M. Chen and S. G. Leblanc.
A four-scale bidirectional reflectance model based on canopy architecture.
IEEE Transactions on geoscience and remote sensing, 35(5): 1316–1337, 1997.

J. M. Chen, P. M. Rich, S. T. Gower, J. M. Norman, and S. Plummer.
Leaf area index of boreal forests: Theory, techniques, and measurements.
Journal of Geophysical Research: Atmospheres, 102(D24):29429–29443, 1997.

J. M. Chen, J. Liu, S. G. Leblanc, R. Lacaze, and J.-L. Roujean.
Multi-angular optical remote sensing for assessing vegetation structure and carbon absorption.
Remote Sensing of Environment, 84(4):516–525, 2003.

J. M. Chen, G. Mo, J. Pisek, J. Liu, F. Deng, M. Ishizawa, and D. Chan.
Effects of foliage clumping on the estimation of global terrestrial gross primary productivity.
Global Biogeochemical Cycles, 26(1), 2012.

Q. Chen, D. Baldocchi, P. Gong, and T. Dawson.
Modeling radiation and photosynthesis of a heterogeneous savanna woodland landscape with a hierarchy of model complexities.
agricultural and forest meteorology, 148(6-7):1005–1020, 2008.

B. Choat, E. C. Lahr, P. J. Melcher, M. A. Zwieniecki, and N. M. Holbrook.
The spatial pattern of air seeding thresholds in mature sugar maple trees.
Plant, Cell & Environment, 28(9):1082–1089, 2005.

J. Chorover, R. Kretzschmar, F. Garcia-Pichel, and D. L. Sparks.
Soil biogeochemical processes within the critical zone.
Elements, 3(5):321–326, 2007.

G. J. Collatz, J. T. Ball, C. Grivet, and J. A. Berry.

Physiological and environmental regulation of stomatal conductance, photosynthesis and transpiration: a model that includes a laminar boundary layer.
Agricultural and Forest meteorology, 54(2-4):107–136, 1991.

G. J. Collatz, M. Ribas-Carbo, and J. Berry.
Coupled photosynthesis-stomatal conductance model for leaves of c4 plants.
Functional Plant Biology, 19(5):519–538, 1992.

I. Cowan and F. GD.
Stomatal function in relation to leaf metabolism and environment.
1977.

E. Cremonese, M. Migliavacca, M. Galvagno, M. Rossini, R. Colombo, E. Pari, L. Busetto, S. Cogliati, M. Lonati, G. Manca, et al.
Alpine grassland phenology: a multi-source data perspective.
In *Phenology 2010: Climate change impacts & adaptations*, pages 20–20. Citeseer, 2010.

G. P. Cressman.
An operational objective analysis system.
Mon. Wea. Rev, 87(10):367–374, 1959.

N. C. Cristea, S. K. Kampf, and S. J. Burges.
Revised coefficients for priestley-taylor and makkink-hansen equations for estimating daily reference evapotranspiration.
Journal of Hydrologic Engineering, 18(10):1289–1300, 2013.

Y. Dai, R. E. Dickinson, and Y.-P. Wang.
A two-big-leaf model for canopy temperature, photosynthesis, and stomatal conductance.
Journal of Climate, 17(12):2281–2299, 2004.

G. Damour, T. Simonneau, H. Cochard, and L. Urban.
An overview of models of stomatal conductance at the leaf level.
Plant, Cell and Environment, 33(9):1419–1438, 2010.
ISSN 01407791.
doi: 10.1111/j.1365-3040.2010.02181.x.

O. David, J. C. Ascough, W. Lloyd, T. R. Green, K. W. Rojas, G. H. Leavesley, and L. R. Ahuja.
A software engineering perspective on environmental modeling framework design: The Object Modeling System.
Environmental Modelling and Software, 39:201–213, 2013.
ISSN 13648152.
doi: 10.1016/j.envsoft.2012.03.006.
URL https://fardapaper.ir/mohavaha/uploads/2017/11/A-software-engineering-perspective-on-environmen pdf.

D. G. De Pury and G. D. Farquhar.
Simple scaling of photosynthesis from leaves to canopies without the errors of big-leaf models.
Plant, Cell and Environment, 20(5):537–557, may 1997.
ISSN 01407791.
doi: 10.1111/j.1365-3040.1997.00094.x.
URL http://doi.wiley.com/10.1111/j.1365-3040.1997.00094.x.

J. W. Deardorff.
Efficient prediction of ground surface temperature and moisture, with inclusion of a layer of vegetation.
Journal of Geophysical Research: Oceans, 83(C4):1889–1903, 1978.

M. C. Demirel, J. Mai, G. M. Gonzalez, J. Koch, L. Samaniego, and S. Stisen.
Combining satellite data and appropriate objective functions for improved spatial pattern performance of a distributed hydrologic model.
Hydrology and Earth System Sciences, 22:1299–1315, 2018.

R. C. Dewar.
The Ball-Berry-Leuning and Tardieu-Davies stomatal models: Synthesis and extension within a spatially aggregated picture of guard cell function.
Plant, Cell and Environment, 25(11):1383–1398, 2002a.
ISSN 01407791.
doi: 10.1046/j.1365-3040.2002.00909.x.

R. C. Dewar.
The ball–berry–leuning and tardieu–davies stomatal models: synthesis and extension within a spatially aggregated picture of guard cell function.
Plant, Cell & Environment, 25(11):1383–1398, 2002b.

D. Duethmann and G. Blöschl.
Why has catchment evaporation increased in the past 40 years? a data-based study in austria.
Hydrology & Earth System Sciences, 22(10), 2018.

R. Duffkova et al.
Difference in canopy and air temperature as an indicator of grassland water stress.
Soil Water Res, 1:127–138, 2006.

C. J. Duffy.
A Two-State Integral-Balance Model for Soil Moisture and Groundwater Dynamics in Complex Terrain.
Water Resources Research, 32(8):2421–2434, aug 1996.

ISSN 00431397.
doi: 10.1029/96WR01049.
URL http://doi.wiley.com/10.1029/96WR01049.

S. Dupire, T. Curt, and S. Bigot.
Spatio-temporal trends in fire weather in the french alps.
Science of the total environment, 595:801–817, 2017.

D. Eamus, A. Huete, and Q. Yu.
Vegetation dynamics.
Cambridge University Press, 2016.

A. Ershadi, M. F. McCabe, J. P. Evans, N. W. Chaney, and E. F. Wood.
Multi-site evaluation of terrestrial evaporation models using FLUXNET data.
Agricultural and Forest Meteorology, 187:46–61, 2014.
ISSN 01681923.
doi: 10.1016/j.agrformet.2013.11.008.
URL http://dx.doi.org/10.1016/j.agrformet.2013.11.008.

J. Evaristo, S. Jasechko, and J. J. McDonnell.
Global separation of plant transpiration from groundwater and streamflow.
Nature, 525(7567):91–94, 2015.

M. Falkenmark and J. Rockström.
The new blue and green water paradigm: Breaking new ground for water resources planning and management, 2006.

J. Famiglietti and E. F. Wood.
Multiscale modeling of spatially variable water and energy balance processes.
Water Resources Research, 30(11):3061–3078, 1994.

Y. Fan, M. Clark, D. M. Lawrence, S. Swenson, L. Band, S. L. Brantley, P. Brooks, W. E. Dietrich, A. Flores, G. Grant, et al.
Hillslope hydrology in global change research and earth system modeling.
Water Resources Research, 55(2):1737–1772, 2019.

G. D. Farquhar.
Models of integrated photosynthesis of cells and leaves.
Philosophical Transactions of the Royal Society of London. B, Biological Sciences, 323(1216):357–367, 1989.

G. D. Farquhar and K. Raschke.
On the Resistance to Transpiration of the Sites of Evaporation within the Leaf.
Plant Physiology, 61(6):1000–1005, 1978.
ISSN 0032-0889.
doi: 10.1104/pp.61.6.1000.
URL http://www.plantphysiol.org/cgi/doi/10.1104/pp.61.6.1000.

G. D. Farquhar and S. Von Caemmerer.
Modelling of photosynthetic response to environmental conditions.
In *Physiological plant ecology II*, pages 549–587. Springer, 1982.

G. D. Farquhar, S. v. von Caemmerer, and J. A. Berry.
A biochemical model of photosynthetic co 2 assimilation in leaves of c 3 species.
Planta, 149(1):78–90, 1980.

S. Fatichi, V. Ivanov, and E. Caporali.
A mechanistic ecohydrological model to investigate complex interactions in cold and warm water-controlled environments:
1. theoretical framework and plot-scale analysis.
Journal of Advances in Modeling Earth Systems, 4(2), 2012.

S. Fatichi, P. Molnar, T. Mastrotheodoros, and P. Burlando.
Diurnal and seasonal changes in near-surface humidity in a complex orography.
Journal of Geophysical Research: Atmospheres, 120(6):2358–2374, 2015.

S. Fatichi, C. Pappas, and V. Ivanov.
Modeling plant–water interactions: an ecohydrological overview from the cell to the global scale, wires water, 3, 327–368, 2016.

T. Foken.
50 years of the monin–obukhov similarity theory.
Boundary-Layer Meteorology, 119(3):431–447, 2006.

T. Foken.
The energy balance closure problem: an overview.
Ecological Applications, 18(6):1351–1367, 2008.

G. Formetta, R. Mantilla, S. Franceschi, A. Antonello, and R. Rigon.
The JGrass-NewAge system for forecasting and managing the hydrological budgets at the basin scale: Models of flow generation and propagation/routing.
Geoscientific Model Development, 4(4):943–955, 2011a.
ISSN 1991959X.
doi: 10.5194/gmd-4-943-2011.
URL www.geosci-model-dev.net/4/943/2011/.

G. Formetta, R. Mantilla, S. Franceschi, A. Antonello, and R. Rigon.
The JGrass-NewAge system for forecasting and managing the hydrological budgets at the basin scale: Models of flow generation and propagation/routing.
Geoscientific Model Development, 4(4):943–955, nov 2011b.

ISSN 1991959X.
doi: 10.5194/gmd-4-943-2011.
URL https://www.geosci-model-dev.net/4/943/2011/.

G. Formetta, R. Mantilla, S. Franceschi, A. Antonello, and R. Rigon.
The jgrass-newage system for forecasting and managing the hydrological budgets at the basin scale: models of flow generation and propagation/routing.
Geoscientific Model Development, 4(4):943, 2011c.

G. Formetta, R. Rigon, J. Chávez, and O. David.
Modeling shortwave solar radiation using the jgrass-newage system.
Geoscientific Model Development, 6(4):915–928, 2013a.

G. Formetta, R. Rigon, J. L. Chávez, and O. David.
Modeling shortwave solar radiation using the JGrass-NewAge system.
Geoscientific Model Development, 6(4):915–928, jul 2013b.
ISSN 1991959X.
doi: 10.5194/gmd-6-915-2013.
URL https://www.geosci-model-dev.net/6/915/2013/.

G. Formetta, A. Antonello, S. Franceschi, O. David, and R. Rigon.
Hydrological modelling with components: A GIS-based open-source framework.
Environmental Modelling and Software, 55:190–200, may 2014a.
ISSN 13648152.
doi: 10.1016/j.envsoft.2014.01.019.

URL https://www.sciencedirect.com/science/article/pii/S1364815214000292.

G. Formetta, A. Antonello, S. Franceschi, O. David, and R. Rigon. Hydrological modelling with components: A gis-based open-source framework. *Environmental Modelling & Software*, 55:190–200, 2014b.

G. Formetta, M. Bancheri, O. David, and R. Rigon. Performance of site-specific parameterizations of longwave radiation. *Hydrology and Earth System Sciences*, 20(11):4641–4654, nov 2016. ISSN 16077938. doi: 10.5194/hess-20-4641-2016. URL https://www.hydrol-earth-syst-sci.net/20/4641/2016/.

A. S. L. Frank P. Incropera, David P. DeWitt, Theodore L. Bergman. *Fundamentals of Heat and Mass Transfer.pdf*, volume 13. 2002. URL http://cds.cern.ch/record/1339915/files/9780471457282{_}TOC.pdf.

E. Freeman, E. Robson, B. Bates, and K. Sierra. *Head first design patterns*. " O'Reilly Media, Inc.", 2008.

A. Friend. Modelling canopy co2 fluxes: are 'big-leaf'simplifications justified? *Global Ecology and Biogeography*, 10(6):603–619, 2001.

M. Galvagno, G. Wohlfahrt, E. Cremonese, M. Rossini, R. Colombo, G. Filippa, T. Julitta, G. Manca, C. Siniscalco, U. Morra di Cella, and M. Migliavacca.
Phenology and carbon dioxide source/sink strength of a subalpine grassland in response to an exceptionally short snow season.
Environmental Research Letters, 8(2):25008, 2013.
URL http://stacks.iop.org/1748-9326/8/i=2/a=025008.

E. Gamma.
Design patterns: elements of reusable object-oriented software.
Pearson Education India, 1995.

E. Gamma, R. Helm, R. Johnson, and J. Vlissides.
Design patterns: Micro-architectures for reusable object-oriented design.
Reading: Addison-Wesley, 1994.

D. M. Gates.
Transpiration and leaf temperature.
Annual Review of Plant Physiology, 19(1):211–238, 1968.

J. M. Gilbert and R. M. Maxwell.
Contrasting warming and drought in snowmelt-dominated agricultural basins: revealing the role of elevation gradients in regional response to temperature change.
Environmental Research Letters, 13(7):074023, 2018.

A. E. Gill.
Atmosphere—ocean dynamics.
Elsevier, 2016.

J. Goudriaan.
Crop micrometeorology: a simulation study.

PhD thesis, Pudoc, 1977.

M. L. Goulden and R. C. Bales.
Mountain runoff vulnerability to increased evapotranspiration with vegetation expansion.
Proceedings of the National Academy of Sciences, 111(39): 14071–14075, 2014.

H. V. Gupta, H. Kling, K. K. Yilmaz, and G. F. Martinez.
Decomposition of the mean squared error and nse performance criteria: Implications for improving hydrological modelling.
Journal of hydrology, 377(1-2):80–91, 2009.

E. Haghighi and D. Or.
Evaporation from porous surfaces into turbulent airflows: Coupling eddy characteristics with pore scale vapor diffusion.
Water Resources Research, 49(12):8432–8442, 2013.
ISSN 00431397.
doi: 10.1002/2012WR013324.

A. Hammerle, A. Haslwanter, M. Schmitt, M. Bahn, U. Tappeiner, A. Cernusca, and G. Wohlfahrt.
Eddy covariance measurements of carbon dioxide, latent and sensible energy fluxes above a meadow on a mountain slope.
Boundary-layer meteorology, 122(2):397–416, 2007.

L. E. Hay and M. Umemoto.
Multiple-objective stepwise calibration using Luca.
U. S. Geological Survey Open-File Report, (2006-1323):25, 2006a.

L. E. Hay and M. Umemoto.
Multiple-objective stepwise calibration using Luca.
Number 2006-1323. US Geological Survey, 2006b.

ISBN OFR - 2006-1323.

R. Hiller, M. J. Zeeman, and W. Eugster.
Eddy-covariance flux measurements in the complex terrain of an alpine valley in switzerland.
Boundary-Layer Meteorology, 127(3):449–467, 2008.

R. Hock.
A distributed temperature-index ice-and snowmelt model including potential direct solar radiation.
Journal of Glaciology, 45(149):101–111, 1999.

N. M. Holbrook, M. J. Burns, and C. B. Field.
Negative xylem pressures in plants: a test of the balancing pressure technique.
Science, 270(5239):1193–1194, 1995.

T. Hölttä, H. Cochard, E. Nikinmaa, and M. Mencuccini.
Capacitive effect of cavitation in xylem conduits: results from a dynamic model.
Plant, Cell & Environment, 32(1):10–21, 2009.

V. Y. Ivanov, R. L. Bras, and E. R. Vivoni.
Vegetation-hydrology dynamics in complex terrain of semiarid areas: 1. a mechanistic approach to modeling dynamic feedbacks.
Water Resources Research, 44(3), 2008.

P. G. Jarvis.
The Interpretation of the Variations in Leaf Water Potential and Stomatal Conductance Found in Canopies in the Field.
Philosophical Transactions of the Royal Society B: Biological Sciences, 273(927):593–610, 1976.
ISSN 0962-8436.
doi: 10.1098/rstb.1976.0035.

URL http://rstb.royalsocietypublishing.org/cgi/doi/10.1098/rstb.1976.0035.

P. G. Jarvis and K. G. Mcnaughton.
Stomatal Control of Transpiration: Scaling Up from Leaf to Region.
Advances in Ecological Research, 15(C):1–49, jan 1986.
ISSN 00652504.
doi: 10.1016/S0065-2504(08)60119-1.
URL https://www.sciencedirect.com/science/article/pii/S0065250408601191.

T. June, J. R. Evans, and G. D. Farquhar.
A simple new equation for the reversible temperature dependence of photosynthetic electron transport: a study on soybean leaf.
Functional plant biology, 31(3):275–283, 2004.

M. Jung, M. Reichstein, P. Ciais, S. I. Seneviratne, J. Sheffield, M. L. Goulden, G. Bonan, A. Cescatti, J. Chen, R. De Jeu, A. J. Dolman, W. Eugster, D. Gerten, D. Gianelle, N. Gobron, J. Heinke, J. Kimball, B. E. Law, L. Montagnani, Q. Mu, B. Mueller, K. Oleson, D. Papale, A. D. Richardson, O. Roupsard, S. Running, E. Tomelleri, N. Viovy, U. Weber, C. Williams, E. Wood, S. Zaehle, and K. Zhang.
Recent decline in the global land evapotranspiration trend due to limited moisture supply.
Nature, 467(7318):951–954, 2010.
ISSN 00280836.
doi: 10.1038/nature09396.
URL http://www.ncbi.nlm.nih.gov/pubmed/20935626http://www.nature.com.ezproxy.library.wisc.edu/nature/journal/v467/n7318/full/nature09396.html{%}5Cnhttp:

//www.nature.com.ezproxy.library.wisc.edu/nature/journal/v467/n7318/pdf/nature09396.pdf.

G. G. Katul, R. Oren, S. Manzoni, C. Higgins, and M. B. Parlange. Evapotranspiration: A process driving mass transport and energy exchange in the soil-plant-atmosphere-climate system, sep 2012.
ISSN 87551209.
URL http://doi.wiley.com/10.1029/2011RG000366.

G. G. Katul, D. Cava, M. Siqueira, and D. Poggi.
Scalar turbulence within the canopy sublayer.
Coherent flow structures at Earth's Surface, pages 73–95, 2013.

H. Kobayashi, D. D. Baldocchi, Y. Ryu, Q. Chen, S. Ma, J. L. Osuna, and S. L. Ustin.
Modeling energy and carbon fluxes in a heterogeneous oak woodland: A three-dimensional approach.
Agricultural and Forest Meteorology, 152:83–100, 2012.

S. Y. Kotchenova, X. Song, N. V. Shabanov, C. S. Potter, Y. Knyazikhin, and R. B. Myneni.
Lidar remote sensing for modeling gross primary production of deciduous forests.
Remote Sensing of Environment, 92(2):158–172, 2004.

C.-T. Lai, G. Katul, R. Oren, D. Ellsworth, and K. Schäfer.
Modeling co2 and water vapor turbulent flux distributions within a forest canopy.
Journal of Geophysical Research: Atmospheres, 105(D21):26333–26351, 2000.

P. Lehmann and D. Or.

Effects of stomata clustering on leaf gas exchange.
New Phytologist, 207(4):1015–1025, sep 2015.
ISSN 14698137.
doi: 10.1111/nph.13442.
URL http://doi.wiley.com/10.1111/nph.13442.

P. Lehmann, S. Assouline, and D. Or.
Characteristic lengths affecting evaporative drying of porous media.
Physical Review E, 77(5):056309, 2008.

P. Lehmann, O. Merlin, P. Gentine, and D. Or.
Soil texture effects on surface resistance to bare-soil evaporation.
Geophysical Research Letters, 45(19):10–398, 2018.

R. Leuning.
Modelling Stomatal Behaviour and and Photosynthesis of Eucalyptus grandis.
Functional Plant Biology, 17(2):159, 1990.
ISSN 1445-4408.
doi: 10.1071/pp9900159.
URL http://www.publish.csiro.au/?paper=PP9900159.

R. Leuning.
A critical appraisal of a combined stomatal-photosynthesis model for C3 plants.
Plant, Cell & Environment, 18(4):339–355, apr 1995.
ISSN 13653040.
doi: 10.1111/j.1365-3040.1995.tb00370.x.
URL http://doi.wiley.com/10.1111/j.1365-3040.1995.tb00370.x.

S. Liu, L. Lu, D. Mao, and L. Jia.

Evaluating parameterizations of aerodynamic resistance to heat transfer using field measurements.
2007.

C. Macfarlane, D. White, and M. Adams.
The apparent feed-forward response to vapour pressure deficit of stomata in droughted, field-grown eucalyptus globulus labill.
Plant, Cell & Environment, 27(10):1268–1280, 2004.

D. S. Mackay, D. E. Roberts, B. E. Ewers, J. S. Sperry, N. G. McDowell, and W. T. Pockman.
Interdependence of chronic hydraulic dysfunction and canopy processes can improve integrated models of tree response to drought.
Water Resources Research, 51(8):6156–6176, 2015.

G. Manoli, S. Bonetti, J.-C. Domec, M. Putti, G. Katul, and M. Marani.
Tree root systems competing for soil moisture in a 3d soil–plant model.
Advances in water resources, 66:32–42, 2014.

R. Mantilla, V. K. Gupta, and O. J. Mesa.
Role of coupled flow dynamics and real network structures on Hortonian scaling of peak flows.
Journal of Hydrology, 322(1-4):155–167, may 2006.
ISSN 00221694.
doi: 10.1016/j.jhydrol.2005.03.022.
URL https://linkinghub.elsevier.com/retrieve/pii/S0022169405001113.

S. Manzoni, G. Vico, G. Katul, S. Palmroth, R. B. Jackson, and A. Porporato.

Hydraulic limits on maximum plant transpiration and the emergence of the safety–efficiency trade-off.
New Phytologist, 198(1):169–178, 2013.

D. L. Martin, D. J. Wehner, and C. Throssell.
Models for predicting the lower limit of the canopy-air temperature difference of two cool season grasses.
Crop science, 34(1):192–198, 1994.

J. Martínez-Vilalta and N. Garcia-Forner.
Water potential regulation, stomatal behaviour and hydraulic transport under drought: deconstructing the iso/anisohydric concept.
Plant, Cell & Environment, 40(6):962–976, 2017.

T. Mastrotheodoros, C. Pappas, P. Molnar, P. Burlando, T. F. Keenan, P. Gentine, C. M. Gough, and S. Fatichi.
Linking plant functional trait plasticity and the large increase in forest water use efficiency.
Journal of Geophysical Research: Biogeosciences, 122(9):2393–2408, 2017.

T. Mastrotheodoros, C. Pappas, P. Molnar, P. Burlando, P. Hadjidoukas, and S. Fatichi.
Ecohydrological dynamics in the alps: Insights from a modelling analysis of the spatial variability.
Ecohydrology, 12(1):e2054, 2019.

T. Mastrotheodoros, C. Pappas, P. Molnar, P. Burlando, G. Manoli, J. Parajka, R. Rigon, B. Szeles, M. Bottazzi, P. Hadjidoukas, et al.
More green and less blue water in the alps during warmer summers.
Nature Climate Change, pages 1–7, 2020.

R. M. Maxwell and L. E. Condon.

Connections between groundwater flow and transpiration partitioning.
Science, 353(6297):377–380, 2016.

K. A. McColl.
Practical and theoretical benefits of an alternative to the penman-monteith evapotranspiration equation.
Water Resources Research, 56(6):e2020WR027106, 2020.

J. McDonough.
A'synthetic scalar'subgrid-scale model for large-eddy simulation of turbulent combustion.
In *Proc. 2002 Spring Tech. Mtg. Central States Sec., Combust. Inst.* Citeseer, 2002.

J. M. McDonough.
Introductory lectures on turbulence: physics, mathematics and modeling.
2007.

K. McNaughton and T. A. Black.
A study of evapotranspiration from a douglas fir forest using the energy balance approach.
Water Resources Research, 9(6):1579–1590, 1973.

B. Medlyn.
A maestro retrospective.
Forests at the land-atmosphere interface, pages 105–122, 2004.

P. Meir, B. Kruijt, M. Broadmeadow, E. Barbosa, O. Kull, F. Carswell, A. Nobre, and P. Jarvis.
Acclimation of photosynthetic capacity to irradiance in tree canopies in relation to leaf nitrogen concentration and leaf mass per unit area.
Plant, Cell & Environment, 25(3):343–357, 2002.

P. Melcher, F. Meinzer, D. Yount, G. Goldstein, and U. Zimmermann.
Comparative measurements of xylem pressure in transpiring and non-transpiring leaves by means of the pressure chamber and the xylem pressure probe.
Journal of Experimental Botany, 49(327):1757–1760, 1998.

L. Mercado, J. Lloyd, F. Carswell, Y. Malhi, P. Meir, and A. D. Nobre.
Modelling amazonian forest eddy covariance data: a comparison of big leaf versus sun/shade models for the c-14 tower at manaus i. canopy photosynthesis.
Acta Amazonica, 36(1):69–82, 2006.

L. M. Mercado, C. Huntingford, J. H. Gash, P. M. Cox, and V. Jogireddy.
Improving the representation of radiation interception and photosynthesis for climate model applications.
Tellus B: Chemical and Physical Meteorology, 59(3):553–565, 2007.

L. Misson, D. P. Rasse, C. Vincke, M. Aubinet, and L. François.
Predicting transpiration from forest stands in Belgium for the 21st century.
Agricultural and Forest Meteorology, 111(4):265–282, jun 2002. ISSN 01681923.
doi: 10.1016/S0168-1923(02)00039-4.
URL https://www.sciencedirect.com/science/article/pii/S0168192302000394.

P. J. Mitchell, E. J. Veneklaas, H. Lambers, and S. S. Burgess.
Using multiple trait associations to define hydraulic functional types in plant communities of south-western australia.
Oecologia, 158(3):385–397, 2008.

M. Molles.

Ecology: concepts and applications.
McGraw-Hill Education, 2015.

J. Monteith.
Solar radiation and productivity in tropical ecosystems.
Journal of applied ecology, 9(3):747–766, 1972.

J. Monteith.
Principles of environmental physics edward arnold.
London, 214p, 1973.

J. Monteith.
Evaporation and surface temperature.
Quarterly Journal of the Royal Meteorological Society, 107(451): 1–27, 1981.

J. Monteith.
Evaporation from land surfaces: progress in analysis and prediction since 1948.
In *National conference on advances in evapotranspiration, Hyatt Regency Chicago, Ill.(USA), 16-17 Dec 1985*. American Society of Agricultural Engineers, 1985.

J. L. Monteith.
Evaporation and environment.
In *Symposia of the society for experimental biology*, volume 19, pages 205–234. Cambridge University Press (CUP) Cambridge, 1965.

R. Moore.
The probability-distributed principle and runoff production at point and basin scales.
Hydrological Sciences Journal, 30(2):273–297, 1985.

M. Moran, A. Rahman, J. Washburne, D. Goodrich, M. Weltz, and W. Kustas.

Combining the penman-monteith equation with measurements of surface temperature and reflectance to estimate evaporation rates of semiarid grassland.
Agricultural and forest Meteorology, 80(2-4):87–109, 1996.

F. I. Morton.
Operational estimates of areal evapotranspiration and their significance to the science and practice of hydrology.
Journal of Hydrology, 66(1-4):1–76, 1983.

K. A. Mott.
Do stomata respond to co2 concentrations other than intercellular?
Plant physiology, 86(1):200–203, 1988.

Y. Mualem.
A new model for predicting the hydraulic conductivity of unsaturated porous media.
Water resources research, 12(3):513–522, 1976.

E. Mukammal and H. Neumann.
Application of the priestley-taylor evaporation model to assess the influence of soil moisture on the evaporation from a large weighing lysimeter and class a pan.
Boundary-Layer Meteorology, 12(2):243–256, 1977.

G. Niedrist, E. Tasser, G. Bertoldi, S. Della Chiesa, N. Obojes, L. Egarter-Vigl, and U. Tappeiner.
Down to future: Transplanted mountain meadows react with increasing phytomass or shifting species composition.
Flora, 224:172–182, 2016.

E. Nikinmaa, R. Sievänen, and T. Hölttä.

Dynamics of leaf gas exchange, xylem and phloem transport, water potential and carbohydrate concentration in a realistic 3-d model tree crown.
Annals of botany, 114(4):653–666, 2014.

P. S. Nobel et al.
Physicochemical & environmental plant physiology.
Academic press, 1999.

S. M. Noe and C. Giersch.
A simple dynamic model of photosynthesis in oak leaves: Coupling leaf conductance and photosynthetic carbon fixation by a variable intracellular CO2 pool.
Functional Plant Biology, 31(12):1195–1204, dec 2004.
ISSN 14454408.
doi: 10.1071/FP03251.
URL http://www.publish.csiro.au/?paper=FP03251.

D. Norbiato, M. Borga, R. Merz, G. Blöschl, and A. Carton.
Controls on event runoff coefficients in the eastern italian alps.
Journal of Hydrology, 375(3-4):312–325, 2009.

J. Norman.
" modelling the complete crop canopy",'modification of the aerial environment of plants'.
Am. Soc. Agr. Eng. Monograph, 2:249–277, 1979.

J. Norman.
Interfacing leaf and canopy light interception models [plant photosynthesis].
1980.

M. E. Olson, D. Soriano, J. A. Rosell, T. Anfodillo, M. J. Donoghue, E. J. Edwards, C. León-Gómez, T. Dawson, J. J. C. Martínez, M. Castorena, et al.
Plant height and hydraulic vulnerability to drought and cold.
Proceedings of the National Academy of Sciences, 115(29):7551–7556, 2018.

D. Or, P. Lehmann, E. Shahraeeni, and N. Shokri.
Advances in Soil Evaporation Physics—A Review.
Vadose Zone Journal, 12(4):0, nov 2013.
ISSN 00222313.
doi: 10.1016/0022-2313(76)90010-7.
URL https://www.soils.org/publications/vzj/abstracts/12/4/vzj2012.0163.

R. Orth and G. Destouni.
Drought reduces blue-water fluxes more strongly than green-water fluxes in europe.
Nature communications, 9(1):1–8, 2018.

D. Papale, M. Migliavacca, E. Cremonese, A. Cescatti, G. Alberti, M. Balzarolo, L. B. Marchesini, E. Canfora, R. Casa, P. Duce, et al.
Carbon, water and energy fluxes of terrestrial ecosystems in italy.
In *The Greenhouse Gas Balance of Italy*, pages 11–45. Springer, 2015.

C. Pappas, S. Fatichi, and P. Burlando.
Modeling terrestrial carbon and water dynamics across climatic gradients: does plant trait diversity matter?
New Phytologist, 209(1):137–151, 2016.

M. B. Parlange and G. G. Katul.
An advection-aridity evaporation model.

Water Resources Research, 28(1):127–132, 1992.

C. A. Paulson.
The mathematical representation of wind speed and temperature profiles in the unstable atmospheric surface layer.
Journal of Applied Meteorology, 9(6):857–861, 1970.

H. L. Penman.
Natural evaporation from open water, hare soil and grass.
Proceedings of the Royal Society of London. Series A, Mathematical and physical sciences, 193(1032):120–145, 1948.
ISSN 09501207.
doi: 10.1098/rspa.1948.0037.

N. Pepin, R. S. Bradley, H. Diaz, M. Baraër, E. Caceres, N. Forsythe, H. Fowler, G. Greenwood, M. Hashmi, X. Liu, et al.
Elevation-dependent warming in mountain regions of the world.
Nature climate change, 5(5):424–430, 2015.

D. Poggi, G. Katul, and J. Albertson.
A note on the contribution of dispersive fluxes to momentum transfer within canopies.
Boundary-layer meteorology, 111(3):615–621, 2004.

L. Prandtl.
7. bericht über untersuchungen zur ausgebildeten turbulenz.
ZAMM-Journal of Applied Mathematics and Mechanics/Zeitschrift für Angewandte Mathematik und Mechanik, 5 (2):136–139, 1925.

L. Prandtl.
Application of the" magnus effect" to the wind propulsion of ships.
National Advisory Committee for Aeronautics, 1926.

I. C. Prentice, X. Liang, B. E. Medlyn, Y. Wang, et al.
Reliable, robust and realistic: the three r's of next-generation land-surface modelling.
2015.

C. H. B. Priestley and R. Taylor.
On the assessment of surface heat flux and evaporation using large-scale parameters.
Monthly weather review, 100(2):81–92, 1972.

T. Pütz, M. Hannesd, and U. Wollschlägere.
Estimating precipitation and actual evapotranspiration from precision lysimeter measurements.
Procedia Environmental Sciences, 19:543–552, 2013.

M. R. Raupach and J. J. Finnigan.
"Single-layer models of evaporation from plant canopies are incorrect but useful, whereas multilayer models are correct but useless': discuss.
Australian Journal of Plant Physiology, 15(6):705–716, 1988.
ISSN 03107841.
doi: 10.1071/PP9880705.
URL http://www.publish.csiro.au/?paper=PP9880705http://www.publish.csiro.au/fp/pdf/PP9880705.

R. Rigon, E. Ghesla, C. Tiso, and A. Cozzini.
The HORTON machine: a system for DEM analysis The reference manual.
Università degli Studi di Trento, 2006.

R. Rigon, P. D'Odorico, and G. Bertoldi.
The geomorphic structure of the runoff peak.
Hydrology and Earth System Sciences, 15(6):1853–1863, jun 2011.

ISSN 1607-7938.
doi: 10.5194/hess-15-1853-2011.
URL https://www.hydrol-earth-syst-sci.net/15/1853/2011/.

A. E. Rizzoli, M. Donatelli, R. Muetzelfeldt, T. Otjens, M. Svensson, F. Evert, F. Villa, and J. Bolte.
Seamframe, a proposal for an integrated modelling framework for agricultural systems.
In *Proceedings of the 8th ESA Congress*, pages 331–332, 2004.

I. Rodrigues-Iturbe.
Ecohydrology: a hydrological perspective of climate-soil-vegetation dynamic.
Water Resource Research, 36(1):3–9, 2000.

C. R. Rollinson and M. W. Kaye.
Modeling monthly temperature in mountainous ecoregions: importance of spatial scale for ecological research.
Climate Research, 64(2):99–110, 2015.

J. A. Rosell, M. E. Olson, and T. Anfodillo.
Scaling of xylem vessel diameter with plant size: causes, predictions, and outstanding questions.
Current Forestry Reports, 3(1):46–59, 2017.

Y. Ryu, D. D. Baldocchi, H. Kobayashi, C. Van Ingen, J. Li, T. A. Black, J. Beringer, E. Van Gorsel, A. Knohl, B. E. Law, and O. Roupsard.
Integration of MODIS land and atmosphere products with a coupled-process model to estimate gross primary productivity and evapotranspiration from 1 km to global scales.
Global Biogeochemical Cycles, 25(4), 2011.
ISSN 08866236.
doi: 10.1029/2011GB004053.

L. Samaniego, S. Thober, R. Kumar, N. Wanders, O. Rakovec, M. Pan, M. Zink, J. Sheffield, E. F. Wood, and A. Marx.
Anthropogenic warming exacerbates european soil moisture droughts.
Nature Climate Change, 8(5):421, 2018.

R. Samson and R. Lemeur.
Energy balance storage terms and big-leaf evapotranspiration in a mixed deciduous forest.
Annals of Forest Science, 58(5):529–541, jul 2001.
ISSN 12864560.
doi: 10.1051/forest:2001143.
URL http://www.edpsciences.org/10.1051/forest:2001143.

B. Sapoval, M. Rosso, and J.-F. Gouyet.
The fractal nature of a diffusion front and the relation to percolation.
Journal de Physique Lettres, 46(4):149–156, 1985.

P. F. Scholander, E. D. Bradstreet, E. Hemmingsen, and H. Hammel.
Sap pressure in vascular plants: negative hydrostatic pressure can be measured in plants.
Science, 148(3668):339–346, 1965.

S. J. Schymanski and D. Or.
Leaf-scale experiments reveal an important omission in the Penman-Monteith equation.
Hydrology and Earth System Sciences, 21(2):685–706, feb 2017.
ISSN 16077938.
doi: 10.5194/hess-21-685-2017.
URL https://www.hydrol-earth-syst-sci.net/21/685/2017/.

P. J. Sellers, M. D. Heiser, and F. G. Hall.
Relations between surface conductance and spectral vegetation indices at intermediate (100 m2 to 15 km2) length scales.
Journal of Geophysical Research: Atmospheres, 97(D17):19033–19059, 1992.

F. Serafin.
Enabling modeling framework with surrogate modeling capabilities and complex networks.
PhD thesis, University of Trento, 2019.

E. Shahraeeni, P. Lehmann, and D. Or.
Coupling of evaporative fluxes from drying porous surfaces with air boundary layer: Characteristics of evaporation from discrete pores.
Water Resources Research, 48(9), 2012.

Z.-S. She, X. Chen, and F. Hussain.
Quantifying wall turbulence via a symmetry approach: a lie group theory.
Journal of Fluid Mechanics, 827:322–356, 2017.

C. Shen, J. Niu, and M. S. Phanikumar.
Evaluating controls on coupled hydrologic and vegetation dynamics in a humid continental climate watershed using a subsurface-land surface processes model.
Water Resources Research, 49(5):2552–2572, 2013.

N. Shokri and D. Or.
What determines drying rates at the onset of diffusion controlled stage-2 evaporation from porous media?
Water Resources Research, 47(9), 2011.

W. J. Shuttleworth and J. Wallace.
Evaporation from sparse crops-an energy combination theory.

Quarterly Journal of the Royal Meteorological Society, 111(469): 839–855, 1985.

T. Sinclair, C. Murphy, and K. Knoerr.
Development and evaluation of simplified models for simulating canopy photosynthesis and transpiration.
Journal of Applied Ecology, pages 813–829, 1976.

M. Siqueira, G. Katul, and A. Porporato.
Soil moisture feedbacks on convection triggers: The role of soil–plant hydrodynamics.
Journal of Hydrometeorology, 10(1):96–112, 2009.

M. Sprintsin, J. M. Chen, A. Desai, and C. M. Gough.
Evaluation of leaf-to-canopy upscaling methodologies against carbon flux data in north america.
Journal of Geophysical Research: Biogeosciences, 117(G1), 2012.

P. C. Stoy, M. Mauder, T. Foken, B. Marcolla, E. Boegh, A. Ibrom, M. A. Arain, A. Arneth, M. Aurela, C. Bernhofer, et al.
A data-driven analysis of energy balance closure across fluxnet research sites: The role of landscape scale heterogeneity.
Agricultural and forest meteorology, 171:137–152, 2013.

A. D. Stroock, V. V. Pagay, M. A. Zwieniecki, and N. Michele Holbrook.
The physicochemical hydrodynamics of vascular plants.
Annual Review of Fluid Mechanics, 46:615–642, 2014.

Z. Su and C. Jacobs.
ENVISAT: actual evaporation.
Beleidscommissie Remote Sensing (BCRS), 2001.

Z. Su, H. Pelgrum, and M. Menenti.
Aggregation effects of surface heterogeneity in land surface processes.

1999.

C. L. Tague, N. G. McDowell, and C. D. Allen.
An integrated model of environmental effects on growth, carbohydrate balance, and mortality of pinus ponderosa forests in the southern rocky mountains.
PLoS One, 8(11), 2013.

F. Tardieu, T. Lafarge, and T. Simonneau.
Stomatal control by fed or endogenous xylem aba in sunflower: interpretation of correlations between leaf water potential and stomatal conductance in anisohydric species.
Plant, Cell & Environment, 19(1):75–84, 1996.

G. Testa, F. Gresta, and S. L. Cosentino.
Dry matter and qualitative characteristics of alfalfa as affected by harvest times and soil water content, volume 34 of *FAO - Food and Agriculture Organization of the United*.
FAO, 2011.
ISBN 0254-5284.
doi: 10.1016/j.eja.2010.12.001.
URL http://www.fao.org/docrep/X0490E/X0490E00.htm.

I. Turton.
Geo tools.
In *Open source approaches in spatial data handling*, pages 153–169. Springer, 2008.

T. E. Twine, W. Kustas, J. Norman, D. Cook, P. Houser, T. Meyers, J. Prueger, P. Starks, and M. Wesely.
Correcting eddy-covariance flux underestimates over a grassland.
Agricultural and Forest Meteorology, 103(3):279–300, 2000.

A. Verhoef and G. Egea.
Modeling plant transpiration under limited soil water: Comparison of different plant and soil hydraulic parameterizations and preliminary implications for their use in land surface models.
Agricultural and Forest Meteorology, 191:22–32, 2014.

T. Vesala, S. Sevanto, T. Grönholm, Y. Salmon, E. Nikinmaa, P. Hari, and T. Hölttä.
Effect of leaf water potential on internal humidity and co2 dissolution: reverse transpiration and improved water use efficiency under negative pressure.
Frontiers in plant science, 8:54, 2017.

D. Viviroli, H. H. Dürr, B. Messerli, M. Meybeck, and R. Weingartner.
Mountains of the world, water towers for humanity: Typology, mapping, and global significance.
Water resources research, 43(7), 2007.

Y. Wang and P. Jarvis.
Influence of crown structural properties on par absorption, photosynthesis, and transpiration in sitka spruce: application of a model (maestro).
Tree physiology, 7(1-2-3-4):297–316, 1990.

Y.-P. Wang and R. Leuning.
A two-leaf model for canopy conductance, photosynthesis and partitioning of available energy i:: Model description and comparison with a multi-layered model.
Agricultural and Forest Meteorology, 91(1-2):89–111, 1998.

R. Weingartner, D. Viviroli, and B. Schädler.

Water resources in mountain regions: a methodological approach to assess the water balance in a highland-lowland-system.
Hydrological Processes: An International Journal, 21(5):578–585, 2007.

M. Weiß and L. Menzel.
A global comparison of four potential evapotranspiration equations and heir relevance to stream flow modelling in semi-arid environments.
Advances in Geosciences, 18:15–23, jun 2008.
ISSN 16807359.
doi: 10.5194/adgeo-18-15-2008.
URL https://www.adv-geosci.net/18/15/2008/.

D. A. White, C. L. Beadle, P. J. Sands, D. Worledge, and J. L. Honeysett.
Quantifying the effect of cumulative water stress on stomatal conductance of Eucalyptus globulus and Eucalyptus nitens: A phenomenological approach.
Australian Journal of Plant Physiology, 26(1):17–27, 1999.
ISSN 03107841.
doi: 10.1071/PP98023.

D. Wilkinson.
Percolation effects in immiscible displacement.
Physical Review A, 34(2):1380, 1986.

G. Wohlfahrt and P. Widmoser.
Can an energy balance model provide additional constraints on how to close the energy imbalance?
Agricultural and forest meteorology, 169:85–91, 2013.

G. Wohlfahrt, A. Haslwanter, L. Hörtnagl, R. L. Jasoni, L. F. Fenstermaker, J. A. Arnone III, and A. Hammerle.

On the consequences of the energy imbalance for calculating surface conductance to water vapour.
Agricultural and forest meteorology, 149(9):1556–1559, 2009.

S. Wong, I. Cowan, and G. Farquhar.
Stomatal conductance correlates with photosynthetic capacity.
Nature, 282(5737):424, 1979.

E. F. Wood, J. K. Roundy, T. J. Troy, L. Van Beek, M. F. Bierkens, E. Blyth, A. de Roo, P. Döll, M. Ek, J. Famiglietti, et al.
Hyperresolution global land surface modeling: Meeting a grand challenge for monitoring earth's terrestrial water.
Water Resources Research, 47(5), 2011.

K. Yang, N. Tamai, and T. Koike.
Analytical solution of surface layer similarity equations.
Journal of Applied Meteorology, 40(9):1647–1653, 2001.

X. Zhou, E. Istanbulluoglu, and E. R. Vivoni.
Modeling the ecohydrological role of aspect-controlled radiation on tree-grass-shrub coexistence in a semiarid climate.
Water Resources Research, 49(5):2872–2895, 2013.

G. Zhu, Y. Su, X. Li, K. Zhang, C. Li, and N. Ning.
Modelling evapotranspiration in an alpine grassland ecosystem on qinghai-tibetan plateau.
Hydrological Processes, 28(3):610–619, 2014.

G. Zuecco.
Processes space-time variability and hydrological response of headwater catchments: role of rainfall, vegetation and antecedent conditions.
2016.